Simulation of dense suspension in pipe flows with homogeneous stationary sediment bed

---

Derrick Njobuenwu* and Michael Fairweather

School of Chemical and Process Engineering, University of Leeds

In this Presentation, ...

- Why do we study particle suspensions?
- Numerical simulation
- Pipe flow with variable bed heights
- On gravity, agglomeration, breakup

Motivation

Motivation

(A) Suspension of particles in fluid are common in many fields, eg

- biological systems (blood)
- natural systems (cloud)
- industrial processing (waste slurries)

(B) We are considering dense suspensions

- four way coupling
- agglomerate breakup
- direction of gravity
- presence of stationary bed

Motivation

(A) Suspension of particles in fluid are common in many fields, eg

- biological systems (blood)
- natural systems (cloud)
- industrial processing (waste slurries)

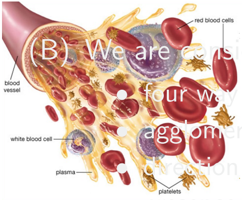

(B) We are considering dense suspensions

- four way coupling
- agglomerate breakup
- direction of gravity
- presence of stationary bed

Motivation

(A) Suspension of particles in fluid are common in many fields, eg

- biological systems (blood)
- natural systems (cloud)
- industrial processing (waste slurries)

(B) We are considering dense suspensions

- four way coupling
- agglomerate breakup
- direction of gravity
- presence of stationary bed

Motivation

(A) Suspension of particles in fluid are common in many fie

- biological systems (blood)
- natural systems (cloud)
- industrial processing (waste slurries)

(B) We are considering dense suspensions

Motivation

(A) Suspension of particles in fluid are common in many fields, eg

- biological systems (blood)
- natural systems (cloud)
- industrial processing (waste slurries)

(B) We are considering dense suspensions

- four way coupling
- agglomerate breakup
- direction of gravity
- presence of stationary bed

Dense Suspensions

Dense suspensions where volume fraction $\alpha_p \geq 10^{-3}$

- four way coupling
- agglomerate breakup
- direction of gravity
- flows with variable bed heights

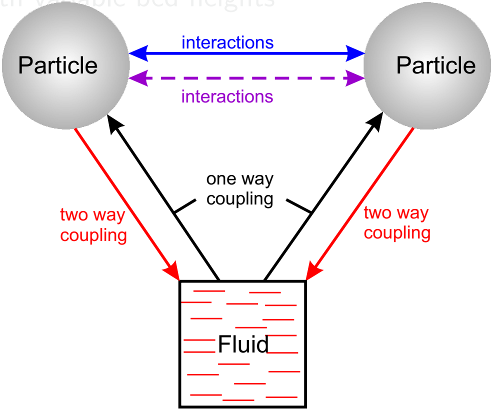

Dense Suspensions

Dense suspensions where volume fraction $\alpha_p \geq 10^{-3}$

- four way coupling
- agglomerate breakup
- direction of gravity
- flows with variable bed heights

- $\sigma(t) \sim \mu \left(\epsilon/\nu\right)^{1/2}$
- $\sigma_{cr} \sim r^{-q} \sim N_{pp}^{-q/d_f}$
- $q = \left[9.2\left(3 - d_f\right) + 1\right]/2$
- Breakup occurs $\sigma > \sigma_{cr}$
- into two equal daughters

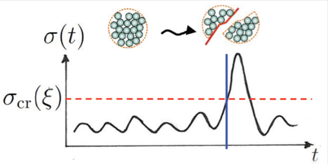

d_f is the fractal dimension

Dense Suspensions

Dense suspensions where volume fraction $\alpha_p \geq 10^{-3}$

- four way coupling
- agglomerate breakup
- direction of gravity
- flows with variable bed heights

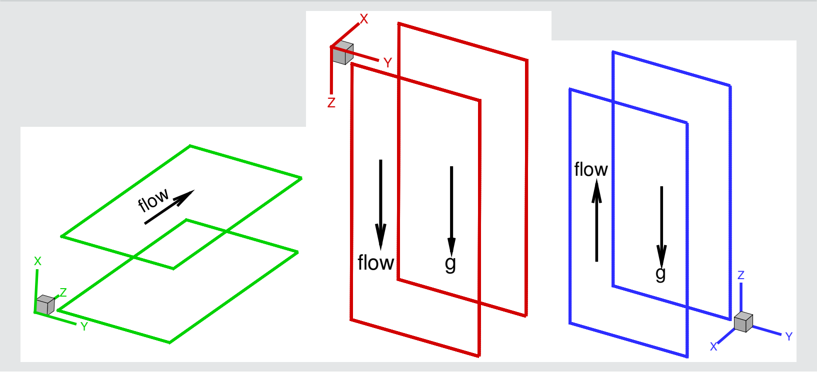

Dense Suspensions

Dense suspensions where volume fraction $\alpha_p \geq 10^{-3}$

- four way coupling
- agglomerate breakup
- direction of gravity
- flows with variable bed heights

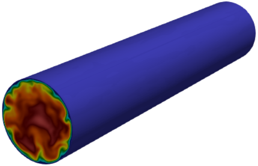

Numerical Methods

Methodology and tools

1. Highly resolved large eddy simulation
2. Robust discrete particle simulation
    - particle dispersion
    - particle collision & agglomeration
    - agglomerate breakup
    - particle deposition
    - particle resuspension
3. UoL high performance computing ARC2, ARC3

Governing Equations

- Navier-Stokes for the fluid phase subject to the continuity

$$\frac{\partial \mathbf{u}}{\partial t} + \mathbf{u} \cdot \nabla \mathbf{u} = -\nabla p + \frac{1}{Re_b} \nabla^2 + f$$

$$\nabla \cdot \mathbf{u} = 0$$

- Newton-Euler for spherical particles

$$m_p \frac{\mathrm{d}\mathbf{v}}{\mathrm{d}t} = \mathbf{F}$$

$$\mathbf{I} \frac{\mathrm{d}\Omega}{\mathrm{d}t} = \mathbf{T}$$

Turbulent Pipe Flow

Streamwise Velocity and Vorticity of Pipe Flow, $B_h = 0$

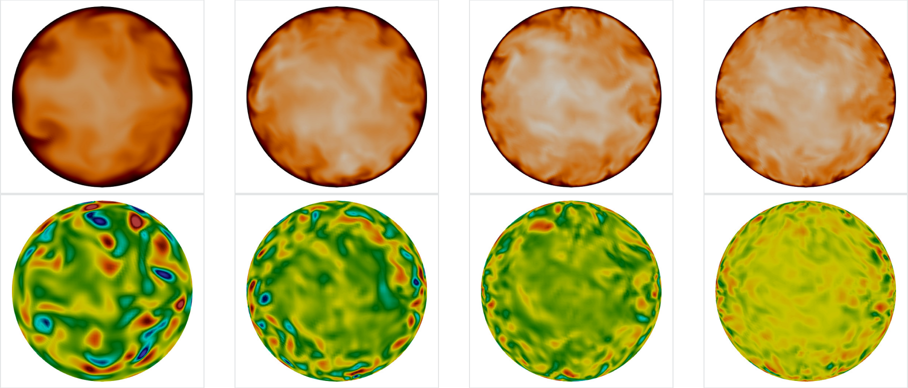

$Re_\tau = 180$	$Re_\tau = 360$	$Re_\tau = 590$	$Re_\tau = 1000$
$Re_b = 5,300$	$Re_b = 11,700$	$Re_b = 19,000$	$Re_b = 37,700$

LES Versus DNS Results of Pipe Flows at $B_h = 0$

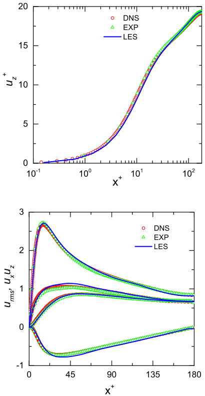

$Re_\tau = 180,$
$Re_b = 5,300$

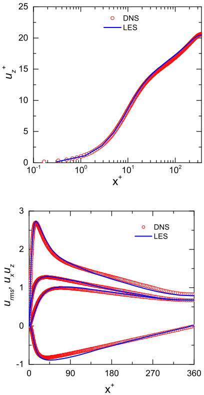

$Re_\tau = 360,$
$Re_b = 11,700$

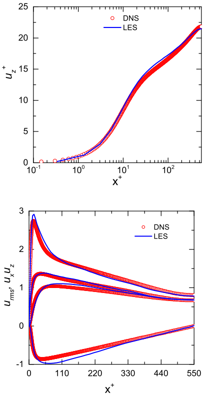

$Re_\tau = 550,$
$Re_b = 19,000$

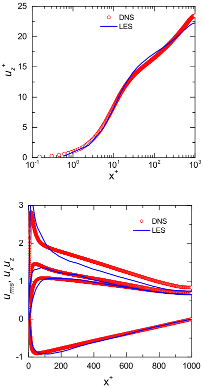

$Re_\tau = 1000,$
$Re_b = 37,700$

Dense Suspension in Channel Flow

Solid-Liquid Flow

Turbulent channel flow

- $Re_\tau = 300 \Rightarrow Re_b \approx 5,100$
- $2h \times 2\pi h \times 4\pi h$; $h = 0.02$ m
- $129 \times 128 \times 128$ grid points
- Periodic boundary conditions in $y-$ and $z-$directions
- No-slip condition on the wall

Calcite Parameters

- $\rho_p = 2170 \ \mathrm{kgm}^{-3}$
- $d_p = 60 \ \mu\mathrm{m}$; $\alpha_p = 10^{-3}$
- $H = 3.8 \times 10^{-10}$ J
- $\delta_0 = 2.0 \times 10^{-10}$ m
- $\bar{\sigma} = 3.0 \times 10^{8}$ Pa
- $N_0 \approx 2,740,000$

Solid-Liquid Flow

Turbulent channel flow

- $Re_\tau = 300 \Rightarrow Re_b \approx 5,100$
- $2h \times 2\pi h \times 4\pi h$; $h = 0.02$ m
- $129 \times 128 \times 128$ grid points
- Periodic boundary conditions in $y-$ and $z-$directions
- No-slip condition on the wall

Calcite Parameters

- $\rho_p = 2170 \ \mathrm{kgm}^{-3}$
- $d_p = 60 \ \mu\mathrm{m}$; $\alpha_p = 10^{-3}$
- $H = 3.8 \times 10^{-10}$ J
- $\delta_0 = 2.0 \times 10^{-10}$ m
- $\bar{\sigma} = 3.0 \times 10^{8}$ Pa
- $N_0 \approx 2,740,000$

Results

Velocity

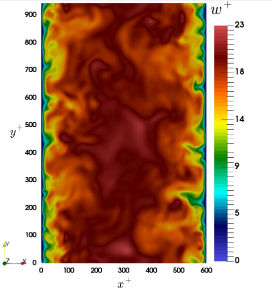

SGS Kinetic Energy

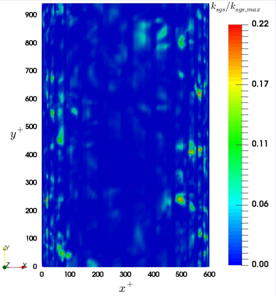

Dissipation Rate

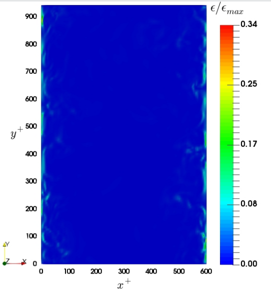

PDF of Wall-normal Position of Breakup Events

$d_p = 60\,\mu m$, $St = 0.1$, DF

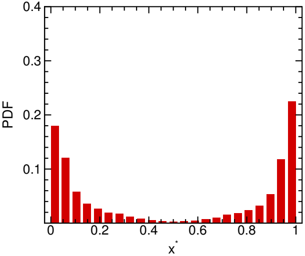

$d_p = 60\,\mu m$, $St = 0.1$, UF

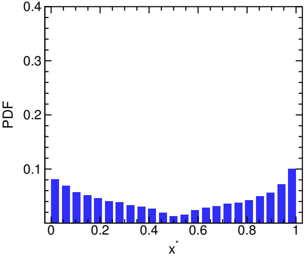

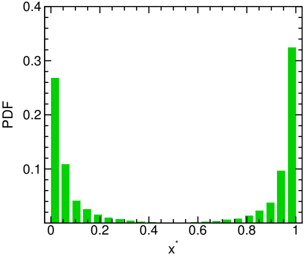

$d_p = 60\,\mu m$, $St = 0.1$, NG

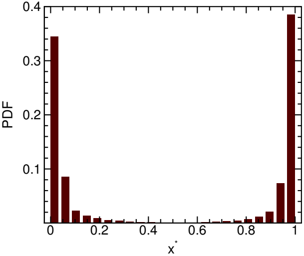

$d_p = 60\,\mu m$, $St = 5$, NG

Population of Primary Particle and Agglomerates

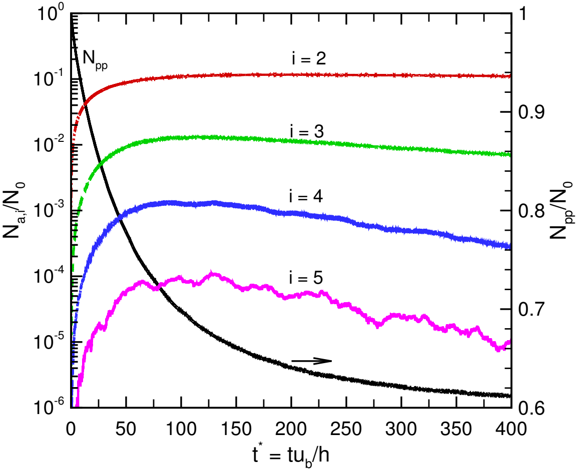

Collision, Agglomeration and Breakup

N_{bk}/N_0 vs t^* Graph

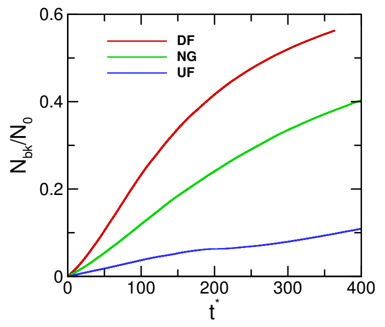

- Particle segregation towards the wall decreases from DF, NG to UF.
- Breakup decreases from DF, NG to UF.

N_{col}/N_0 vs t^* Graph

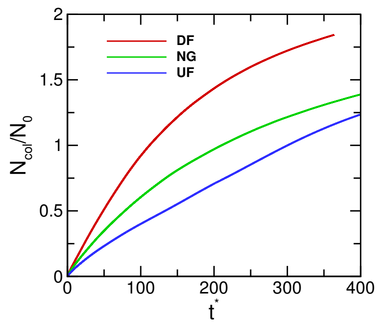

- More collisions occur from DF, NG to UF and with t^+
- Breakup populates agglomerates with smaller N_{pp} with higher collision rate.

Collision, Agglomeration and Breakup

N_{agg}/N_0 vs t^* Graph

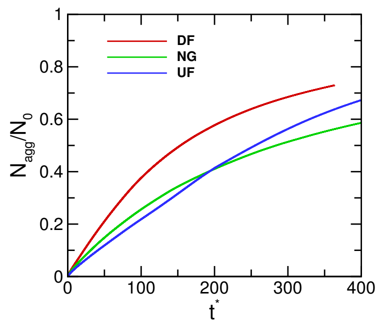

- More collision means more agglomeration.
- Agglomeration decreases in the order DF, NF and UF.

N_a/N_0 vs t^* Graph

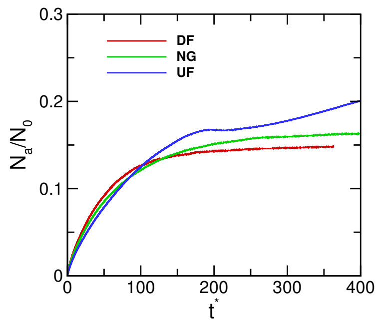

- N_{bk} and N_a are inversely proportional
- Agglomerates population increases in the order, DF, NG and DF

Turbulence modulation

$z-$direction

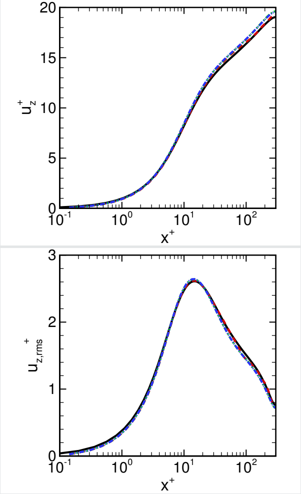

$x-$ & $y-$directions

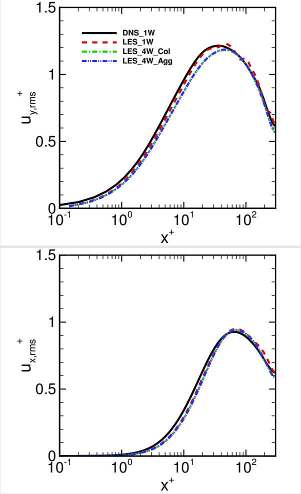

Effect of Gravity on Fluid Velocity Statistics

$z-$direction

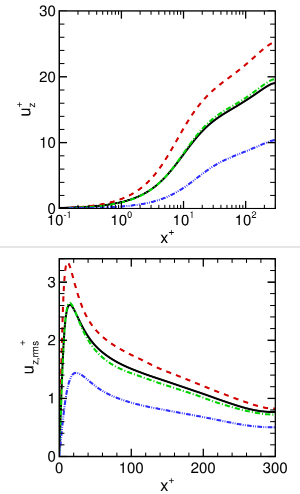

$x-$ & $y-$directions

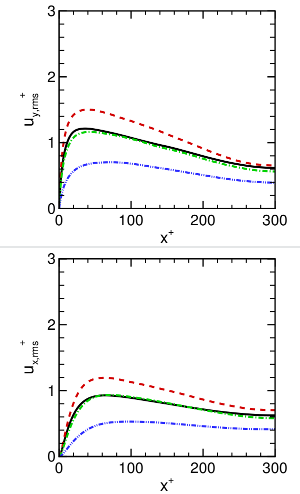

downward flow; no-gravity flow; upward flow; DNS no-gravity flow

Conclusions

Conclusions

- LES of turbulent pipe flow is looking good. The pipe flows with variable bed height will be shown later.
- Successfully implemented particle-particle interactions (collision, agglomeration and breakup events) in BOFFIN LES code.
- Turbulence intensity and direction of gravity influence the particle segregation with respect to the wall
- PSD and gravity have weak and strong influence on the turbulence modulation.
- Particle dynamics in pipe flow with variable bed height is ongoing.

Acknowledgements

Thank you for listening!

Any Question?

MANCHESTER
1824
The University of Manchester

In-situ Characterisation of Sludge in the Legacy Ponds

Olusola Ayoola
PhD Researcher | The University of Manchester

Penrith 2017

Supervisors: Prof. Barry Lennox, Dr. Simon Watson and Dr. Geoff Randall

The University of Manchester

In-Situ (On-Site) Measurements

The University of Manchester

In-situ Characterisation of Sludge in the Legacy Ponds

About Sludge

- A semi solid slurry
- A result of settled suspensions.
- Caused by material corrosion and environmental debris.

Radioactive sludge from the NPP A1 Jaslovske Bohunice Reactor, Slovakia

About Sludge Characterisation

- An analysis of chemical and physical properties
- A quantitative measurement of sludge behaviour
- It provides an understanding of the cost and hazards (if any).

The Big Questions

- How often should sludge be characterised ?

- What are the challenges involved ?

The University of Manchester

A Sludge Simulant Tank at NNL

Year 2011

A Sludge Simulant Tank at NNL

Year 2011

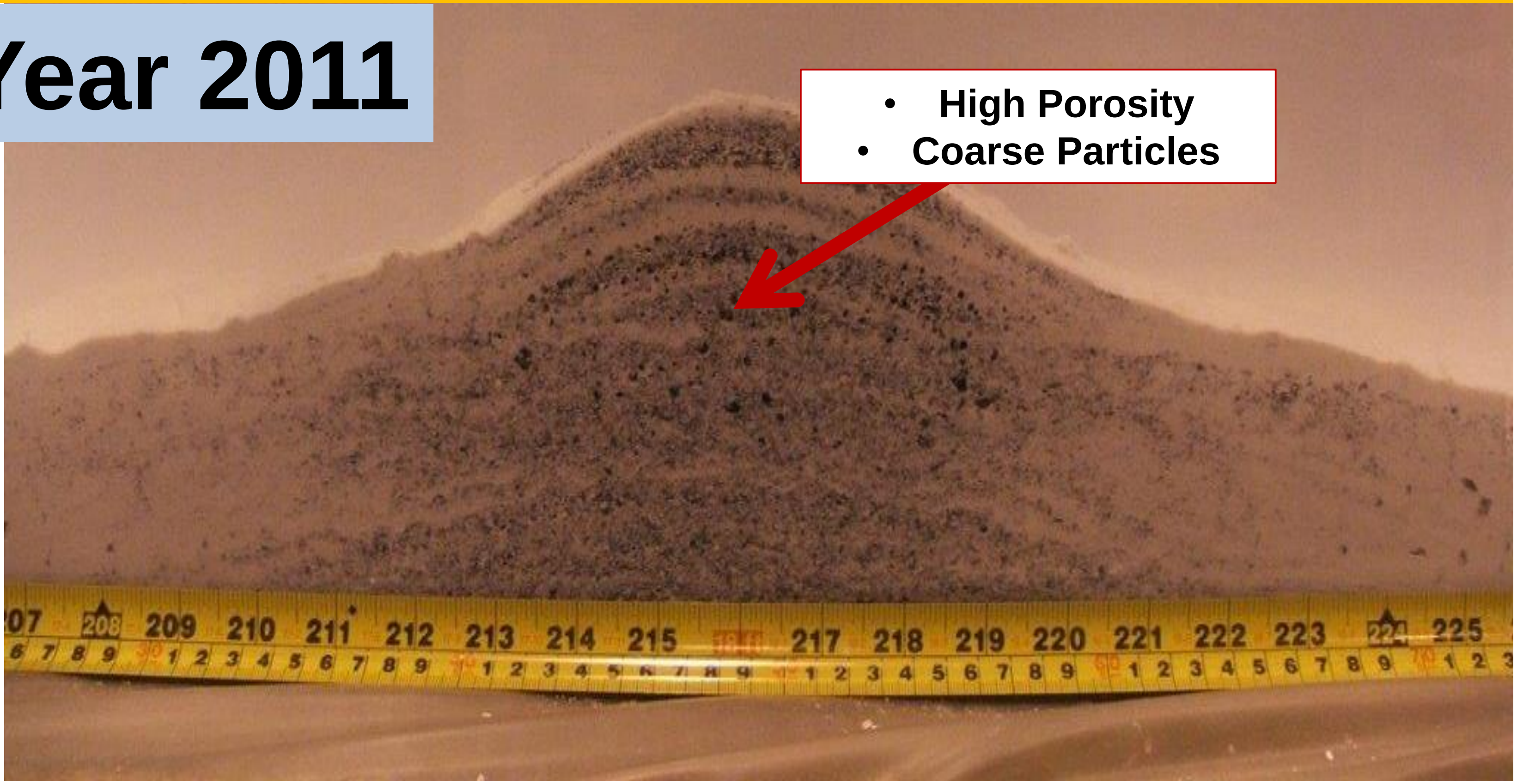

- High Porosity
- Coarse Particles

MANCHESTER
1824
The University of Manchester

A Sludge Simulant Tank at NNL

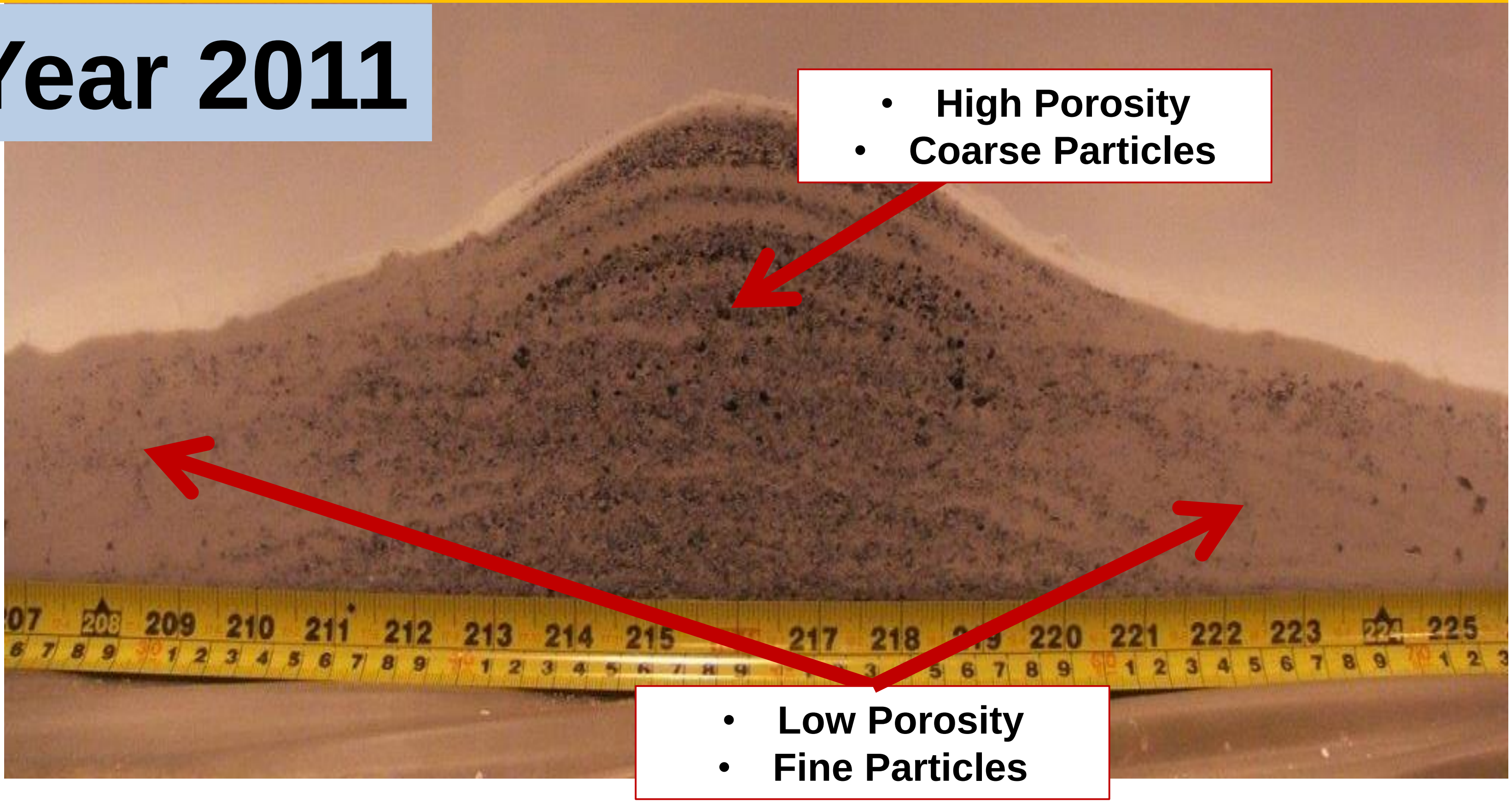

Year 2011

- High Porosity
- Coarse Particles

- Low Porosity
- Fine Particles

MANCHESTER
1824
The University of Manchester

A Sludge Simulant Tank at NNL

Year 2011

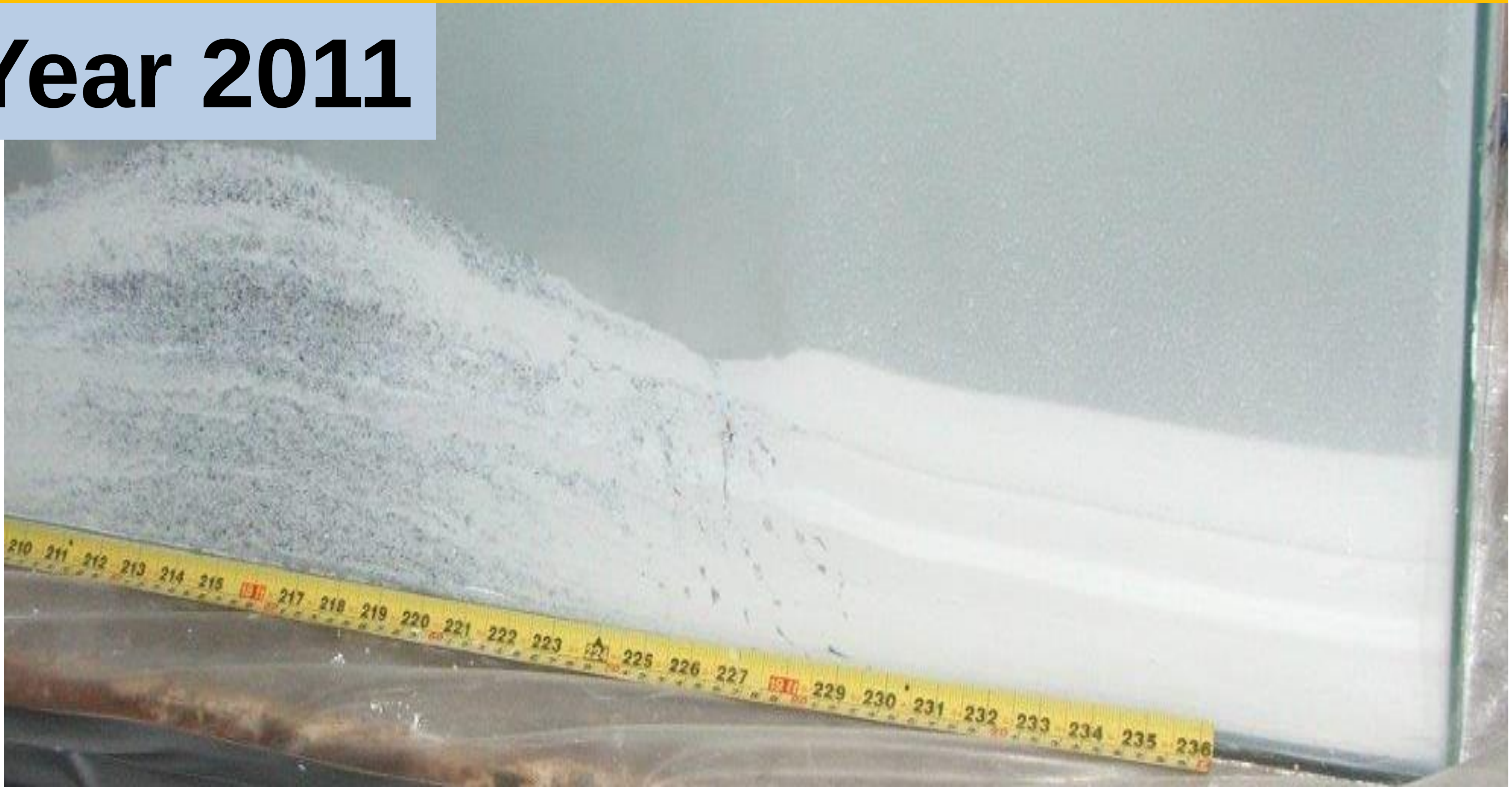

The University of Manchester

A Sludge Simulant Tank at NNL

Year 2017

A Sludge Simulant Tank at NNL

Year 2017

A Sludge Simulant Tank at NNL

Year 2017

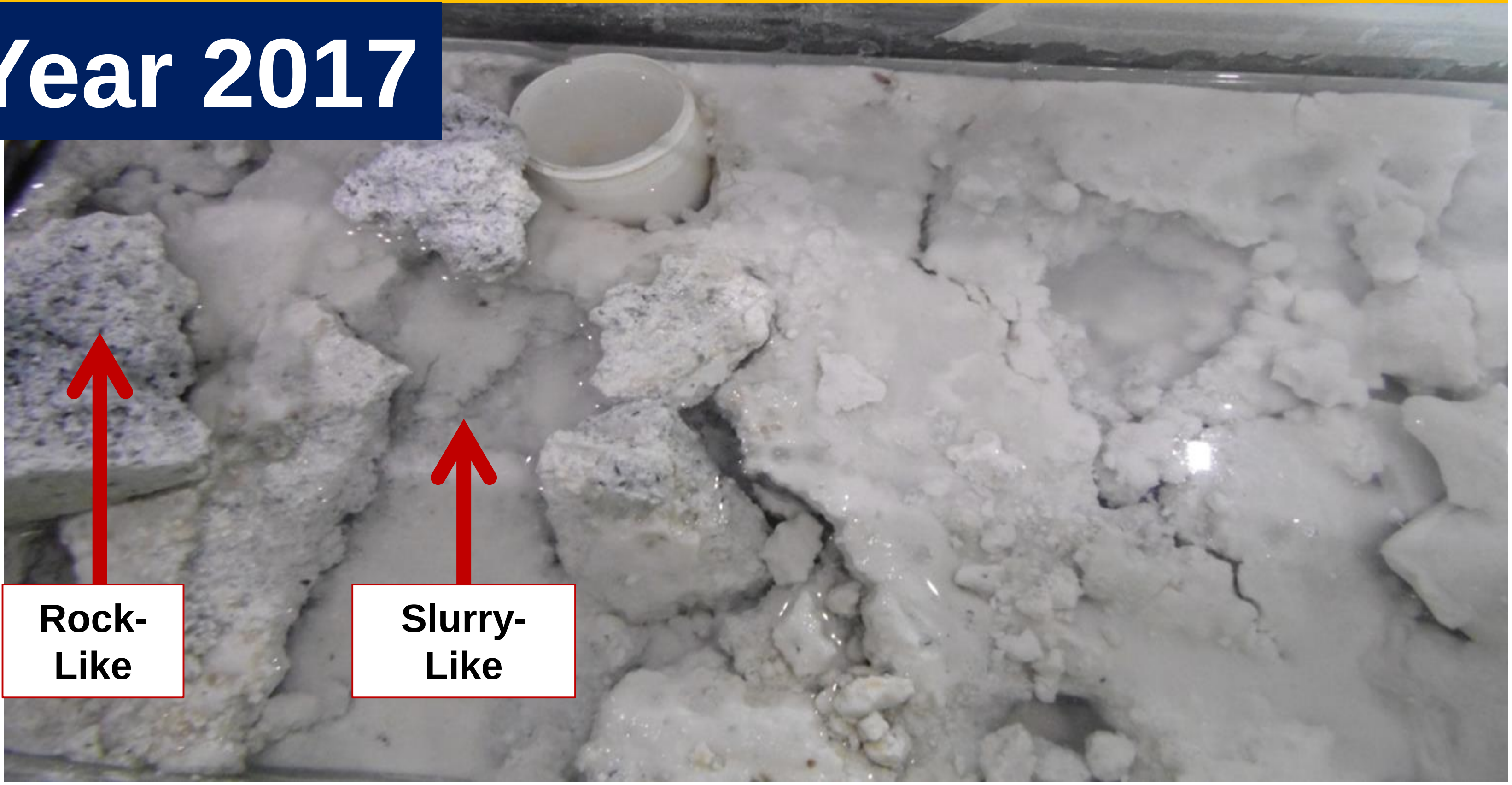

A Sludge Simulant Tank at NNL

Year 2017

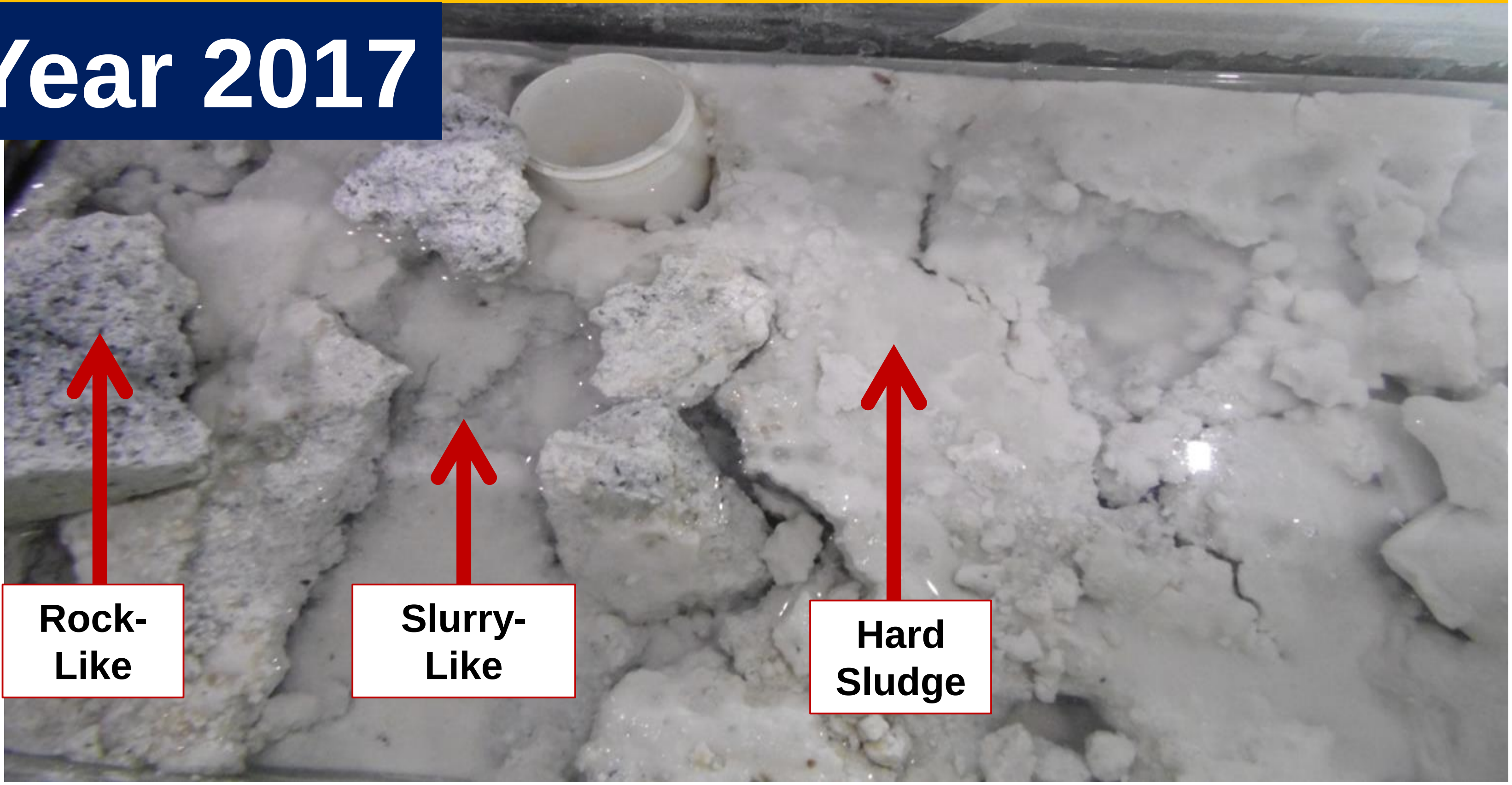

A Sludge Simulant Tank at NNL

Year 2017

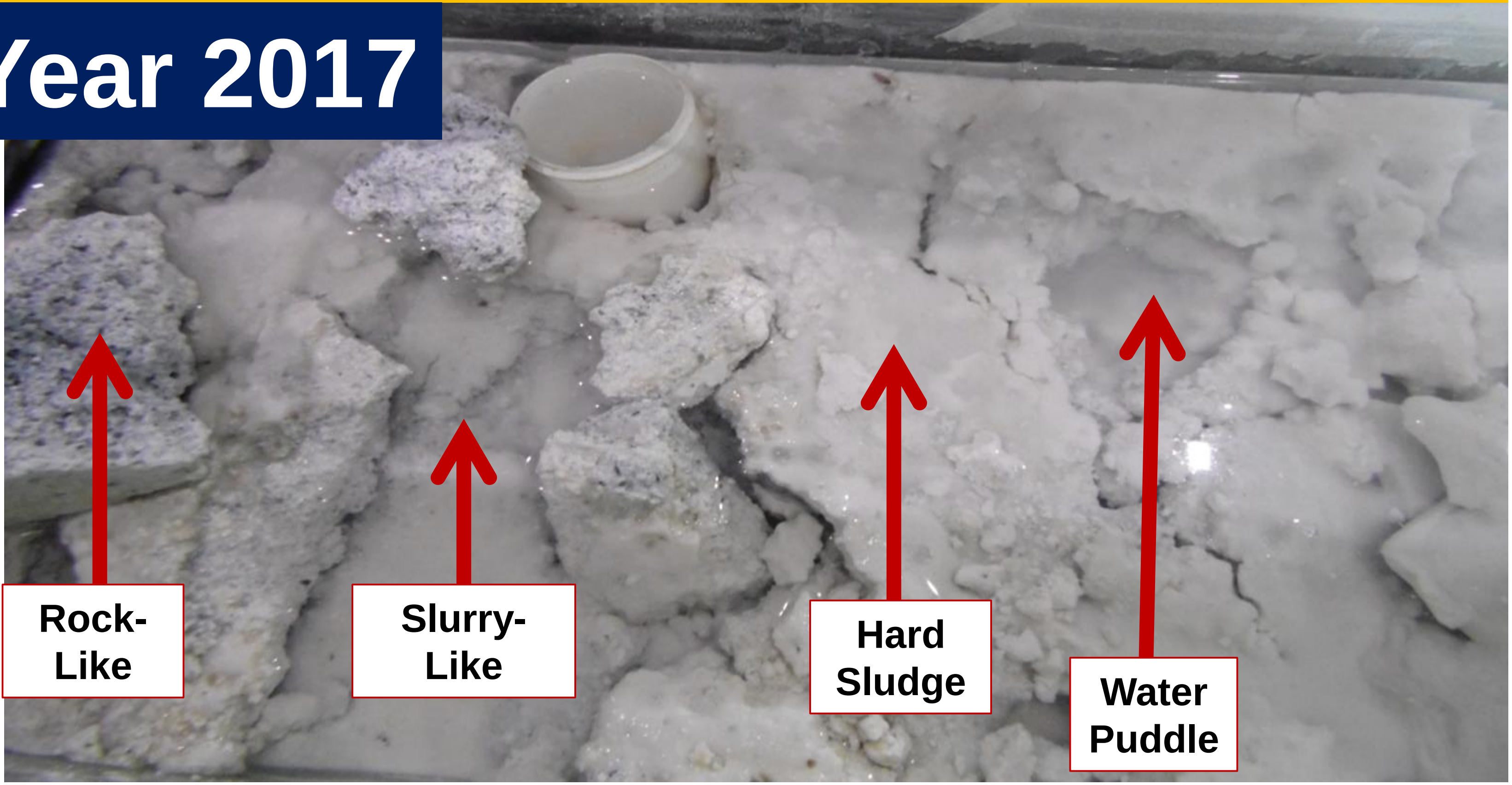

A Sludge Simulant Tank at NNL

Year 2011

Year 2017

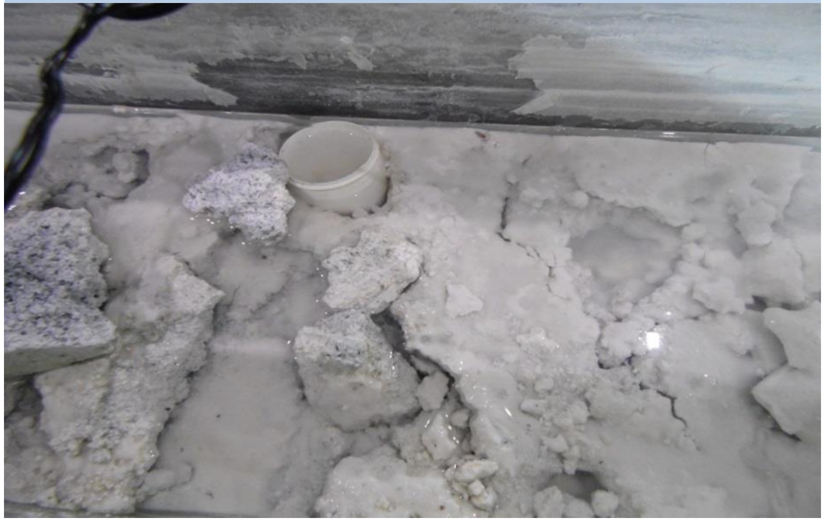

Methods of Sludge Characterisation

- Ex-Situ (Off – Site) method
- In-Situ (On – Site) method

Ex-Situ Sludge Characterisation?

Collect Samples

Ex-Situ Sludge Characterisation?

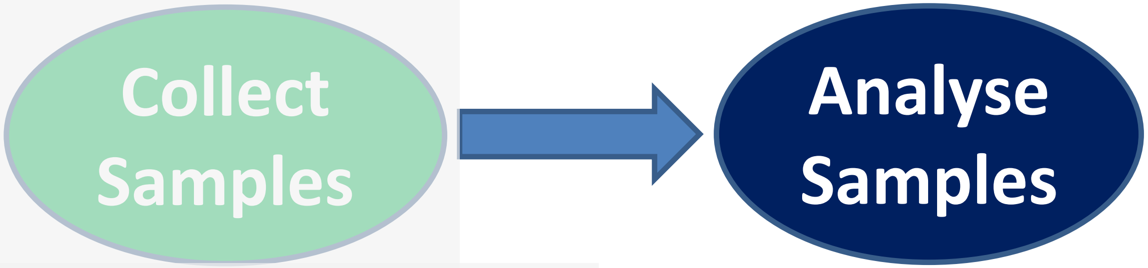

Collect Samples

Analyse Samples

Ex-Situ Sludge Characterisation?

Collect Samples → Analyse Samples → Process Data

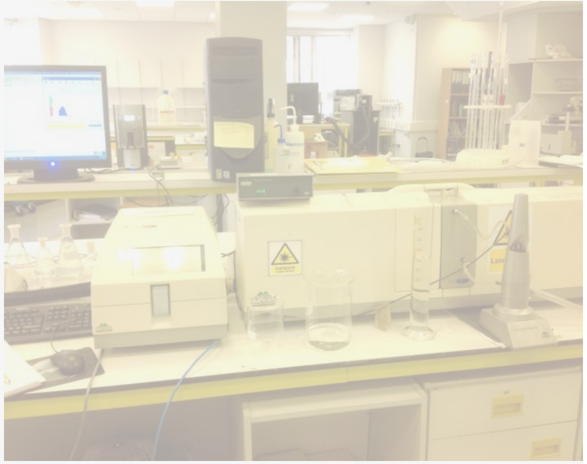

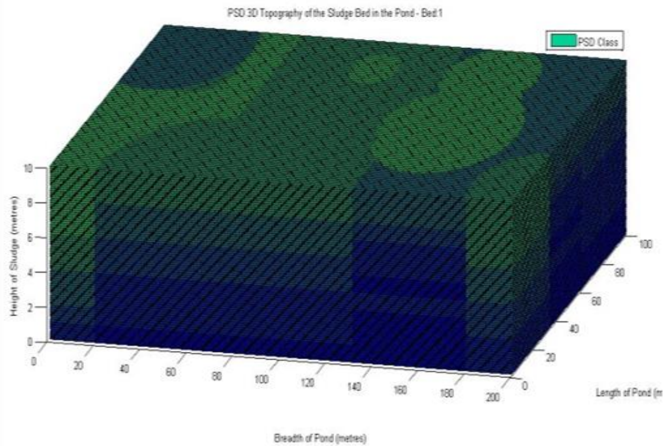

Ex-Situ Sludge Characterisation?

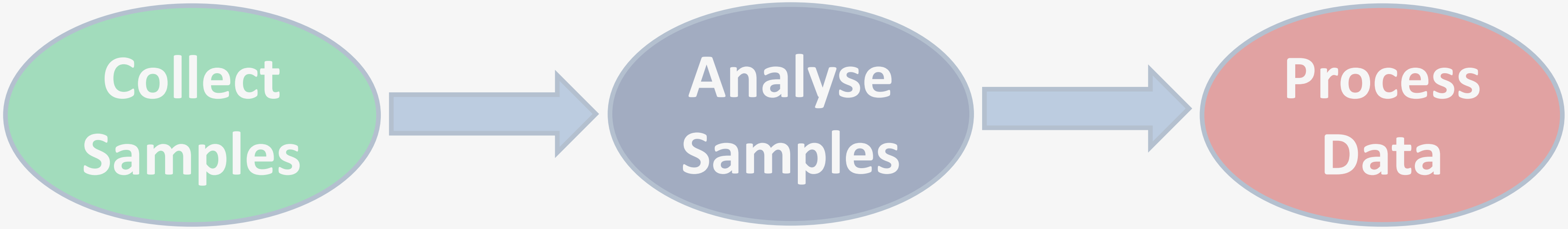

Challenges

- **Limited accessibility around the pond**
- **Exposure limitations**
- **Storage limitations**

The Interest

- Provide real-time mapping
- Further improve safety
- Increase confidence in results

The University of Manchester

The Interest

Hence the need to migrate from

Ex-Situ to In-Situ

sludge characterisation

In-Situ Sludge Characterisation?

Deploy a Remote Operated Vehicle

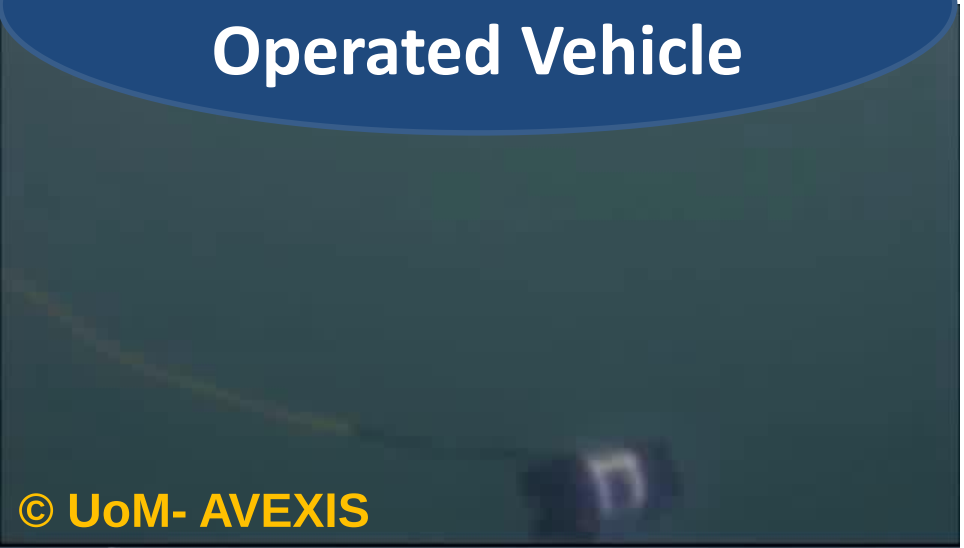

© UoM- AVEXIS

© JF Nuclear

In-Situ Sludge Characterisation?

Deploy a Remote Operated Vehicle

Mount a Mobile Sampler-Analyser

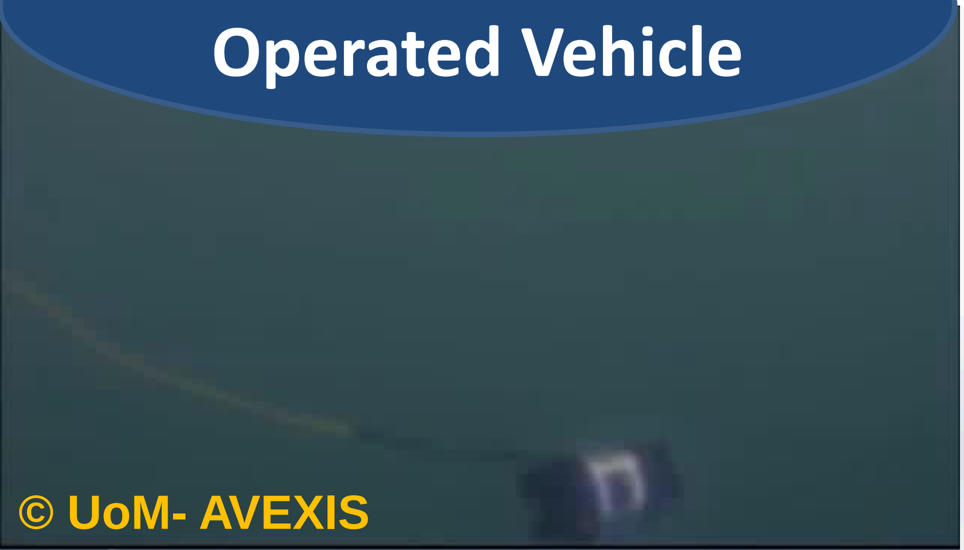

© UoM- AVEXIS

© JF Nuclear

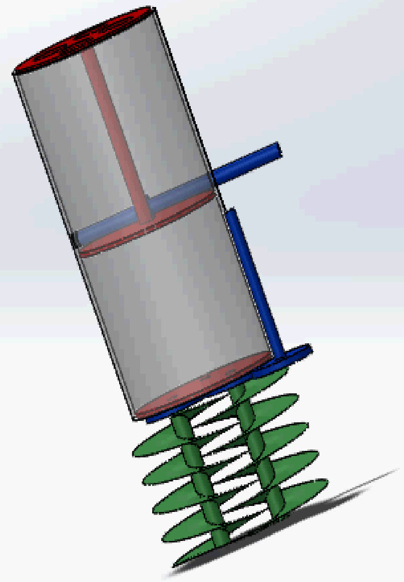

In-Situ Sludge Characterisation?

Challenges

- Capacity of the Remote Operated Vehicle (ROV)
- The efficiency of the sampling mechanism
- The feasibility of a mobile analyser (for particle size analysis)

In-Situ Sludge Characterisation?

Challenges

- Capacity of the Remote Operated Vehicle (ROV)
- The efficiency of the sampling mechanism
- The feasibility of a mobile analyser (for particle size analysis)

MANCHESTER 1824
The University of Manchester

The Sampling Mechanism Idea

- Collect 100ml of sludge and 900ml of clean water (10 % v/V)
- Have an in-house PSD analyser
- Be self cleansing

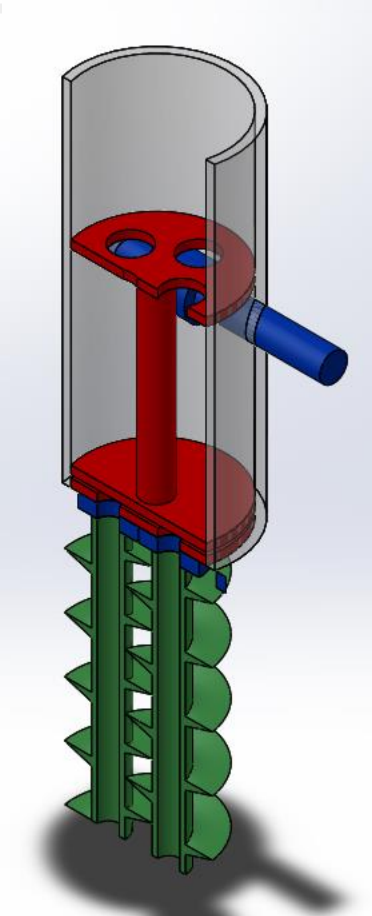

In-Situ Sludge Characterisation?

Challenges

- Capacity of the Remote Operated Vehicle (ROV)
- The efficiency of the sampling mechanism
- The feasibility of a mobile analyser (for particle size analysis)

Mobile PSD Analyser for Underwater Applications

Laser Diffraction Method

www.malvern.com
www,particle.dk/

Mobile PSD Analyser for Underwater Applications

Laser Diffraction Method

Dynamic Light Scattering

www.wyatt.com/

Mobile PSD Analyser for Underwater Applications

Laser Diffraction Method

Dynamic Light Scattering

Focused Beam Reflectance Method

www.mt.com

Mobile PSD Analyser for Underwater Applications

Laser Diffraction Method

Dynamic Light Scattering

Focused Beam Reflectance Method

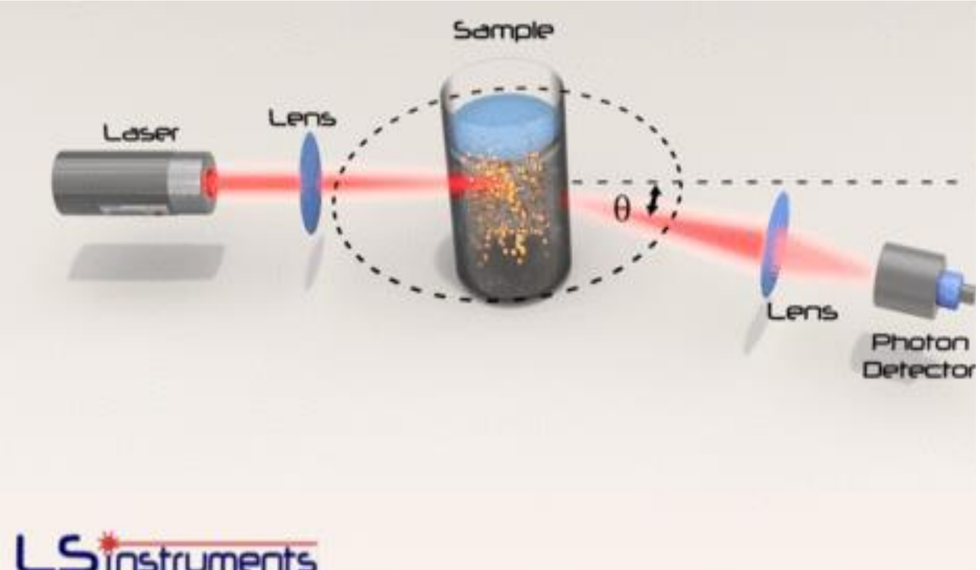

Mobile PSD Analyser for Underwater Applications

Laser Diffraction Method

Dynamic Light Scattering

Focused Beam Reflectance Method

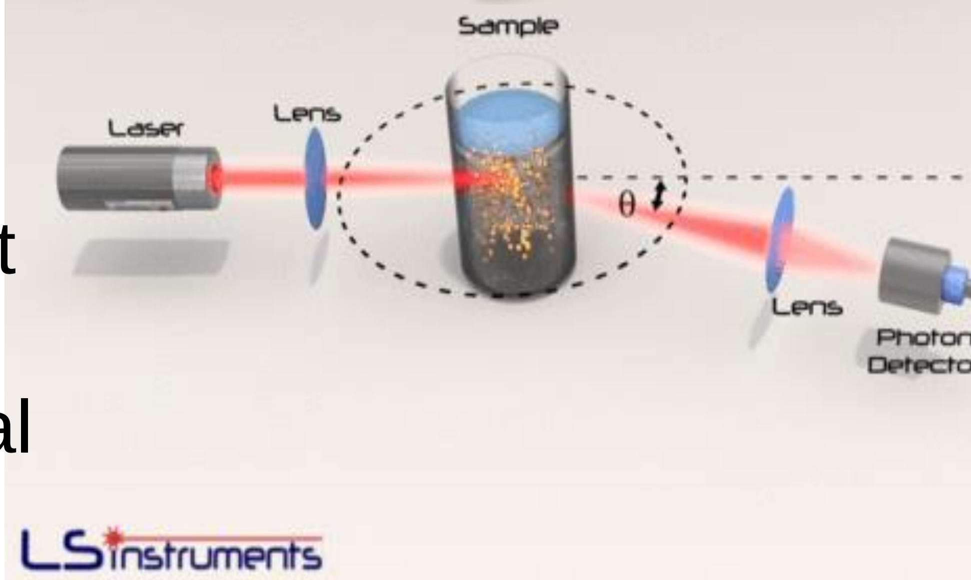

Features

- Delicate optical alignment
- Susceptible to mechanical disturbances

The University of Manchester

Mobile PSD Analyser for Underwater Applications

ULTRASONIC SPECTROSCOPY

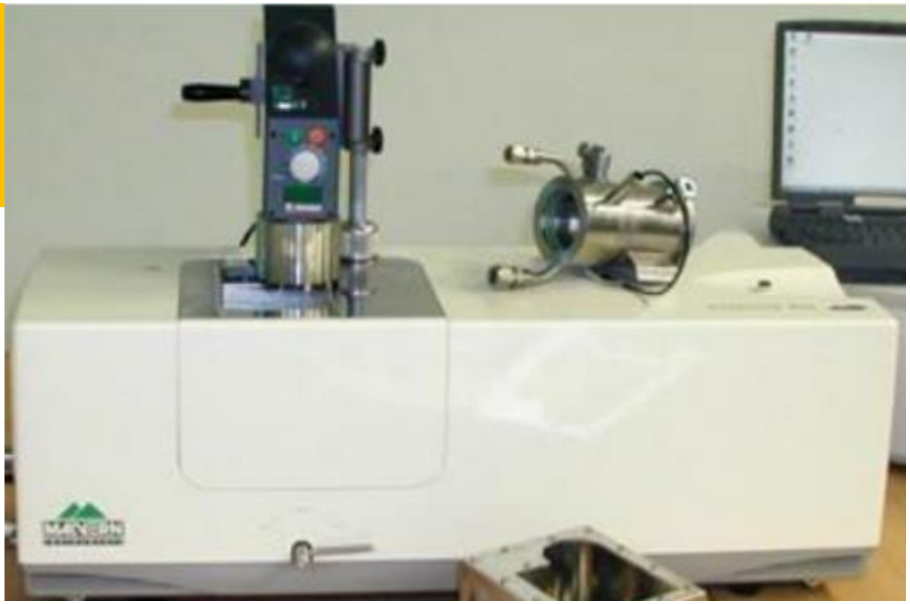

www.researchgate.net/figure/45901368_fig1_Figure-1-The-Malvern-Ultrasizer-11-with-its-associated-temperature-control-unit

Ultrasonic Spectroscopy

- Uses sound waves in the range 1 – 100 MHz
- The transmission of sound waves through the particulate samples
- The measurement of the ultrasonic attenuation spectrum (UAS).
- The conversion of the UAS to particle size distribution (PSD)

Ultrasonic Spectroscopy: How It Works

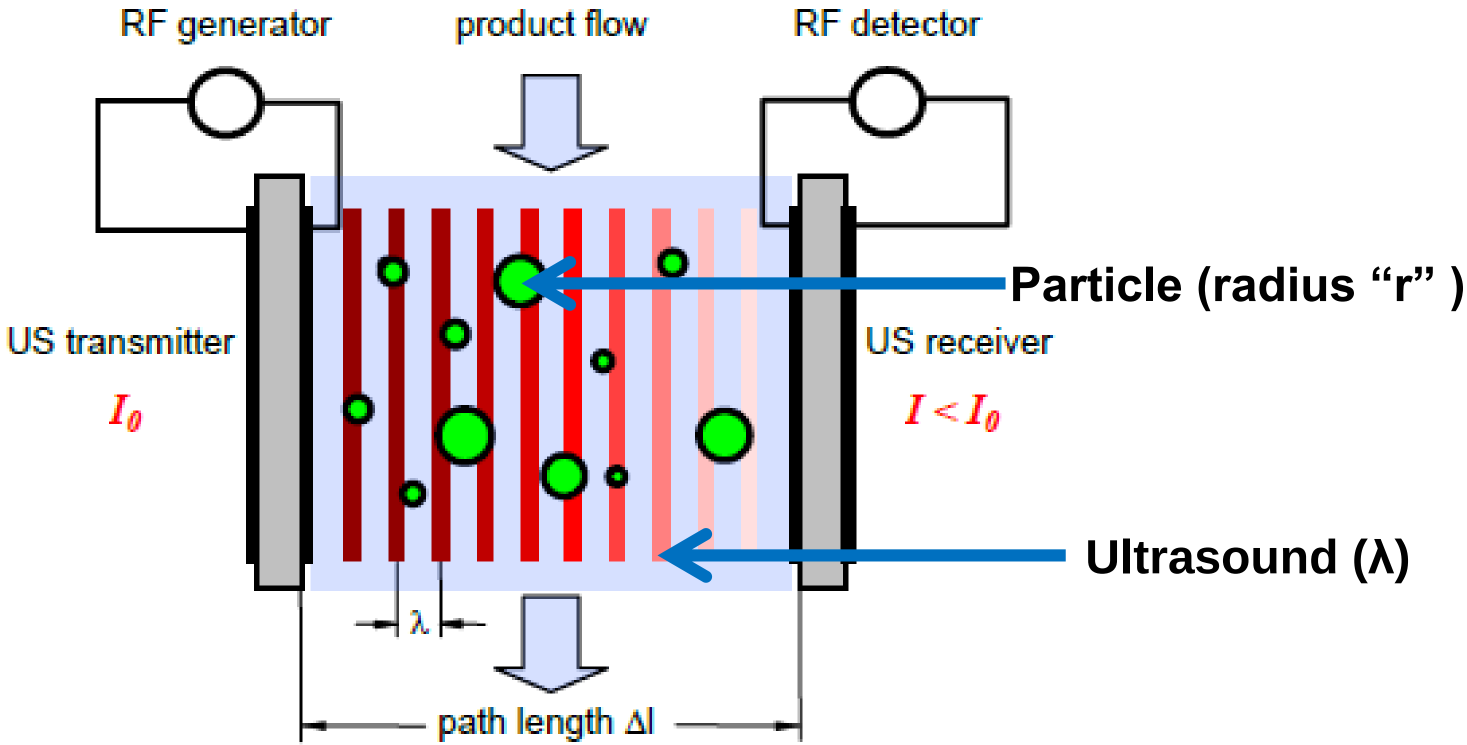

Ultrasonic Measurement Principle (Sympatec OPUS)

Ultrasonic Spectroscopy: The Theory

Causes of acoustic attenuation (Energy losses):

- Wave-Scattering Losses (Wave theory)*
- Absorption Losses (Mechanics theory)*
- Thermal Losses (Heat theory)**
- Visco-inertial Losses (Viscosity theory)**

*($\lambda << r$) **($\lambda >> r$)

Mathematical Interpretation Challenge

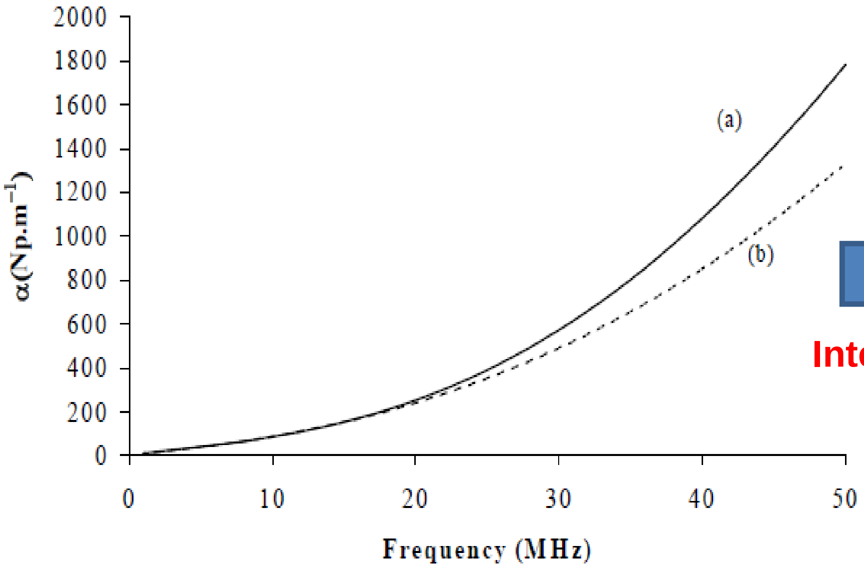

Data

Interpretation

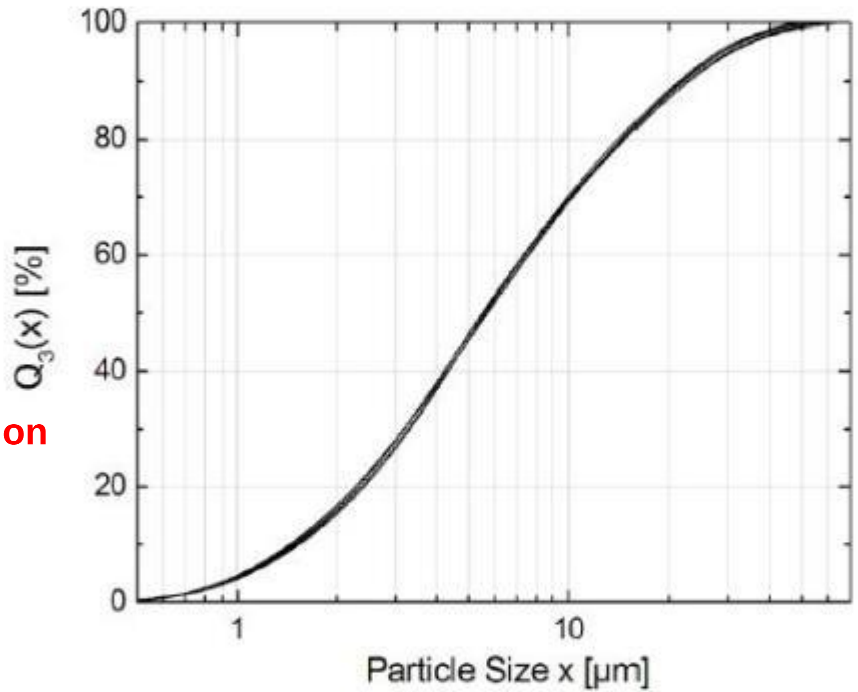

Ultrasonic Attenuation Spectrum (UAS)

Particle Size Distribution (PSD)

Mathematical Interpretation Challenge

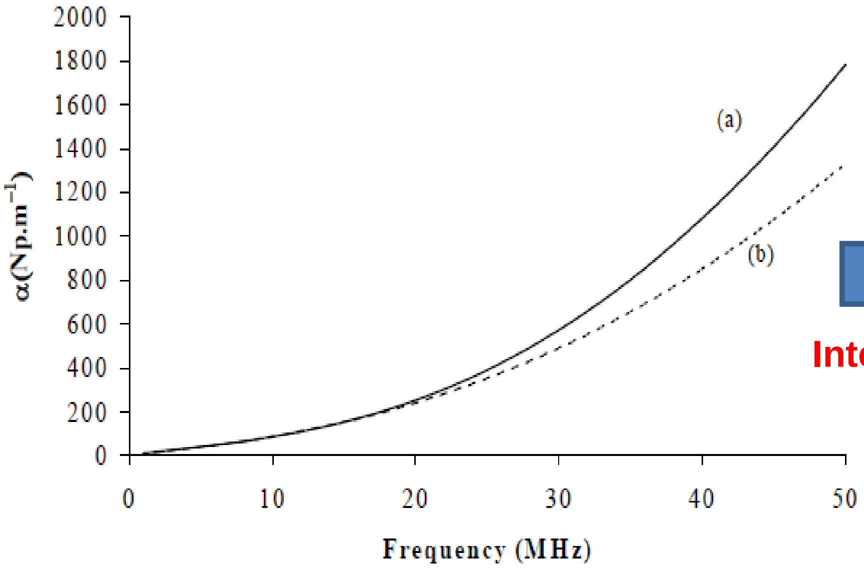

Data

Interpretation

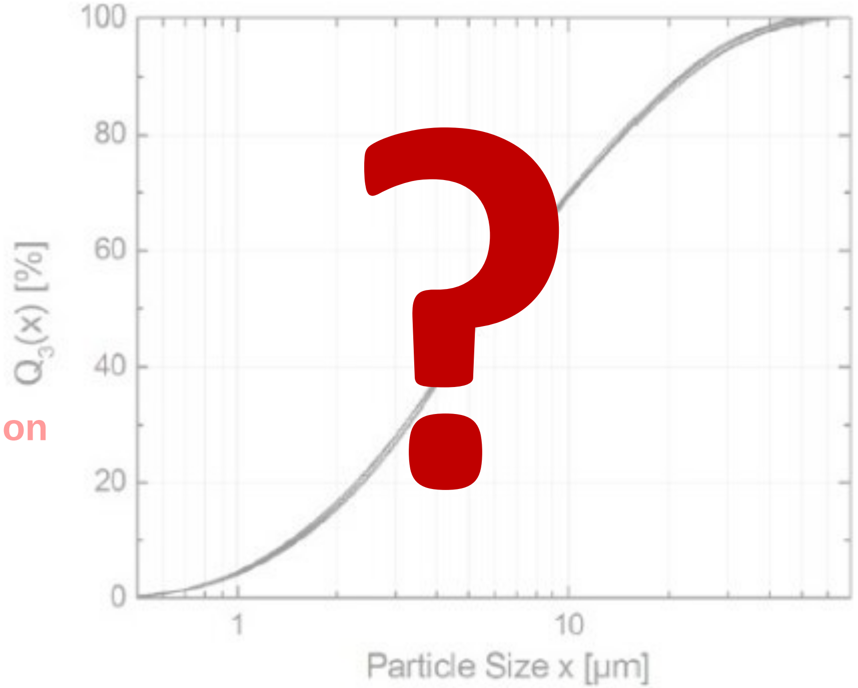

Ultrasonic Attenuation Spectrum (UAS)

Particle Size Distribution (PSD)

MANCHESTER
1824
The University of Manchester

Mathematical Interpretation Challenge

- $A_i\,(w, x_i) = A(w, 0)\; e^{-\alpha(w)x_i}\; e^{\frac{jwx}{c(w)}}$ (1)
- $\frac{w}{c(w)} + j\alpha(w) = k_c\left(1 + \frac{3\varphi}{jk_c^3\,R^3}\right)(A_o + 3A_1 + 5A_2)^{0.5}$ (2)
- $A_n(r, f) = \; -j\sin\big(\eta_n(r, f)\big)\,.\,e^{-\eta_n(r,f)}$ (3)
- $K_{i,j} \;=\; -\frac{4\pi}{K_c^2}\sum_0^n(2n+1)\left|A_n\left(r_i, f_j\right)\right|^2$ (4)
- $\alpha(f) = \; C_{p.a}\Delta L\; K(x, f)dQ_3(r)$ (5)

Mathematical Interpretation Challenge

- $\alpha(f) = C_{p.a} \Delta L \, K(x, f) dQ_3(r)$

UAS

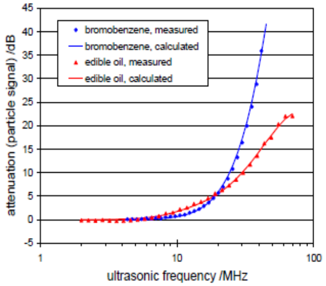

Frequency dependent Properties of the (unknown) sludge

PSD

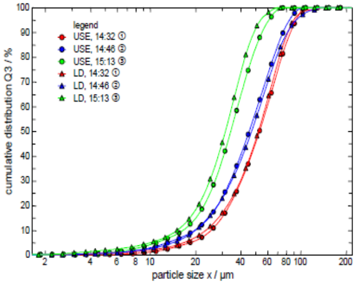

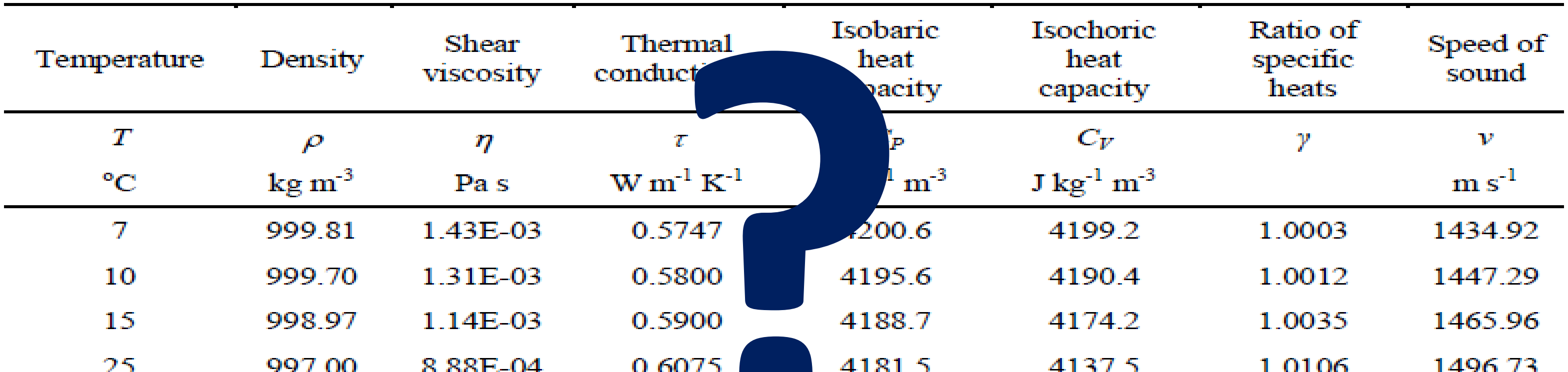

Temperature	Density	Shear viscosity	Thermal conduct	Isobaric heat pacity	Isochoric heat capacity	Ratio of specific heats	Speed of sound
T °C	ρ kg m^{-3}	η Pa s	τ W m^{-1} K^{-1}	$_P$ ^{1} m^{-3}	C_V J kg^{-1} m^{-3}	γ	v m s^{-1}
7	999.81	1.43E-03	0.5747	200.6	4199.2	1.0003	1434.92
10	999.70	1.31E-03	0.5800	4195.6	4190.4	1.0012	1447.29
15	998.97	1.14E-03	0.5900	4188.7	4174.2	1.0035	1465.96
25	997.00	8.88E-04	0.6075	4181.5	4137.5	1.0106	1496.73

Mathematical Interpretation Challenge

- Requires a database of parameters for all the materials present in the sample.

- Not feasible for a largely unknown sample

The University of Manchester

Proposed Solution

- $\alpha(f) = C_{p.a} \Delta L\, K(x, f) dQ_2(r)$

- $$\begin{matrix} α\_1 \\ α\_2 \\ α\_n \end{matrix} = \begin{bmatrix} k\_(11) & \cdots & k\_(1n) \\ \vdots & \ddots & \vdots \\ k\_(n1) & \cdots & k\_(nn) \end{bmatrix} \begin{matrix} q\_1 \\ q\_2 \\ q\_n \end{matrix}$$

- $A_n = K_n \; Q_n$
- Let AA_{nm} = $[A_{n1} \;\; A_{n2} \;\; \ldots \; A_{nm}\;]$
- and QQ_{nm} = $[Q_{n1} \;\; Q_{n2} \;\; \ldots \; Q_{nm}\;]$

- $AA_{nm} = \; KK_{nm}\, QQ_{nm}$

- $$\begin{bmatrix} α\_(11) & \cdots & α\_(1m) \\ \vdots & \ddots & \vdots \\ α\_(n1) & \cdots & α\_(nm) \end{bmatrix} = \begin{bmatrix} k\_(11) & \cdots & k\_(1n) \\ \vdots & \ddots & \vdots \\ k\_(n1) & \cdots & k\_(nn) \end{bmatrix} \begin{bmatrix} q\_(11) & \cdots & q\_(1m) \\ \vdots & \ddots & \vdots \\ q\_(n1) & \cdots & q\_(nm) \end{bmatrix}$$

MANCHESTER
1824
The University of Manchester

Proposed Solution

- Obtain the $\boldsymbol{KK_{nm}}$ Matrix by:

  a) analysing the UAS (AA_{nm}) and PSD (QQ_{nm}) properties of some ex-situ samples over time .

  b) Or by creating a database of thermo-mechanical properties through lab-based experiments.

- Calculate the percentage confidence in the $\boldsymbol{KK_{nm}}$ Matrix as no single K-Matrix will fit all.

Conclusion

- In-situ characterisation offers the advantage of continuous data gathering and high amount of sampled data.

- In the absence of a reliable data interpretation algorithm, the ultrasonic attenuation data does provides sufficient information about changes within the sludge bed.

Thank You For Listening

Lancaster University

ab initio Molecular Dynamics Studies of Hydrated Hydroxide Complexes

- 16th October 2017
- Olivia Lynes
- Supervisor: Andy Kerridge
- Industrial supervisor: Jonathan Austin

NATIONAL NUCLEAR LABORATORY

NDA
Nuclear
Decommissioning
Authority

DISTINCTIVE

Talk Overview

- Initial aims of the project
- Aquo complexes
- Hydroxide complexes
  - Monohydroxides
  - Dihydroxides
- Mineral surface – CeO_2
- Final stages of the project
- Conclusion

Project Aims

Computational simulations of storage pond sludge disturbances

- Understanding the interactions of:
  - Strontium, caesium, uranium with particulates.
  - *ab initio* molecular dynamics:
    - Large amount of data
    - Novel research method for this area.

- Studying:
  - Hydration Structure
  - Absorption effects/ surface interaction.
  - pH Effects

Methodology

- CP2K (version 3)
  - Periodic planewave code

- *ab initio* molecular dynamic (AIMD) calculations.
  - Total simulation time of 20 picoseconds.
  - 5 picosecond equilibration period
  - 0.5 fs timestep- 1/10th smallest vibration

- Gaussian Augmented Planewave method (GAPW)
  - Goedecker-Teter-Hutter (GTH) pseudopotentials
  - PBE/DZVP with Grimme d2/d3 dispersion

- Nosè-Hoover thermostat- 400 K

Aquo Complexes

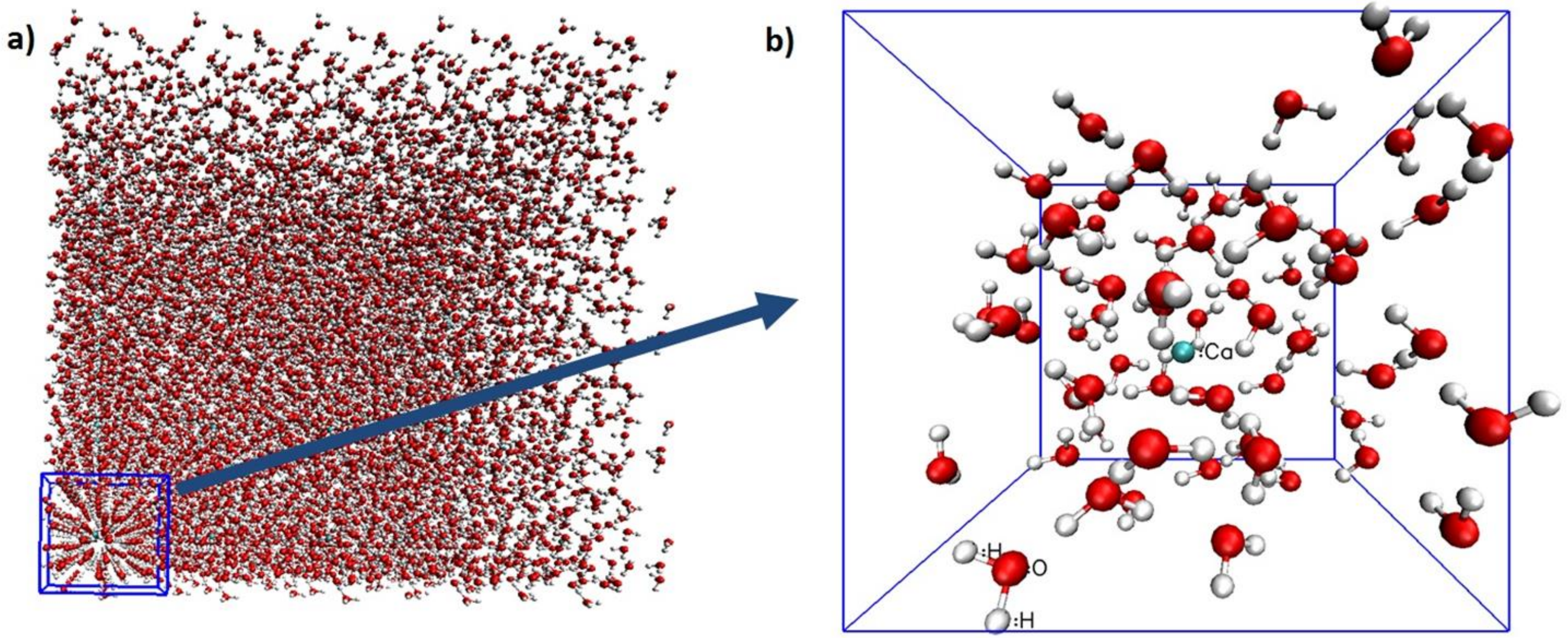

Figure 1: a) Periodic representation of the system. B) Single unit of 64 H_2O molecules with central metal ion (Ca^{2+})

- Studied to establish the model. Well studied in the literature.
- Builds on previous gas phase calculations in the group.
- Ponds are wet!

Aquo Complexes

Coordination Number (CN)

- Number of oxygens coordinated to the metal ion.
- Any CN which lasted less than 0.1 ps discounted as “not a true transition”

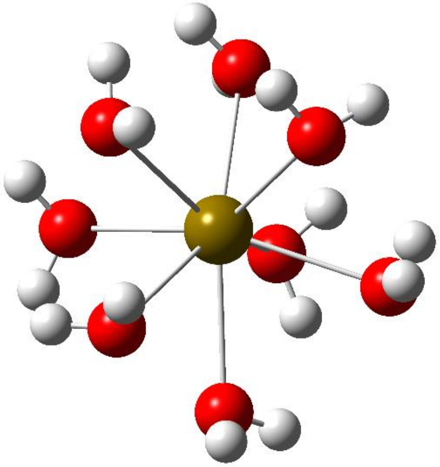

Figure 2: Octahydrated Sr^{2+}

Bond Length

- Average bond length for the first solvation shell.

	CN Residence time %								
	6	**7**	**8**	**9**	**10**	Av. CN	Lit Value	Av. Bond Length/ Å	Lit Value/Å
Mg	100	-	-	-	-	6.00	6	2.13	2.07-2.12
Ca	3.38	45.69	48.29	2.63	-	7.50	6-8	2.44	2.35-2.68
Sr	0.23	14.09	69.57	15.28	0.83	8.02	7-9	2.69	2.52-2.69

Hydroxide Complexes

- Next stage in the research – unexplored in literature
  - AIMD is particularly novel in this area
  - Interested in the dynamics of proton transfer
- Look at the effects of higher pH on solvation structure
- Ponds are generally kept at 11-12 pH
- Looked at mono, di and tri hydroxide complexes

Sr Monohydroxide: OH^- Distance from ion

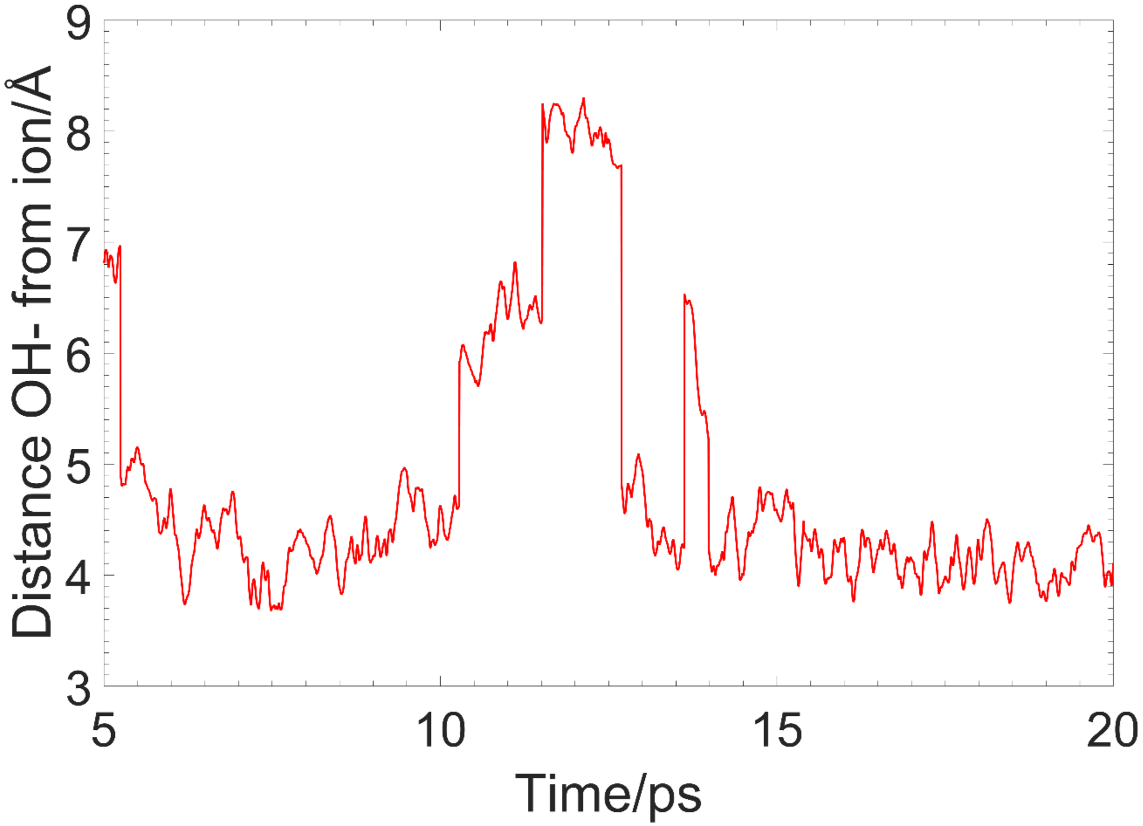

- Single hydroxide with varying initial conditions
- 100 ps of data collected in total
- Proton transfer or hydroxide migration?

Sr Monohydroxide: Oxygen Number

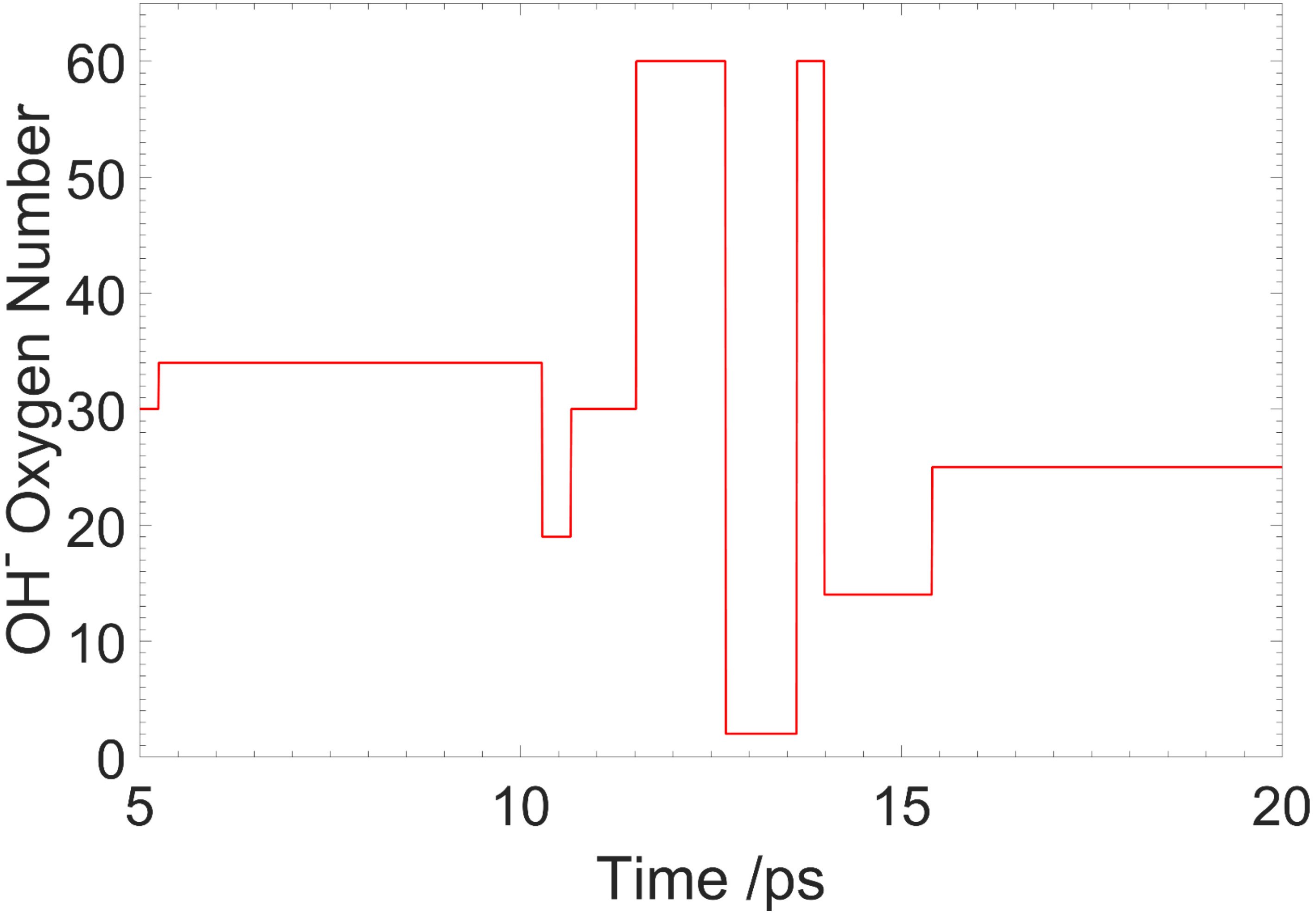

Sr Monohydroxide:
Proton Transfer Events (PTE)

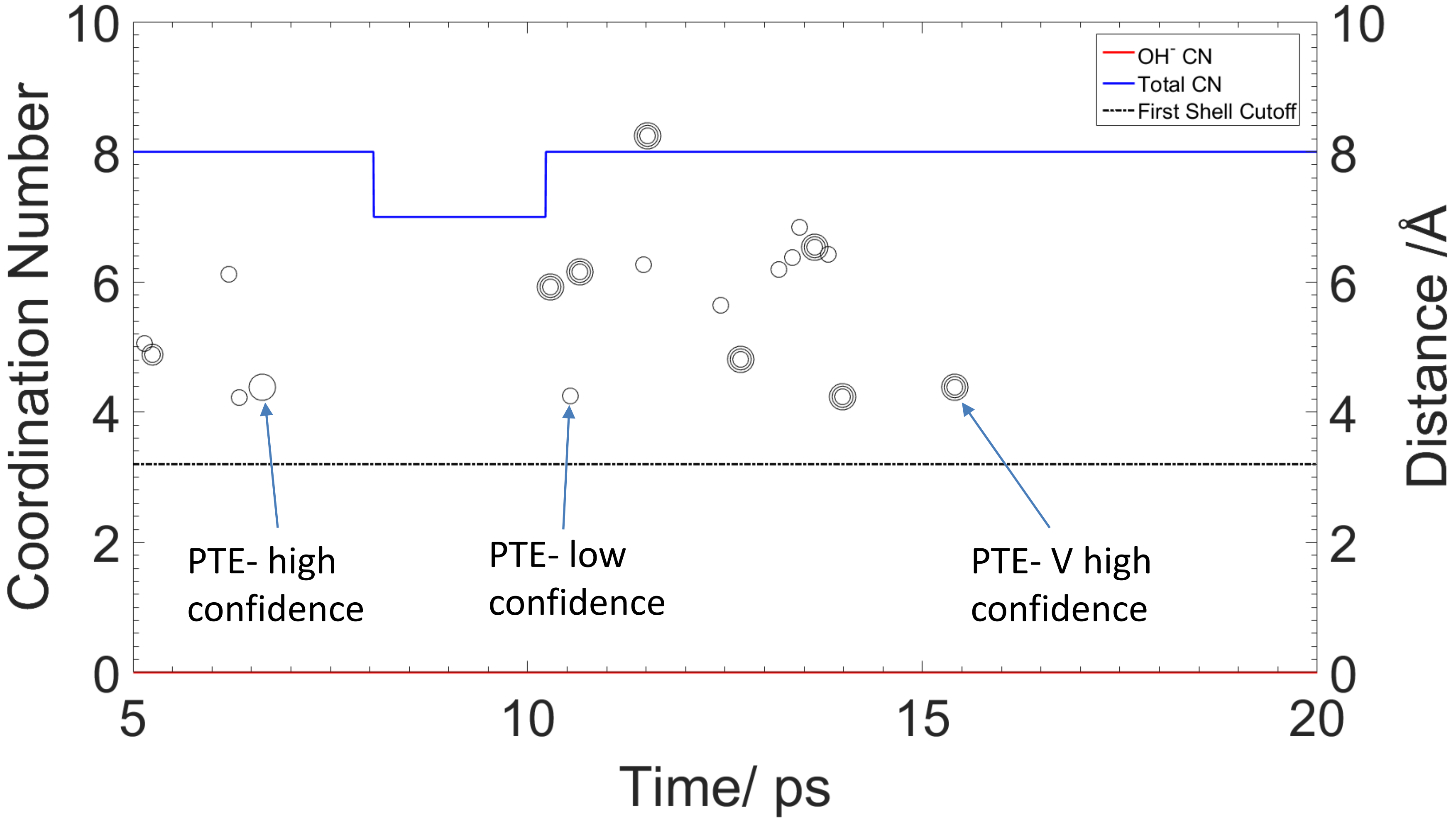

PTE- high confidence

PTE- low confidence

PTE- V high confidence

Alkali Earth Dihydroxides

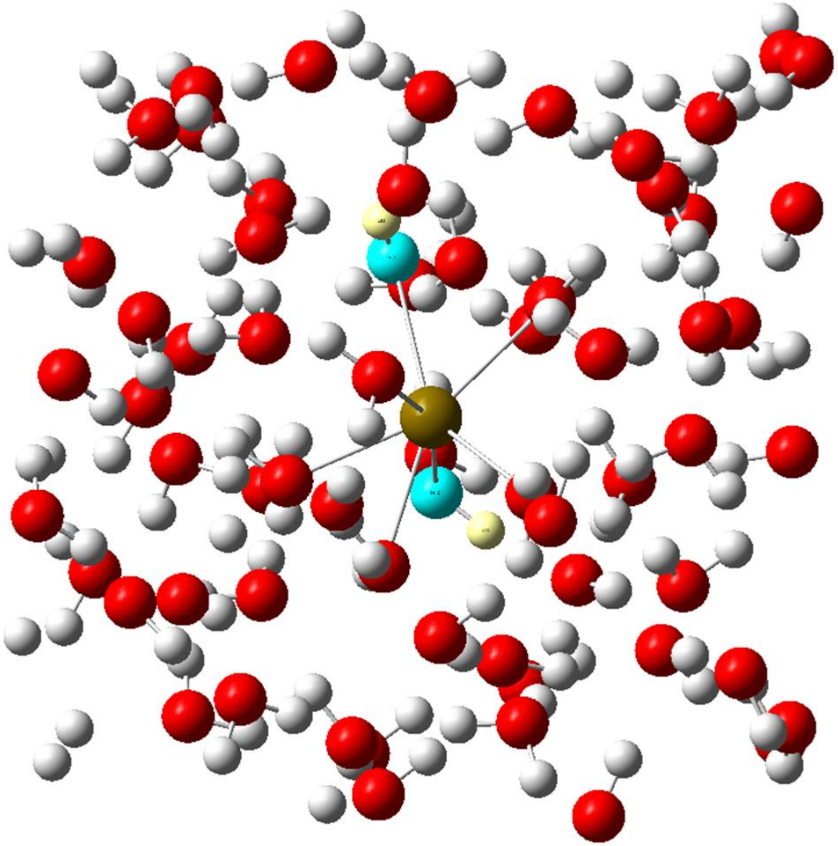

Figure 3: Visual representation of a strontium di-hydroxide. 2 OH- ions (O blue, H yellow) with a Sr^{2+} ion (brown) in the centre.

- Mg^{2+}
- Ca^{2+}
- Sr^{2+}
- Placement of the OH^- was varied in each of the trajectory runs.
- 300 ps trajectory was collected per ion.

Changes in CN and Bond Length

Average Bond Length/ Å

	Water	1OH$^-$	2OH$^-$
Mg	2.13	-	2.15
Ca	2.44	-	2.47
Sr	2.69	2.70	2.69

Overall First Shell CN

	Water	1OH$^-$	2OH$^-$
Mg	6	-	5.92
Ca	7.5	-	6.63
Sr	8.02	7.97	7.61

Hydroxide First Shell CN

	1OH$^-$	2OH$^-$
Mg	-	0.95
Ca	-	0.7
Sr	0.1	0.26

Residence times / %

	0	1	2
Mg	24.77	55.9	19.34
Ca	44.44	41.42	14.14
Sr	76.42	21.65	1.93

Proton Transfer Events

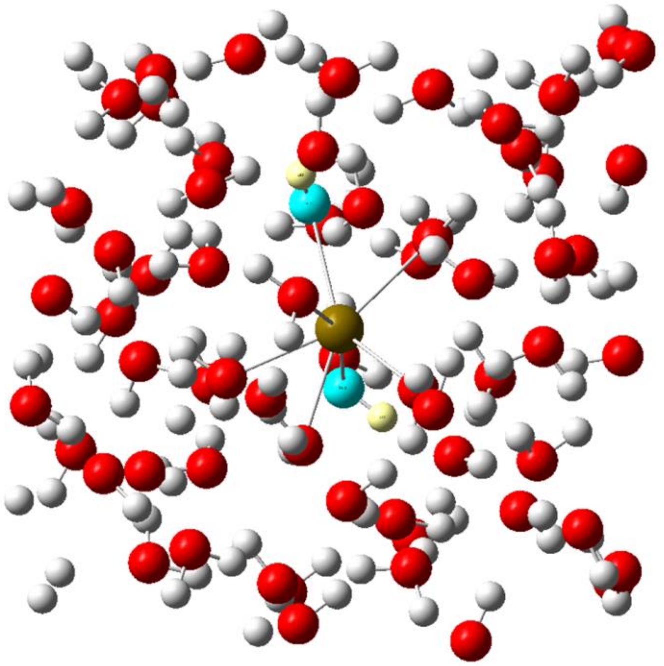

Figure 4: Visual representation of a strontium di-hydroxide. 2 OH^- ions (O blue, H yellow) with a Sr^{2+} ion (brown) in the centre.

	Av. PTE	Outside First Shell /%
Mg	27.67	56.2
Ca	32.53	73.79
Sr	33.33	85.81

UO_2^{2+} Water and Hydroxide Comparison

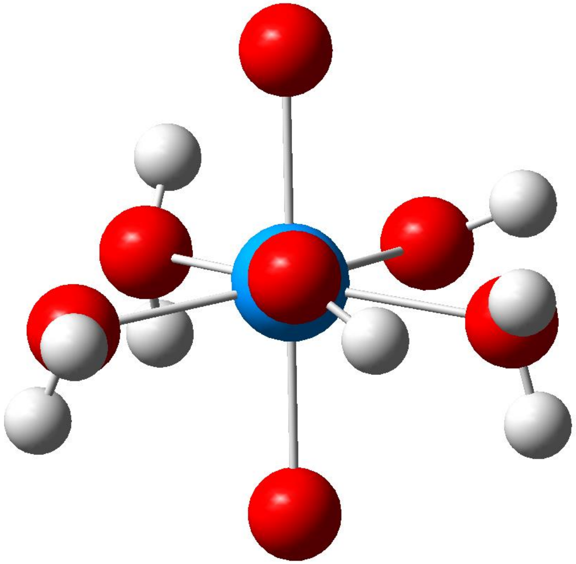

Figure 5: First solvation shell of UO_2^{2+} coordinated by 3 H_2O and 2 OH^-

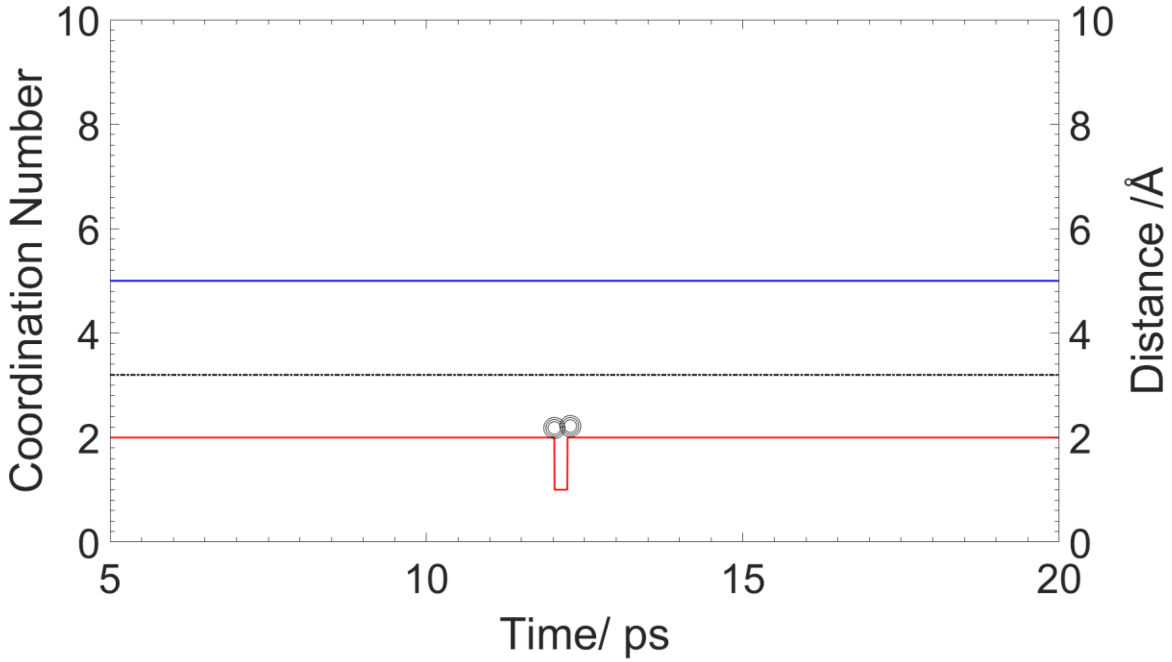

	Water	$2OH^-$
Av. Bond Length/Å	2.42	2.40
Total CN	5.00	4.69
OH- CN	N/A	1.98

Hydroxide Summary

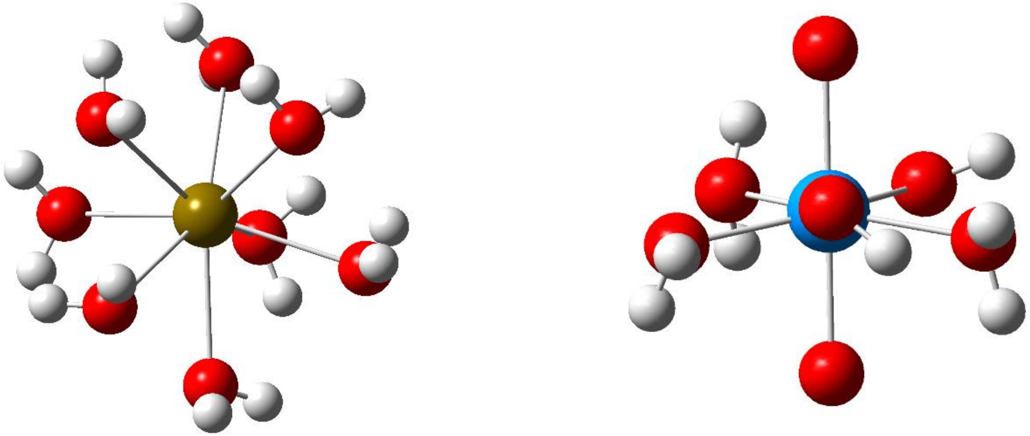

- Introduction of hydroxides had little effect on average bond length.
- The movement of hydroxides through the system occurs through proton transfer events.
- PTEs are more likely to occur outside of the first solvation shell.
- Uranyl binds tightly to hydroxide molecules with little or no PTE occurring.

Oxide Surface- CeO_2

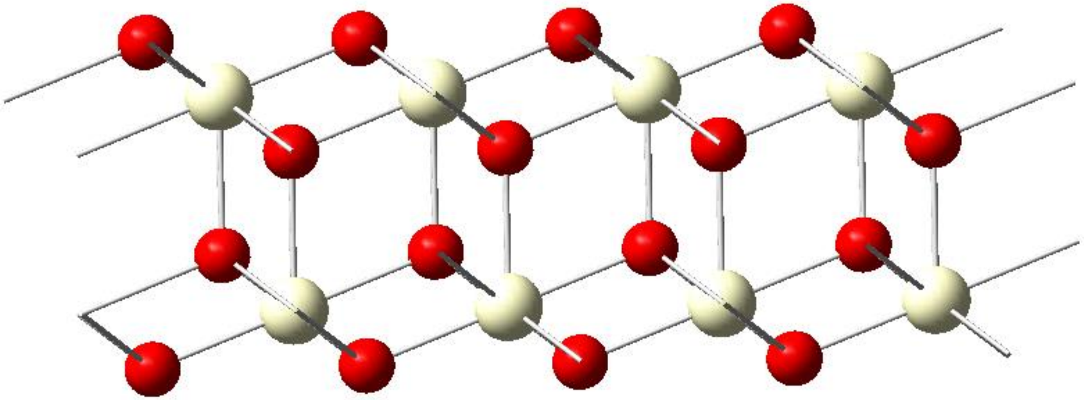

Figure 8: visual representation of the CeO_2 111 surface

- UO_2 is one of the main minerals of interest.
- CeO_2 is a well known analogue for uranium dioxide, as it closely resembles the mineral structure of fuel grade UO_2.
- It is already used both computationally and experimentally with good results.

System Set Up

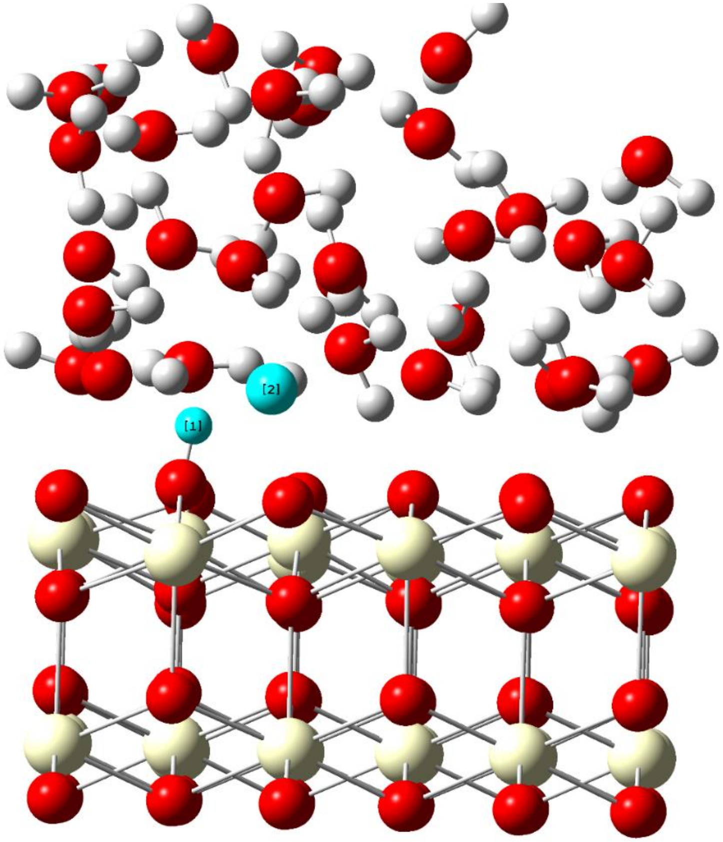

Figure 9: visual representation of the CeO_2 111 surface with a 32 water molecule layer

- CeO_2 (111) Surface – built and optimised
- Using a 4x3x2 surface
- 32 waters on top
- 15 Å vacuum above the water

System Set Up

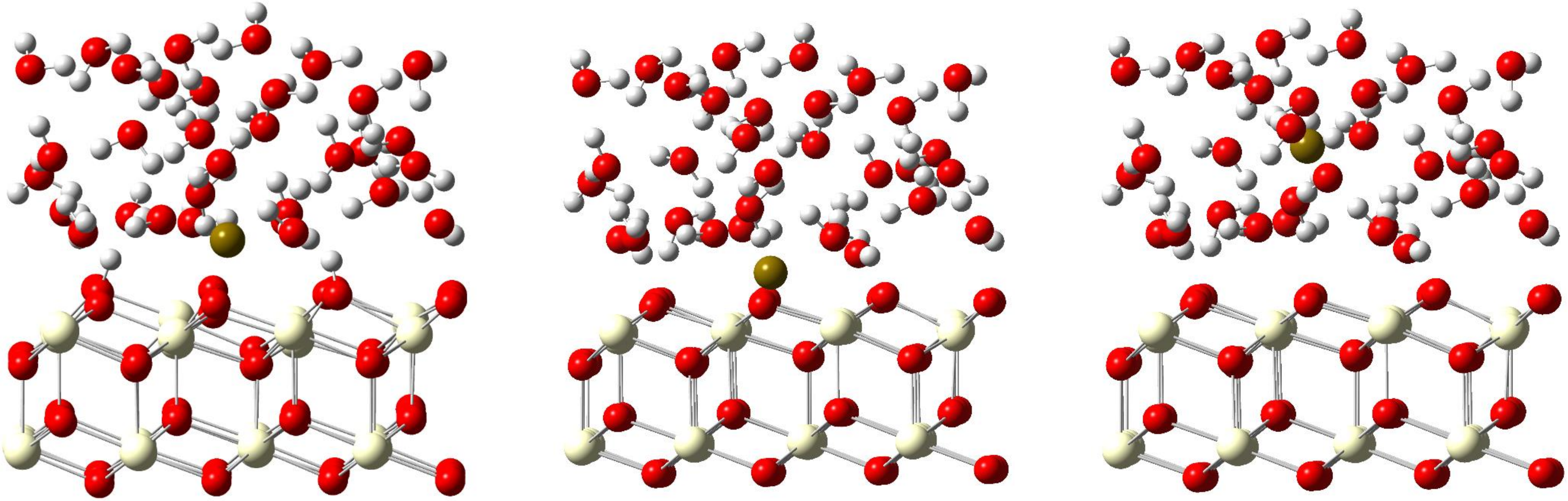

Figure 10: visual representations of the CeO_2 111 surface with a 32 water molecule layer with Sr^{2+}

- Ion environment varied.
- Geometry optimisations of each system will be carried out.
- Comparisons of the energetics of each system.
- Potentially time available to investigate the dynamics.

Final Stages of the Project

- Hydroxide Systems AIMD
  - Monohydroxide for UO_2^{2+} – ongoing, 20 ps left.
  - Dihydroxide – complete.
  - Trihydroxide for La^{3+} and Lu^{3+} – ongoing, 40 ps left.

- CeO_2 Oxide Surface DFT + U
  - Optimisation of surface structure – complete.
  - Optimisation of surface with water structure – ongoing.
  - Optimisation of surface with waters and ions– ongoing.
  - Potentially- AIMD run of a CeO_2 water/ion system.

Conclusion

- Successfully developed an accurate solvation model.
- Investigated the effect of the introduction of hydroxide on the solvation model.
- Developed an analysis method for the dynamics of proton transfer.
- Set up a viable analogue model for the mineral surface in the storage ponds.

Any Questions?

- Theme 3 Annual Meeting
- 16th October 2017
- Olivia Lynes
- o.lynes@lancaster.ac.uk

Tailored Cs/Sr Ion Exchange in Sn-Umbite by Framework Substitution

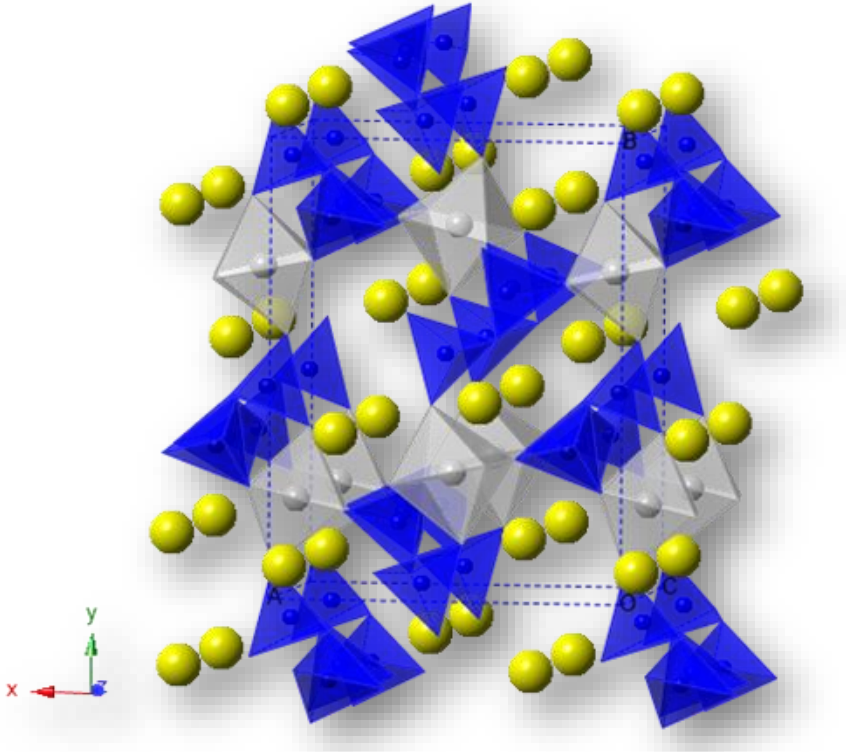

Tzu-Yu (Evin) Chen
16/10/17

Umbite
$K_2SnSi_3O_9 \cdot H_2O$

UNIVERSITY OF BIRMINGHAM

DISTINCTIVE

School of Chemistry

Zeotype materials

There is scope for novel ion exchangers that have

- **improved stability,**
- **ion exchange selectivity,**
- **easy conversion pathways into dense ceramics for long term storage**

- **Microporous framework materials**
- **Chemically and thermally stable materials**
- **Various M^{IV} (M = Ti, Zr, Sn) silicates or germanates based on stable minerals.**

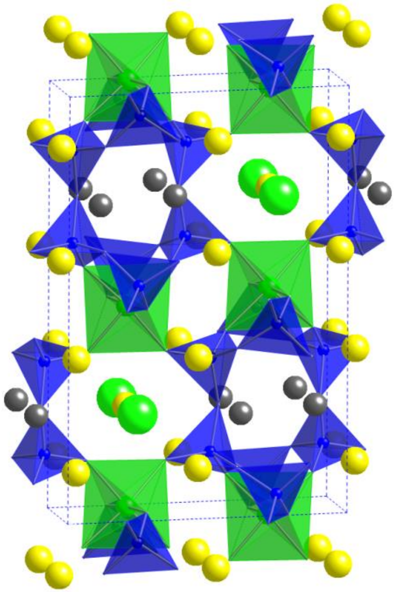

Petarasite (AV-3)
$Na_5Zr_2Si_6O_{18}(Cl,OH)\cdot 2H_2O$

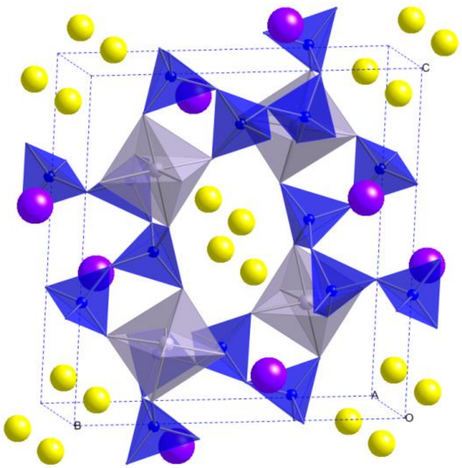

Sn-Kostylevite (AV-7)
$Na_{0.5}K_{1.5}SnSi_3O_9\cdot H_2O$

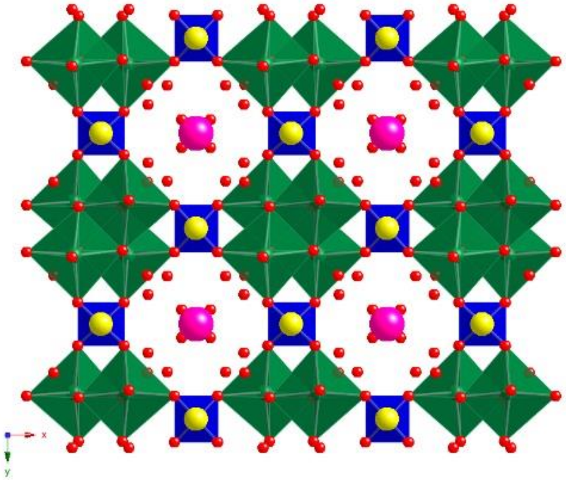

Nb-CST:
$Na_{1.5}Ti_{1.5}Nb_{0.5}O_3SiO_4\cdot 2H_2O$
as found in IONSIV

Sn-umbite

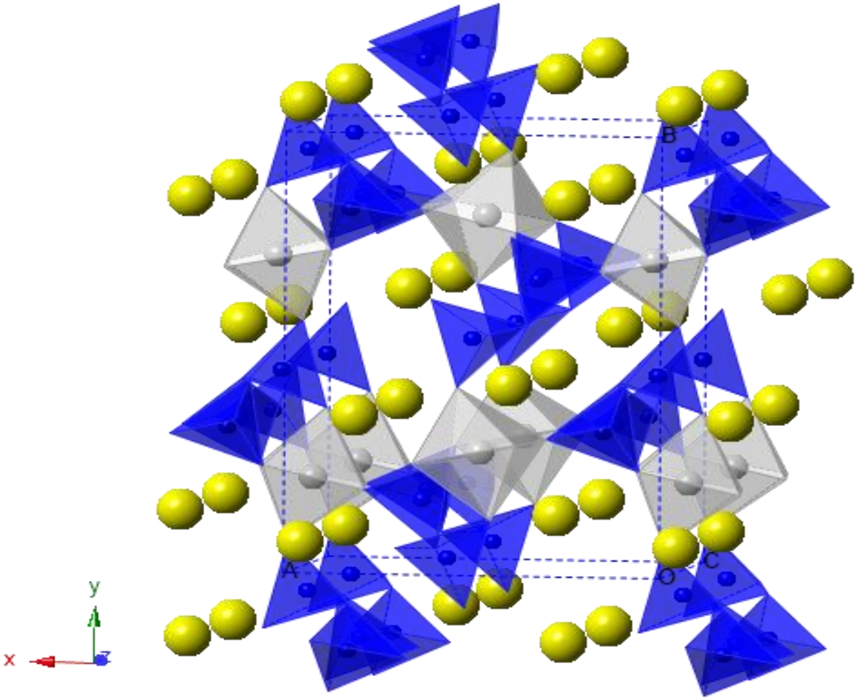

Sn-Umbite,
$K_2SnSi_3O_9{\cdot}H_2O$
Orthorhombic, $P2_12_12_1$
a = 10.101, b = 13.136, c = 7.157 Å

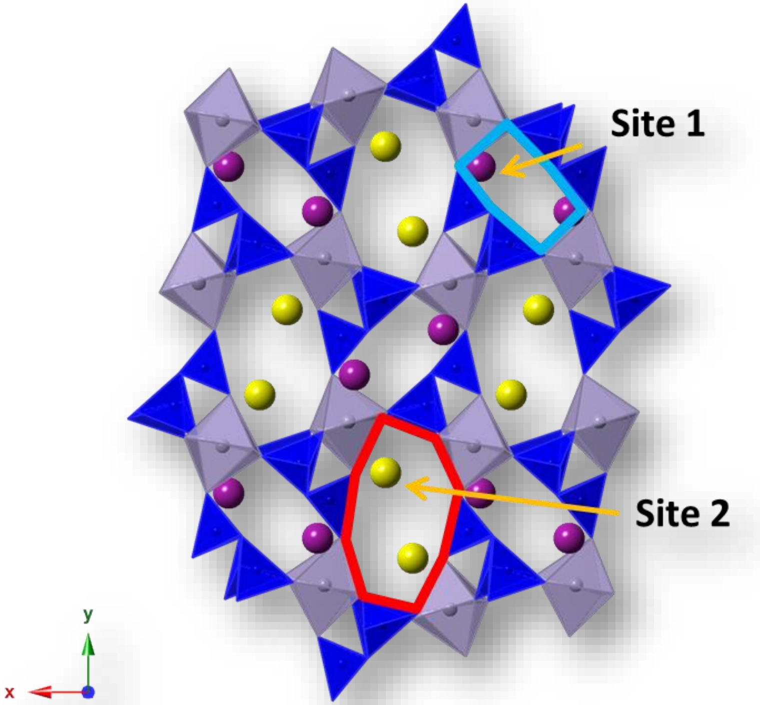

2 ion exchange sites:

- Site 1 is in a 8MR tunnel consisting of six SiO_4 tetrahedra and two SnO_6 octahedra;
- Site 2 is in another 8MR tunnels composing of four SiO_4 tetrahedra and four SnO_6 octahedra.
- H_2O molecules only locate in channels along with Site 2 cations.

Lattice parameters (Pawley fitting)

	a	b	c	V
Sn-umbite	10.114	13.1521	7.1641	953.004
Sn_25Ge	10.1257	13.2200	7.2120	965.409
25Nb	10.1109	13.1983	7.1674	956.478
25Sb	10.1236	13.1665	7.1688	955.542
25(Y,Nb)	10.1533	13.2088	7.1672	961.299
25(Sc,Nb)	10.0990	13.1524	7.1592	950.928

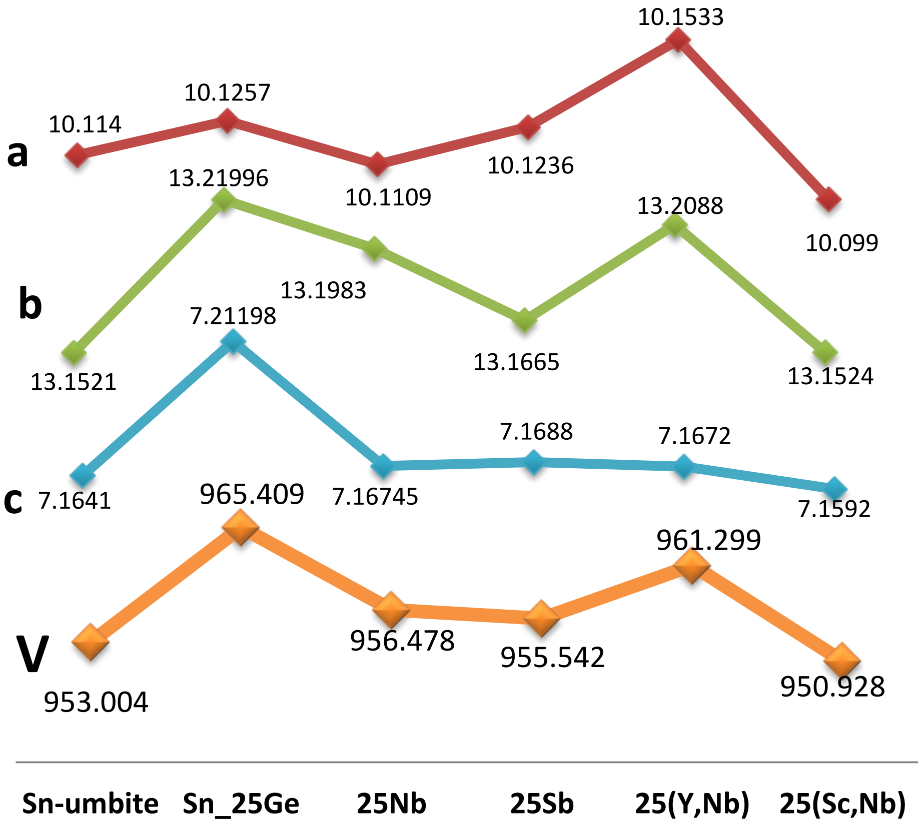

Static batch ion exchange test

- 0.1M $CsNO_3$ or $Sr(NO_3)_2$, V/m=100 mL/g, shake for 1 day.
- XRF analysis on loose powder

Normalised molar ratio of Sr/Cs uptake to octahedral elements in the substituted umbites

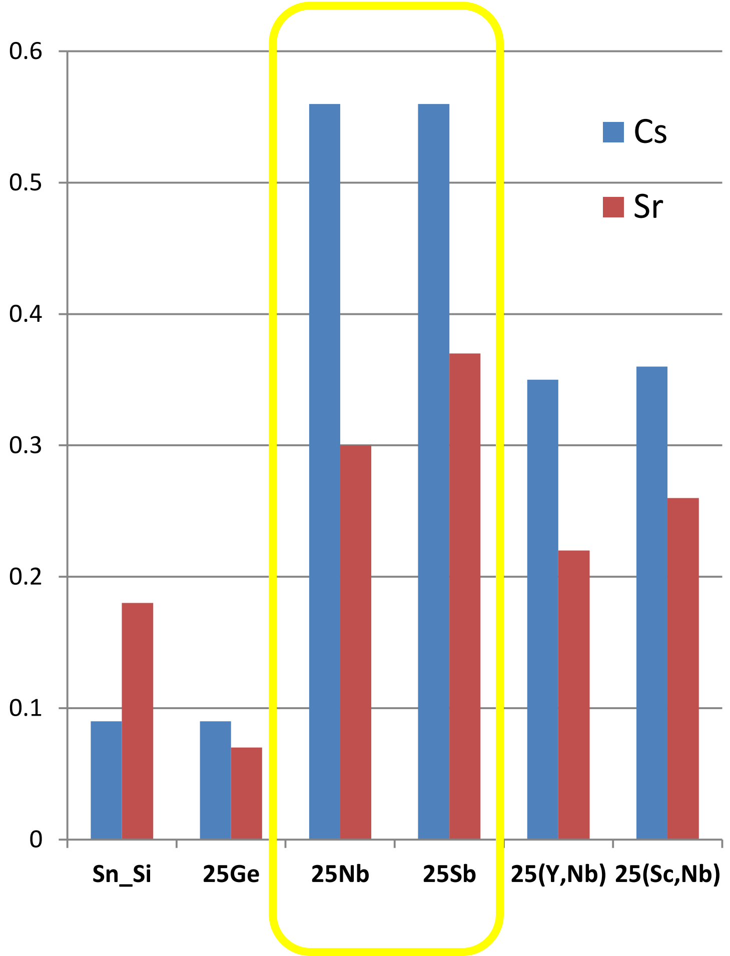

Possible Factors

- **Different tunnel /pore size** due to partial substitution.
- When replacing Sn^{4+} with pentavalent elements such as Nb^{5+} or Sb^{5+}, less K^+ cations are required for charge neutralisation forming **less crowded tunnels** to accommodate more hydrated Cs or Sr.

Structural studies

- Pore chemistry
- Coordination environment

Cation mobility

- Ionic conductivity
- NMR
- Computational studies

Rietveld Refinement (Neutron data)

6 CN	*Radius (Å)*
Sn^{4+}	0.69
Nb^{5+}	0.64
Sb^{5+}	0.60

25Sb umbite
Deuterated sample
TOF neutron data

	Sn-umbite	25Nb	25Sb
a	10.11(3)	10.10(8)	10.12(4)
b	13.15(4)	13.16(11)	13.16(5)
c	7.16(2)	7.18(6)	7.17(3)
V	**952.3(50)**	**954.2(13)**	**954.8(66)**
Porosity (unit cell)	**55.73%**	**55.85%**	**55.80%**

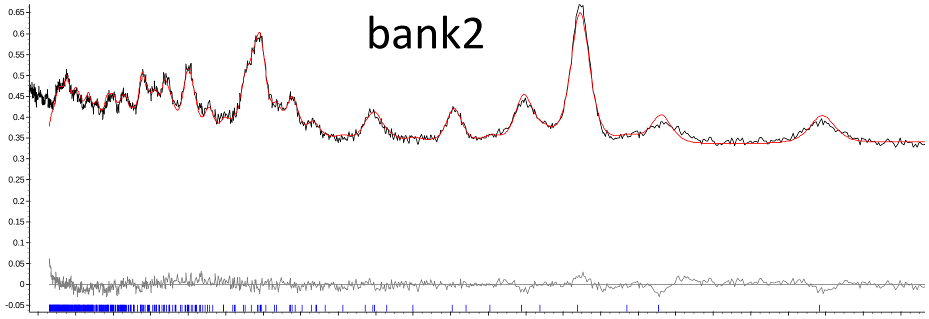

χ^2 1.543
R_{wp} 1.73
R_p 1.64

Almost no change in unit cell volume or pores

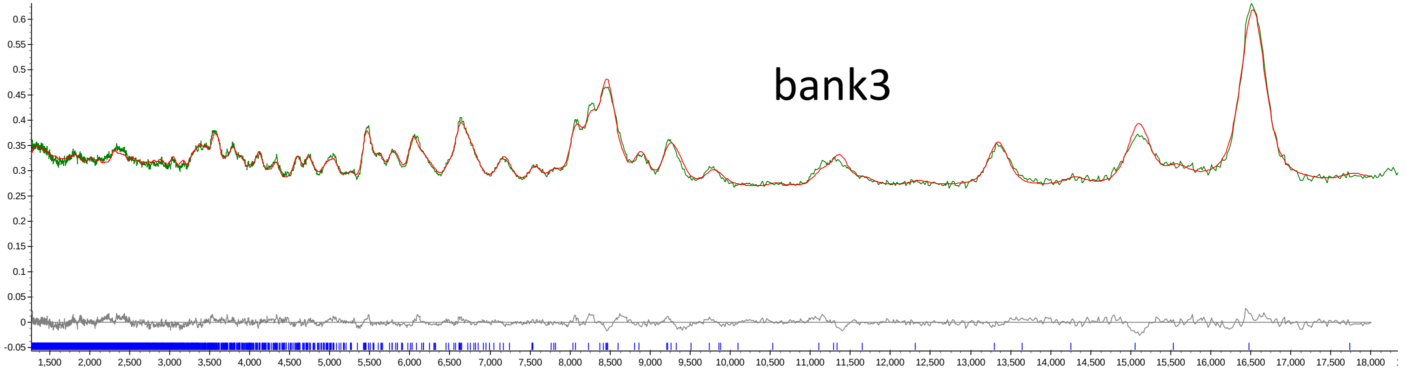

Ionic conductivity

- ☐ Ionic conductivity studies in a number of aluminosilicate zeolites have been made, with special focus on the ion-exchange properties of zeolite samples and on the effect of different channel dimensions (e.g., aperture size) on the ionic conductivity.
- ☐ ***Low conductivity*** in zeolitic materials :

1. the negatively charged **framework** structure of traditional zeolites has very strong attraction for **cations**, which hinders ion migration;
2. the **size of channels** or cages in some of the zeolites is so large that the mobile ions are trapped on the walls of the channels or cages

466 *Chem. Mater., Vol. 4, No. 2, 1992*

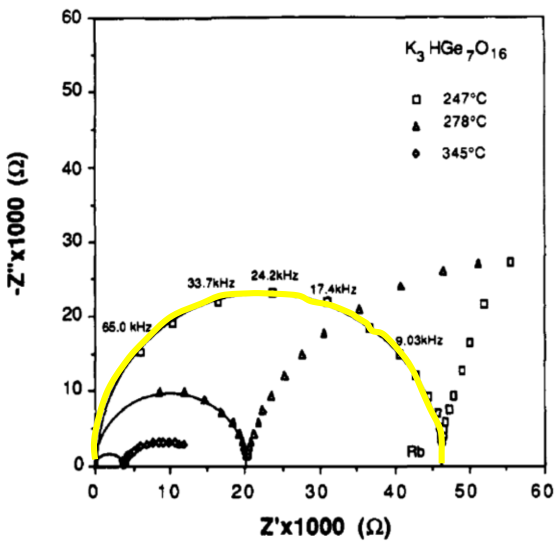

Figure 8. Ac impedance spectra for dehydrated $K_3HGe_7O_{16}$ at selected temperatures, 247, 278, and 345 °C; R_b is bulk resistance; solid line is drawn to guide the eye.

$\sigma = (1/R)*(d/A)$, where d is the thickness of sample and A is the area of electrode

Temperature dependent conductivity

Activation energy for transport could be calculated by fitting conductivity data to Arrhenius equation

$$\sigma T = \sigma_o \exp\left(-\frac{\boxed{E_a}}{kT}\right)$$

Activated energy

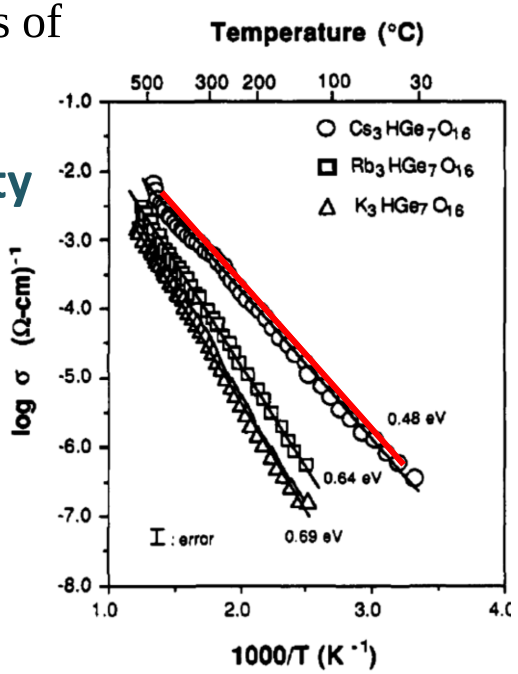

How mobile?

Impedance

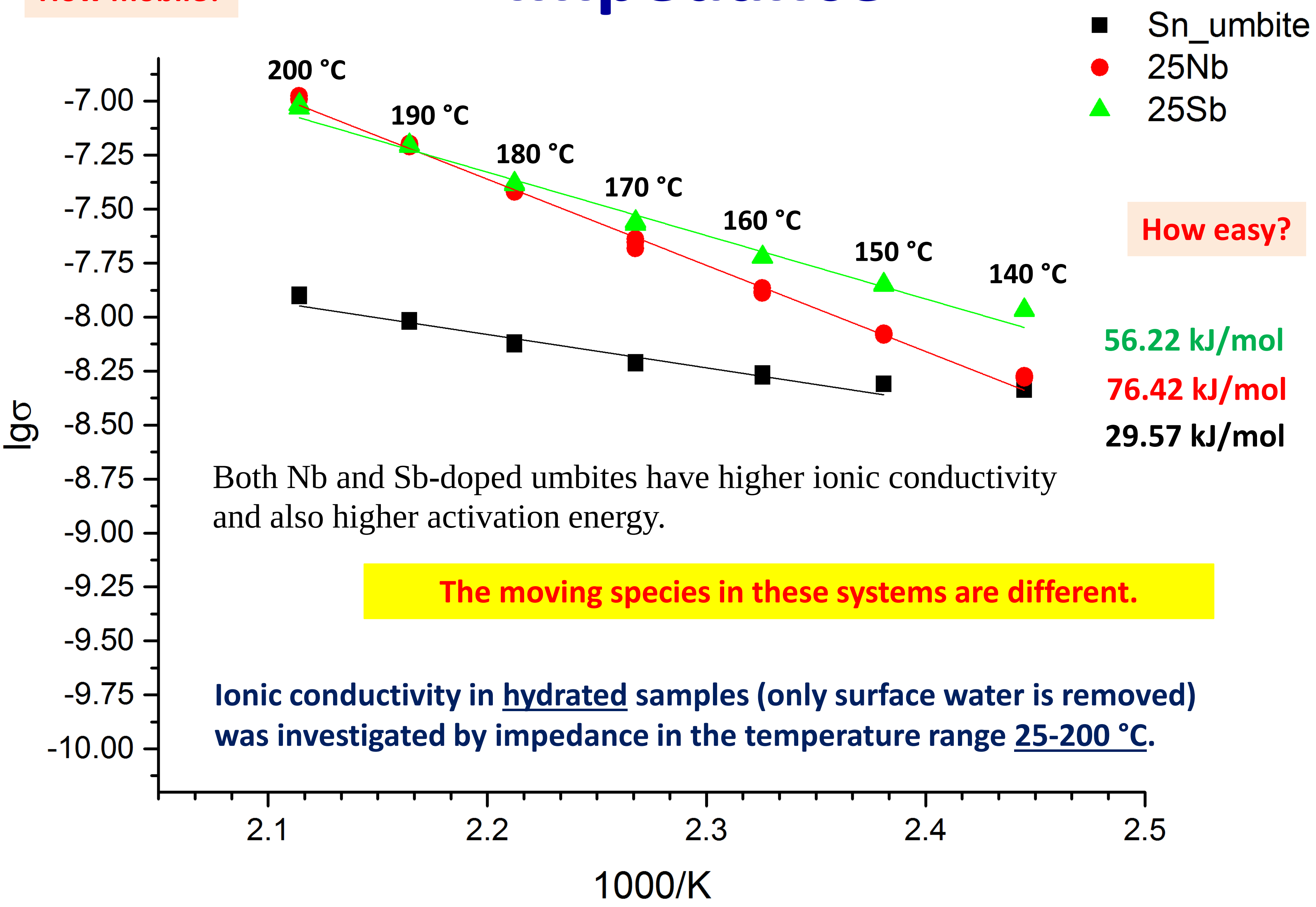

How easy?

56.22 kJ/mol

76.42 kJ/mol

29.57 kJ/mol

Both Nb and Sb-doped umbites have higher ionic conductivity and also higher activation energy.

The moving species in these systems are different.

Ionic conductivity in hydrated samples (only surface water is removed) was investigated by impedance in the temperature range 25-200 °C.

Impedance

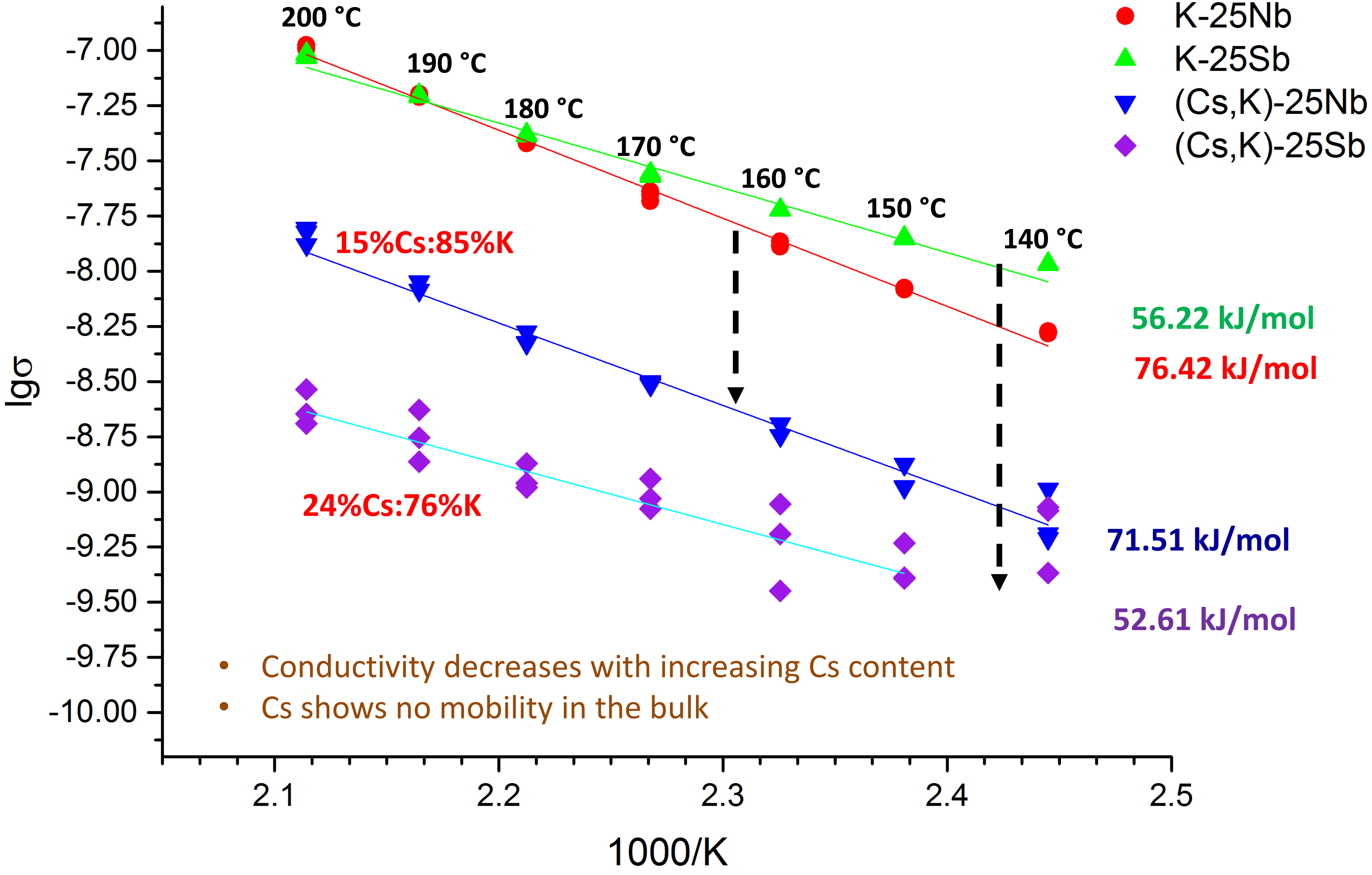

- Conductivity decreases with increasing Cs content
- Cs shows no mobility in the bulk

Various pH

Cs

- ☐ 0.05 N CsCl-CsOH solution
- ☐ molar ratio of CsCl/CsOH= 1:9
- ☐ pH adjusted with HNO_3
- ☐ V/m=100 mL/g
- ☐ shake for 1 day
- ☐ XRF analysis on loose powder
- ▪ K/octahedral elements
- ▪ Cs/octahedral elements

Sn-umbite

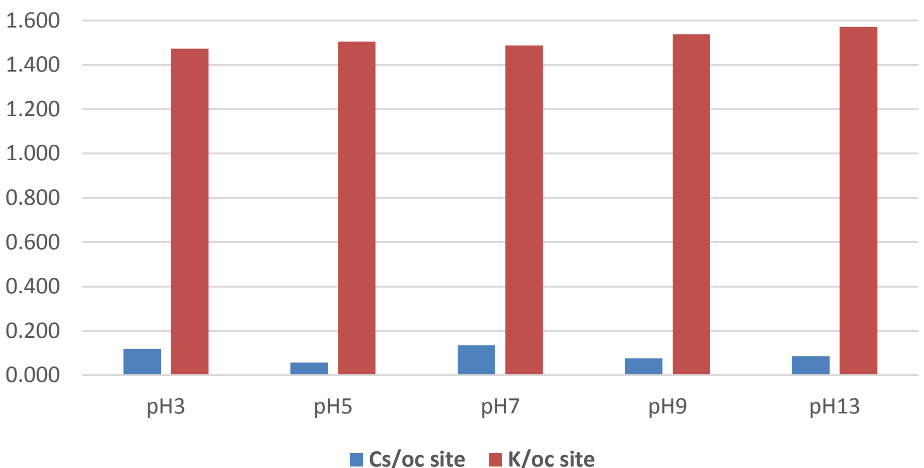

pH independent

25Nb Sn-umbite

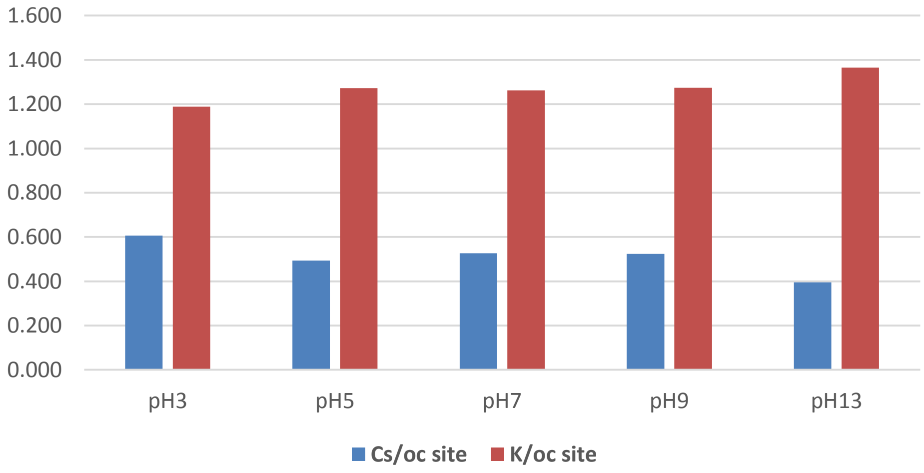

25Sb Sn-umbite

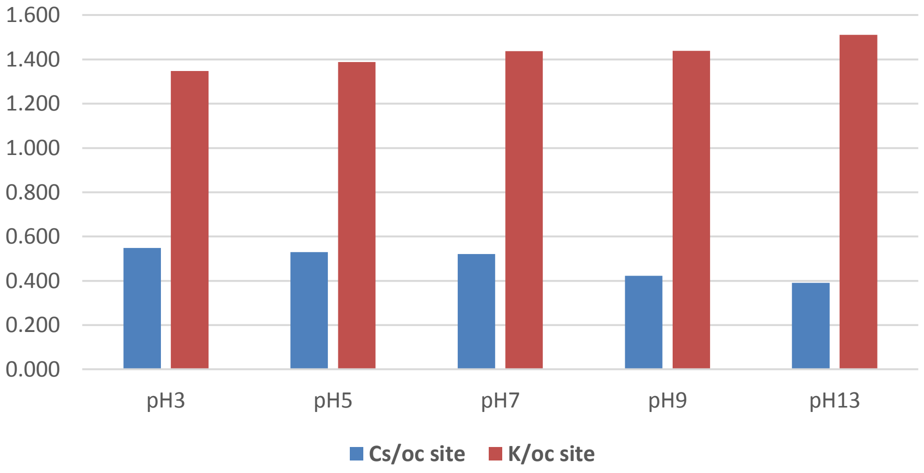

Various pH

Sr

- 0.05 N $SrCl_2$-$Sr(OH)_2$ solution
- molar ratio of $SrCl_2/Sr(OH)_2$= 9:1
- pH adjusted with HNO_3
- V/m=100 mL/g
- shake for 1 day
- XRF analysis on loose powder
- K/octahedral elements
- Cs/octahedral elements

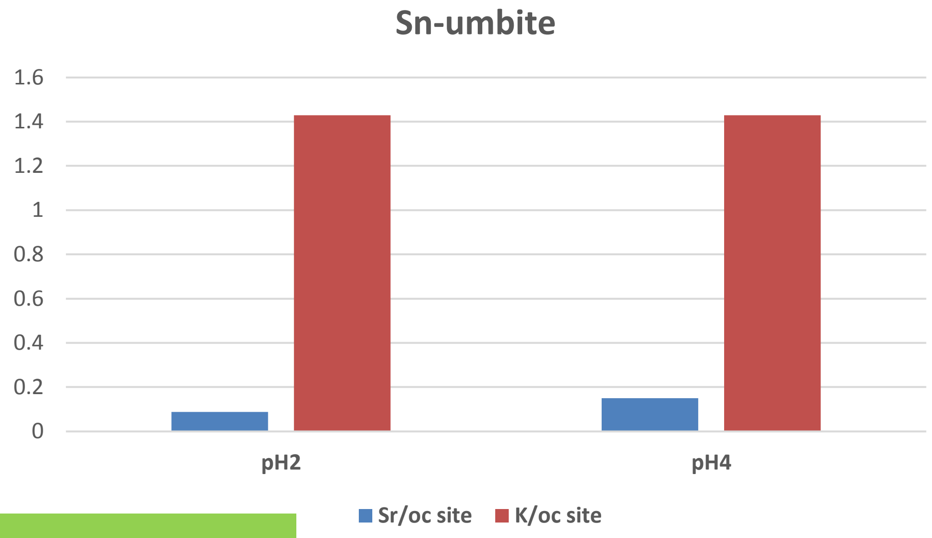

pH independent

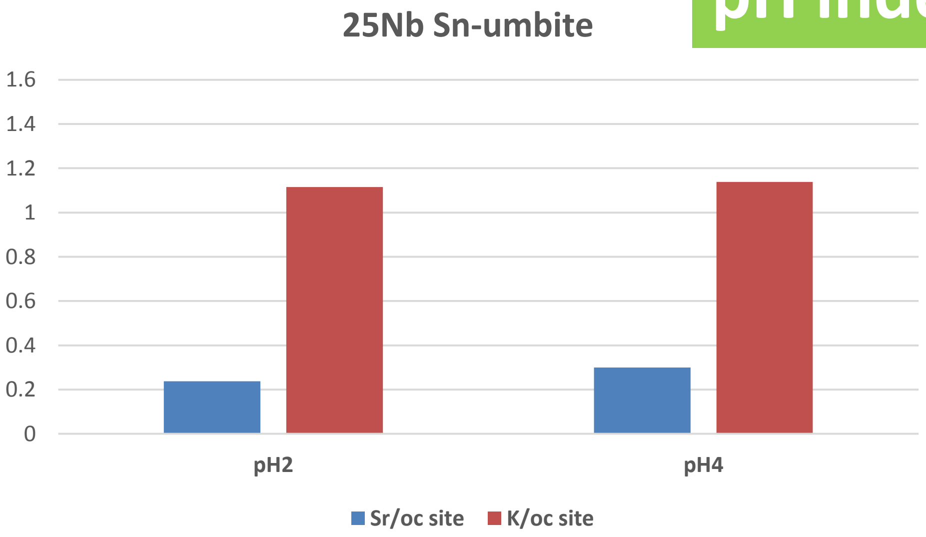

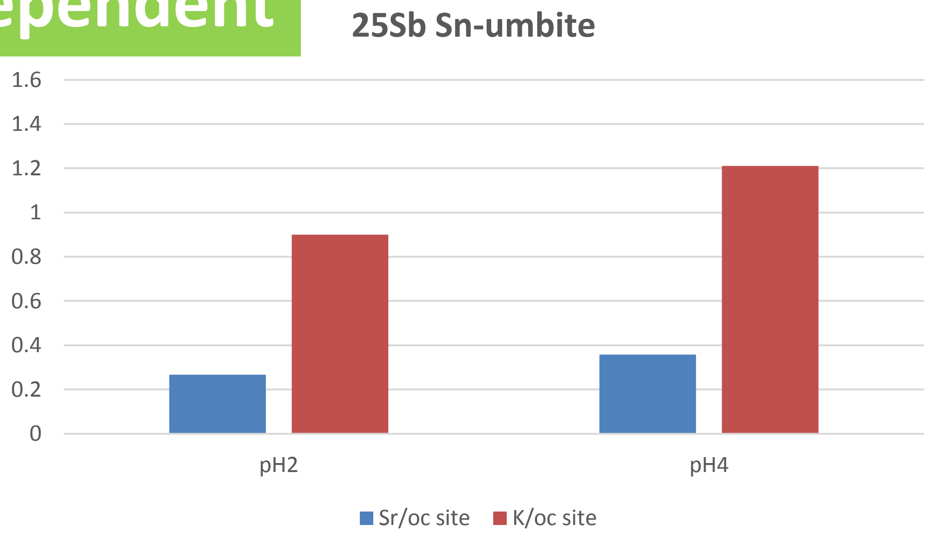

Simulants

- Harwell simulants

Na	100 ppm
Ca	1.5 ppm
Cl	5.57 ppm
Mg	0.99 ppm
Cs	20 ppb
Sr	4 ppb

Competitive

100 ppm **of Na, Mg, Ca, Cs, and Sr**
V/m=100 mL/g, shake for 1 day
XRF on loose powder

	Sn-umbite	**25Nb**	**25Sb**	**25(Y,Nb)**	**25(Sc,Nb)**
Na	■				■
Mg	■	■	■		■
Ca	■	■	■	■	■
Cs	■	■	■	■	■
Sr	■	■	■	■	■

- Hanford simulants

Be	**NO_3**
Ca	**PO_4**
Cd	**SO_4**
Cr	**OH**
Cs	**CO_3**
Cu	**Formate**
Fe	**Acetate**
Na	**Oxalate**
Ni	
Pb	
Si	

- Sellafield simulants

	Case 1	**Case 2**	**Case 3**	**Case 4**
pH	**11.2**	**11**	**10**	**>10**
^{137}Cs	0.001	0.362	0.302	1.51
^{90}Sr	0.000015	0.0153	0.0567	0.032
Na	70	130	60	210
K	0.2	10	20	250
Ca	0.2	3	1.2	60
Mg	0.1	3	140	30
U		2	200	

numbers shown in ppm

Conclusion

- Ion exchange in umbites can be tailored by framework substitutions.
- Cs and Sr uptake drastically improves with increasing Nb/Sb content.
- It is possibly attributed to the less crowded pores formed and a subsequent increase in ion mobility.

1100 °C, 150 MPa, Ar, 2 hrs, mild steel can

HIPed Cs-25Nb-umbite

- **Interaction with the mild steel**
- **Amorphous Sn-Fe-Si glass formation**
- **HIP condition (pressure induced) affecting the thermal conversion**

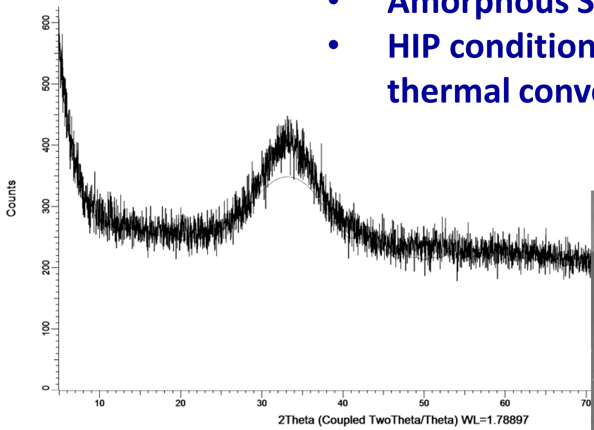

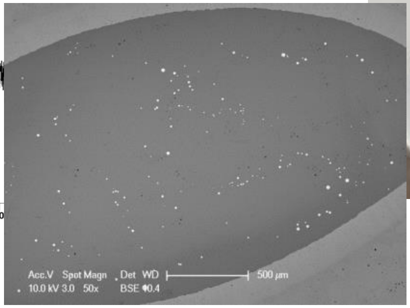

Further Work

- NMR measurements for cation conductivity
- Ion exchange in the presence of competitive cations

Acknowledgement

UNIVERSITY OF
BIRMINGHAM

School of Chemistry

EPSRC

Engineering and Physical Sciences
Research Council

DISTINCTIVE

investing
in **your** future
European Regional Development Fund
European Union

Advantage
West Midlands

www.advantagewm.co.uk

Imperial College
London

Centre for Nuclear
Engineering

Durability of heterogeneous ILW glass/ceramic wasteforms

for complex waste streams

Paul C. M. Fossati, Michael J. D. Rushton & William E. Lee

p.fossati@imperial.ac.uk

DISTINCTIVE

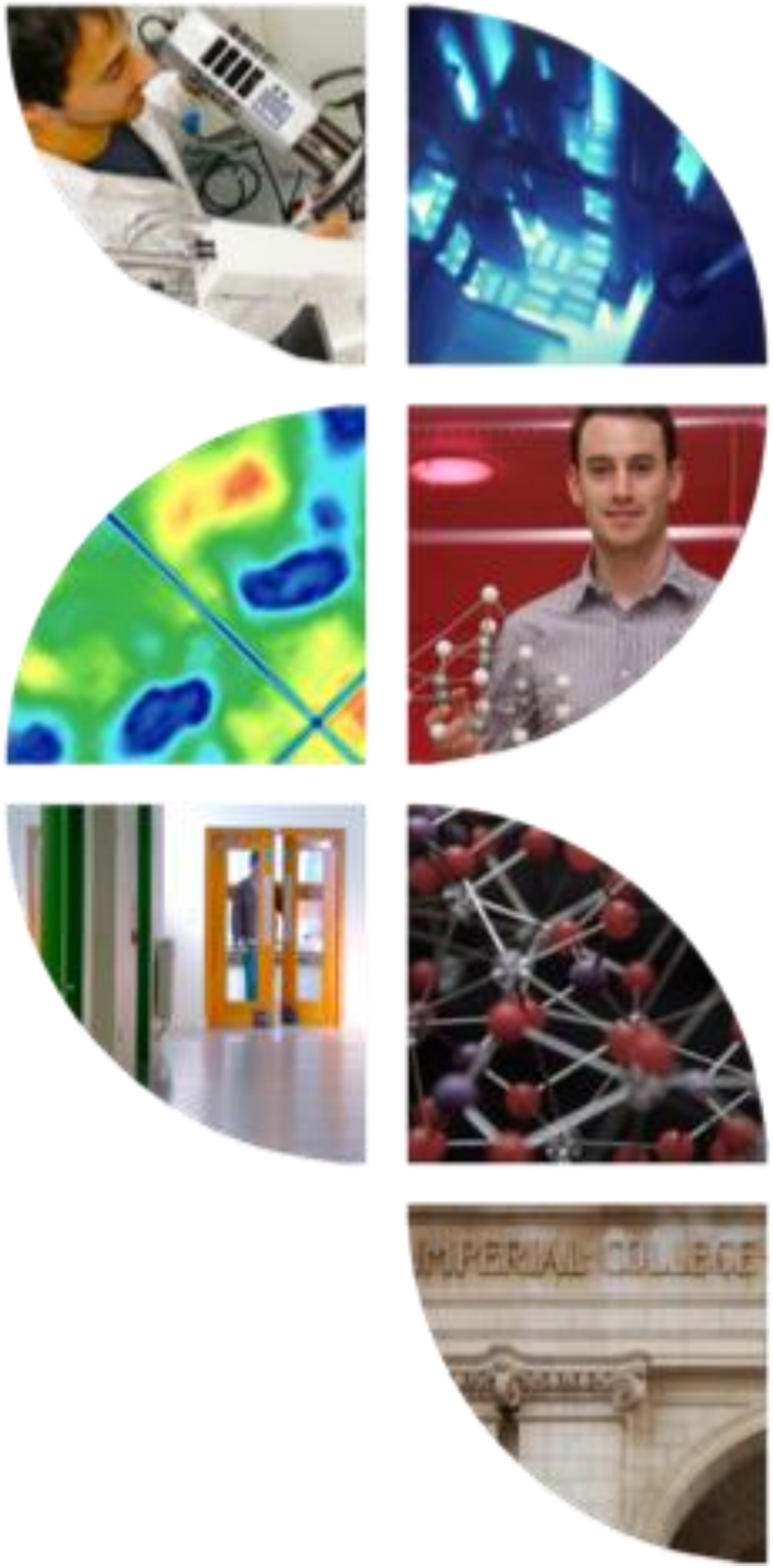

16 October 2017

Plan

Modelling side of previous work by R.K. Chinnam

Purpose: modelling durability of interfaces in GCC at the atomic scale

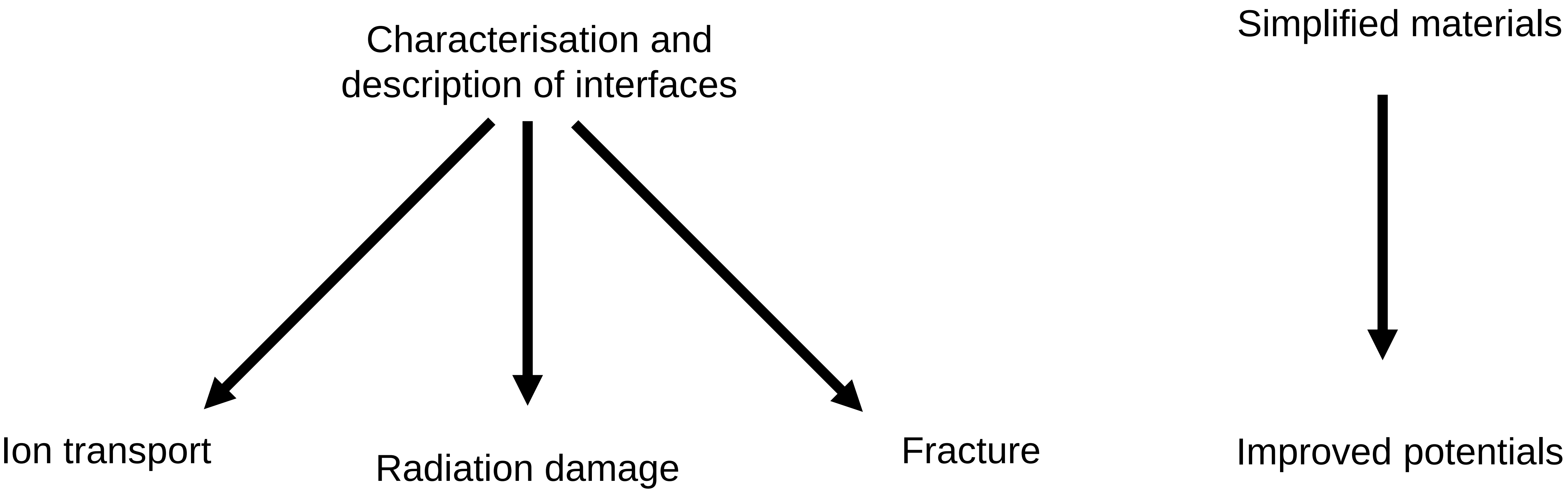

Characterisation and description of interfaces

Ion transport

Radiation damage

Fracture

Simplified materials

Improved potentials

Plan

Modelling side of previous work by R.K. Chinnam

Purpose: modelling durability of interfaces in GCC at the atomic scale

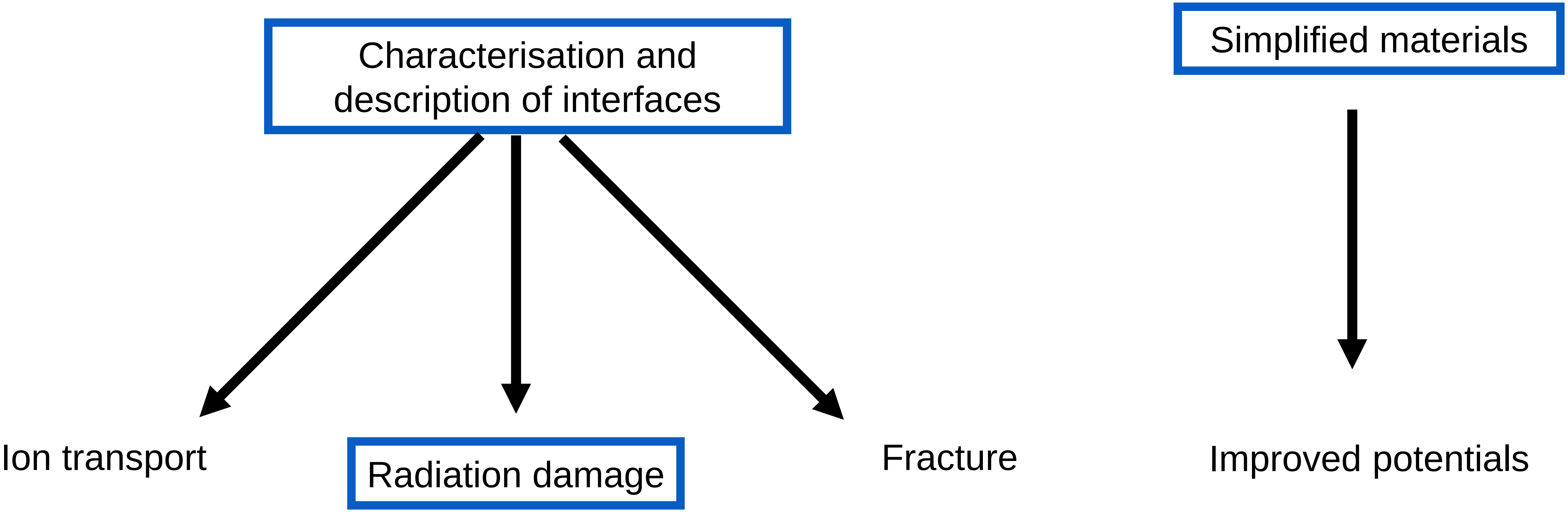

Characterisation and description of interfaces

Simplified materials

Ion transport

Radiation damage

Fracture

Improved potentials

Material of interest

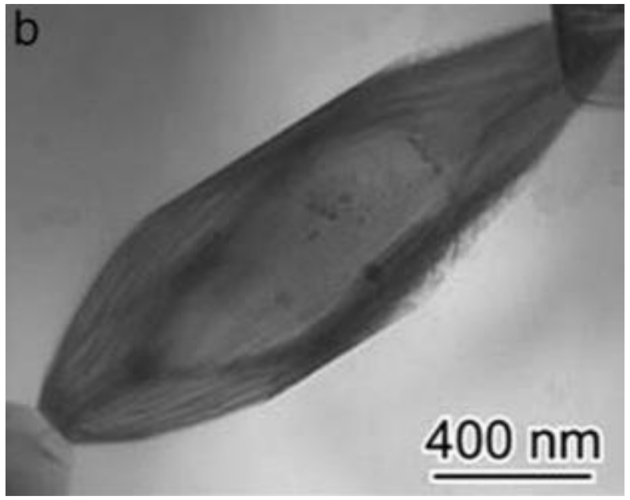

RuO_2 crystals in borosilicate glass
- Common crystallite in glass waste forms
- Simple structure

Effect of secondary phases
- Change melt and glass thermophysical properties
- Change radiation resistance?
- Change long-term behaviour?

Crystal picture: Rose *et al.*, 2011

Modelling approach: material

Simplified material

- Sodium silicate glass $(Na_2O)_x(SiO_2)_{1-x}$
- Rutile TiO_2, isomorphous with RuO_2
- Parameter 1: Na concentration (glass polymerisation)
- Parameter 2: crystal orientation (interface topology)

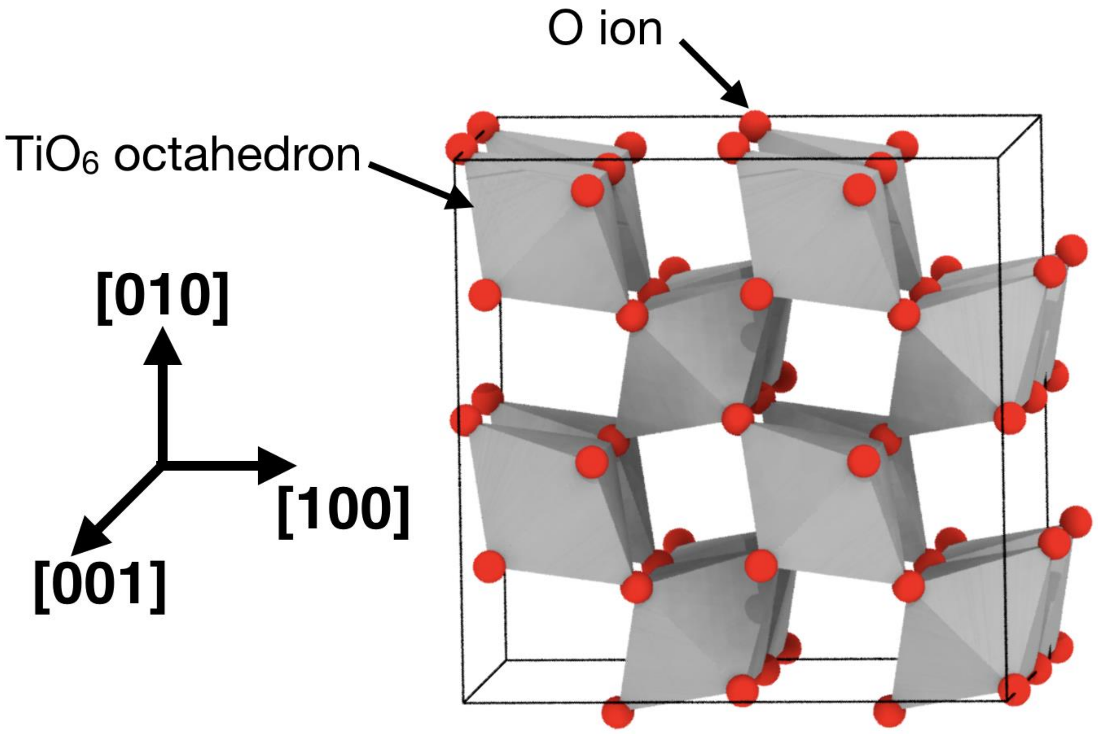

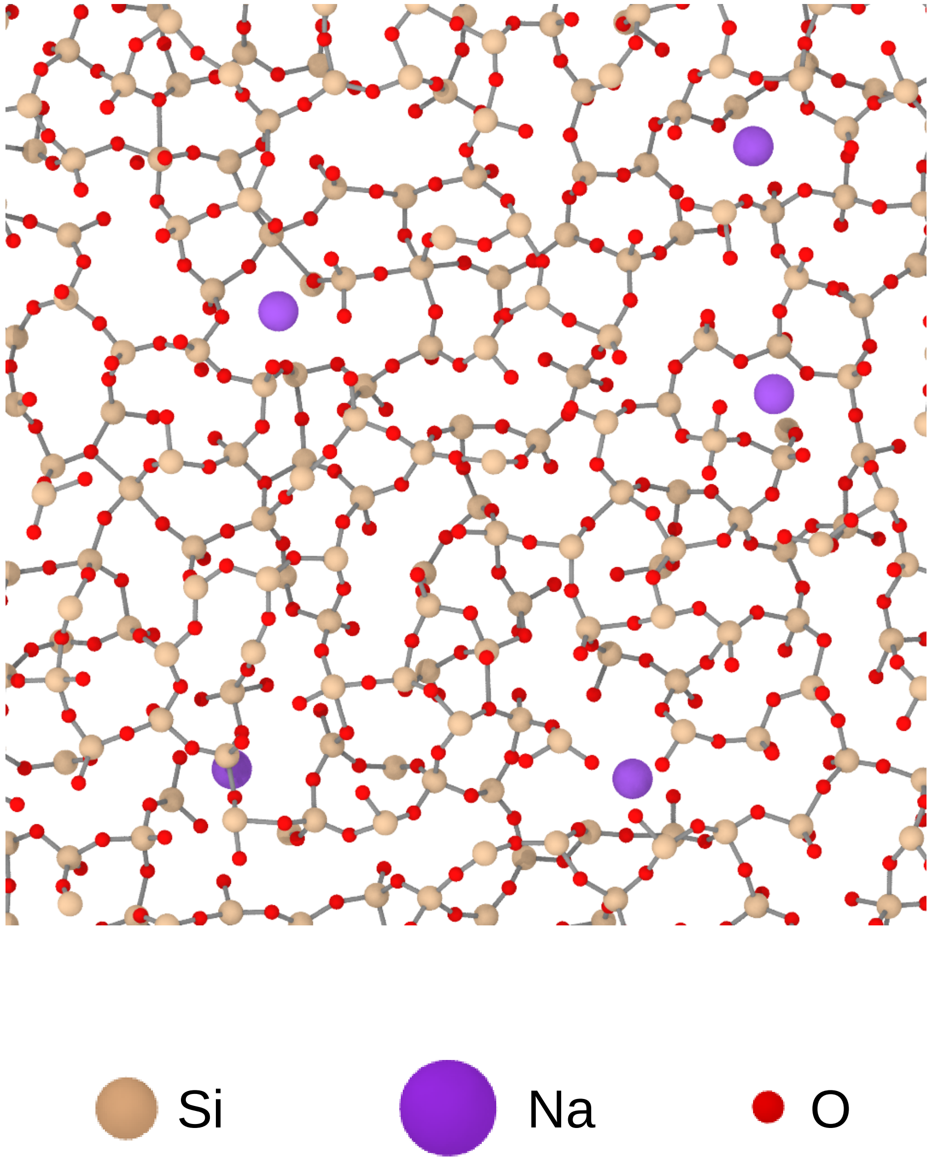

Molecular Dynamics model

Atomistic model
- Empirical (classical) force fields
- Calculate atomic trajectories

Empirical potentials
- Rigid-ion
- Pair interactions (simple and efficient)
- Wide range of compounds

Simulation parameters
- ~ 300 000 atoms
- ~ 130x130x180 Å
- Quench rate: 2.5 K/ps

Scalable
- ~ ns simulation time, necessary for diffusion
- million+ atoms, necessary for fracture

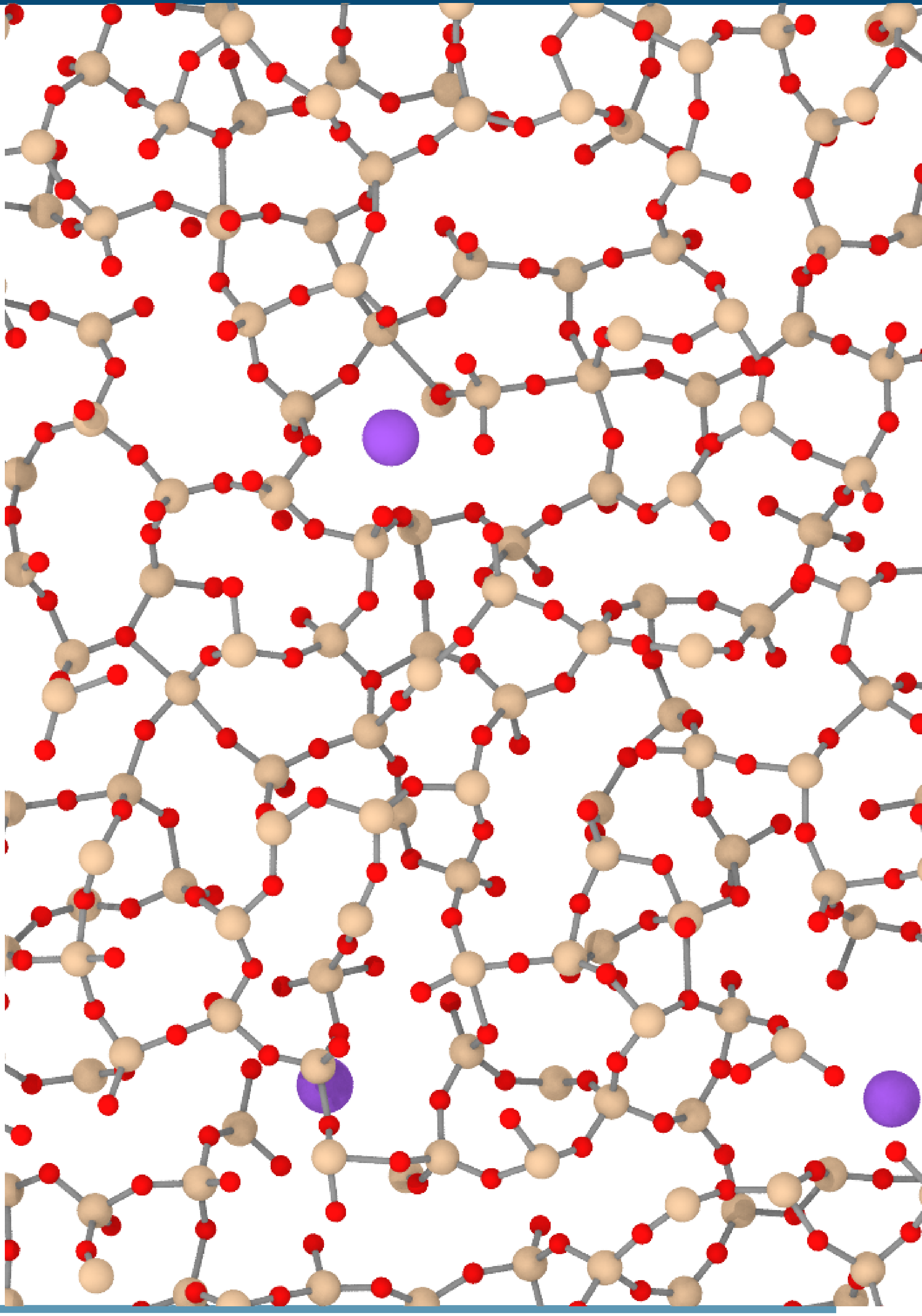

Potential: Pedone *et al.*, 2006

Glass/Crystal Composite (GCC) creation

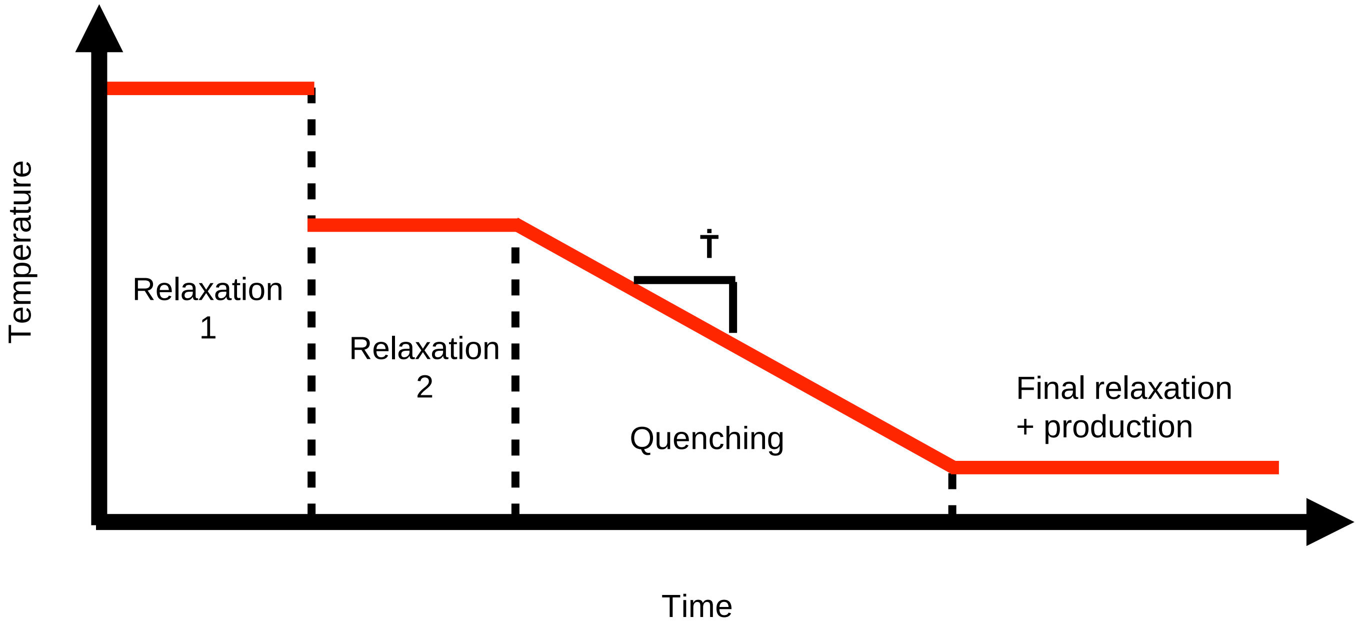

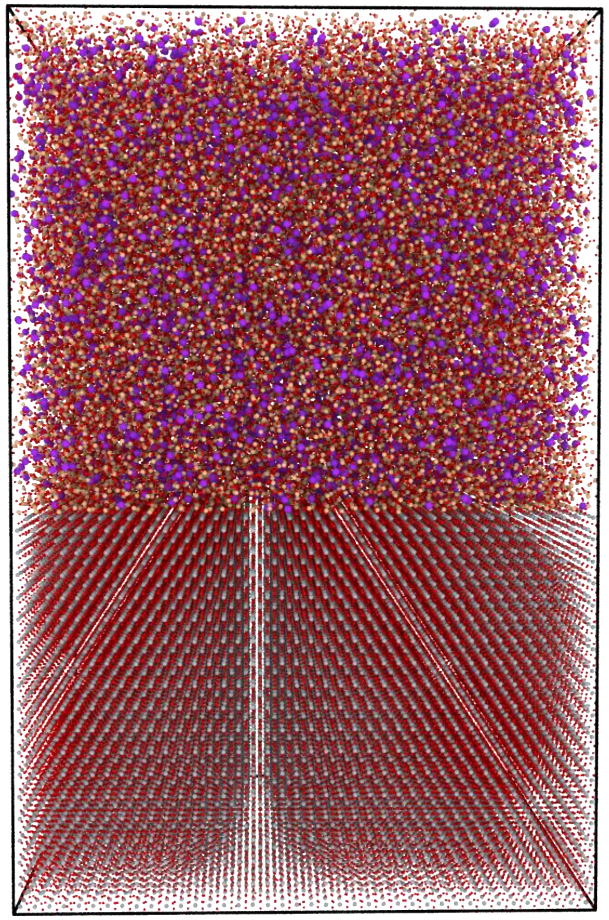

Glass

Crystal
Frozen during quenching

Critical parameter: quench rate Ṫ

- as small as practically possible (but still very high)
- needs to be consistent across simulations

Fixed parameter: glass density

- fixed to experimental room-temperature values
- volume kept constant during quenching

Variations considered

- crystal orientation (12 interfaces with indices lower than 3)
- glass composition (0%, 10% and 20% Na_2O)

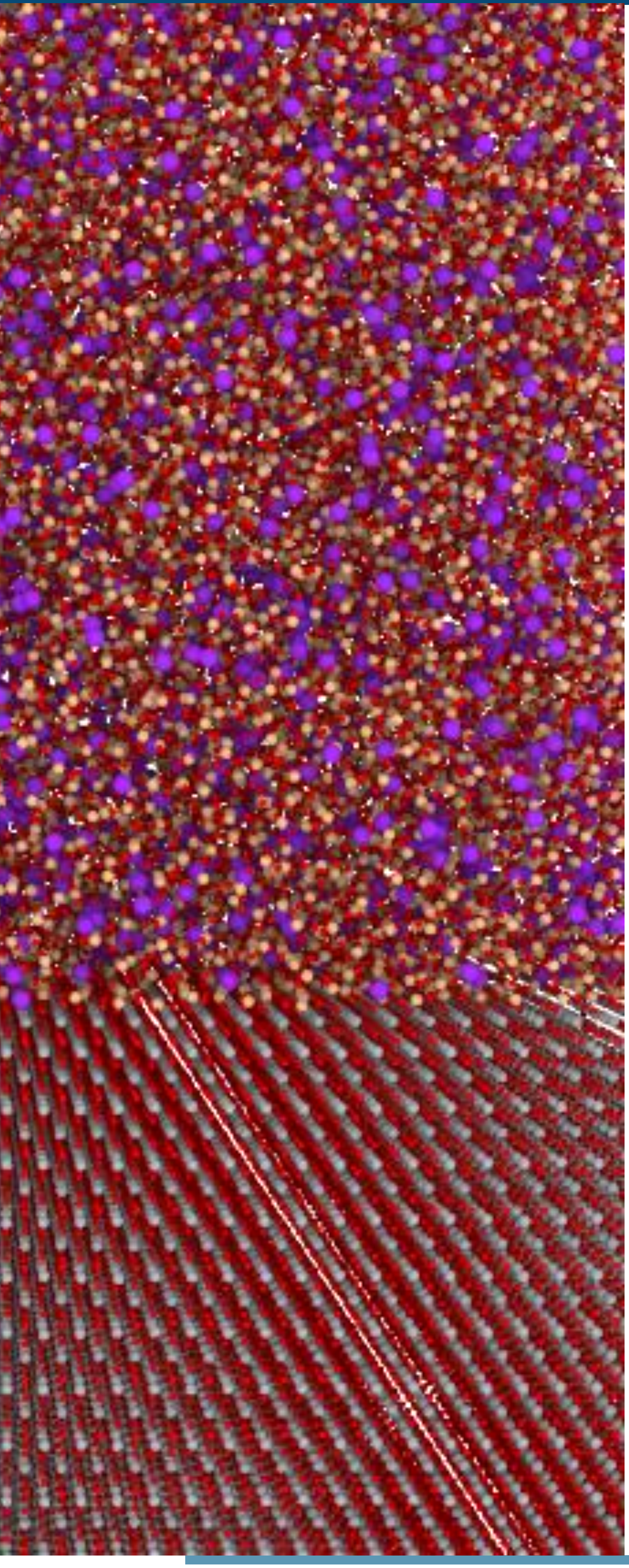

GCC interfaces

Interfaces

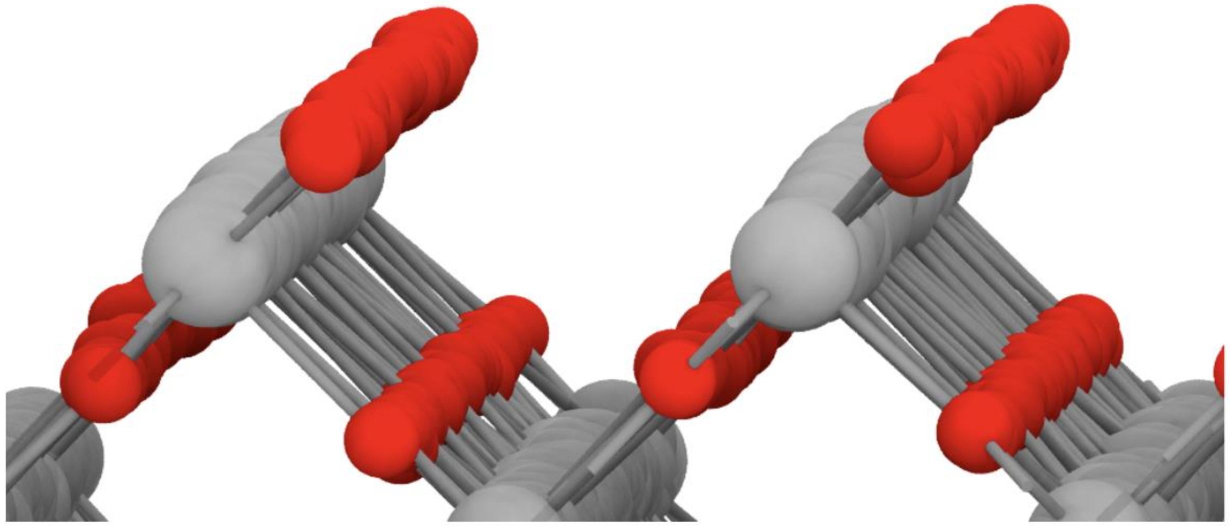
(100) rutile surface

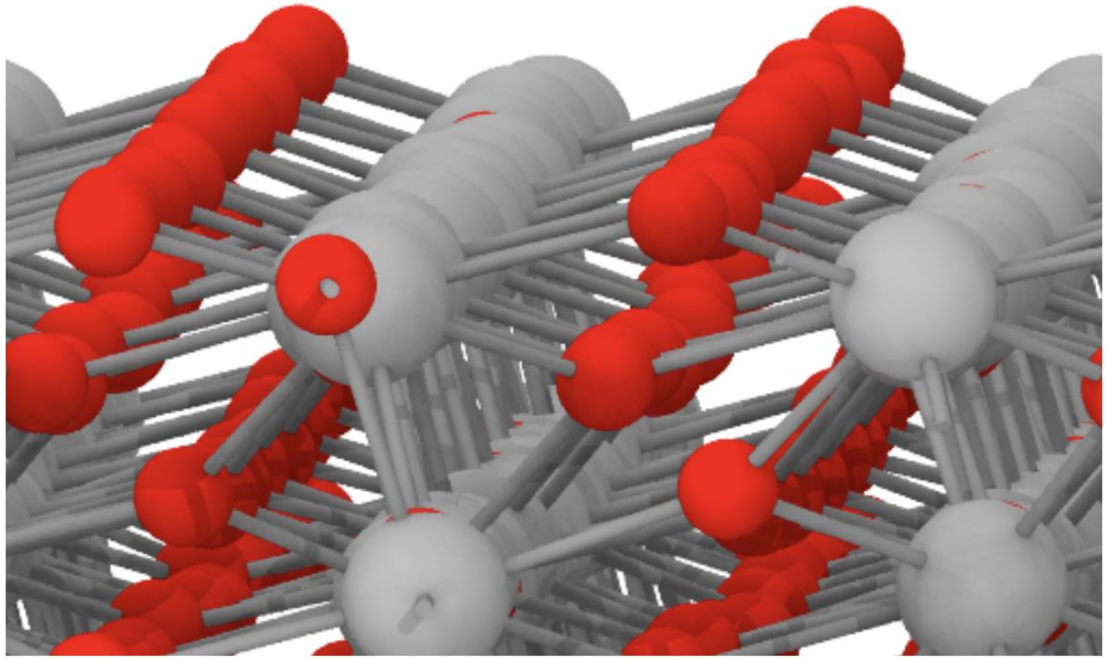
(121) rutile surface

Interface orientations

- All planes with indices ≤ 2 tested
- Examples shown here: (100) and (121)

Segregation on GCC interfaces

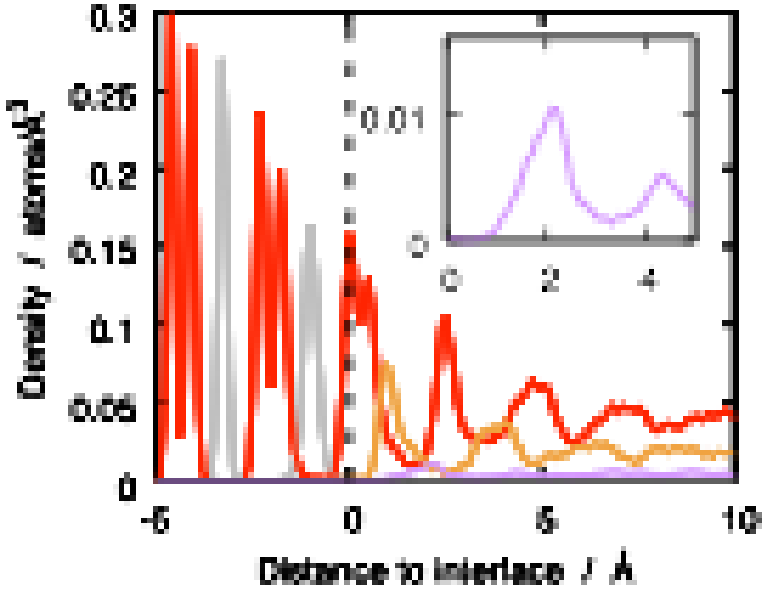

(100) interface; 10% Na_2O

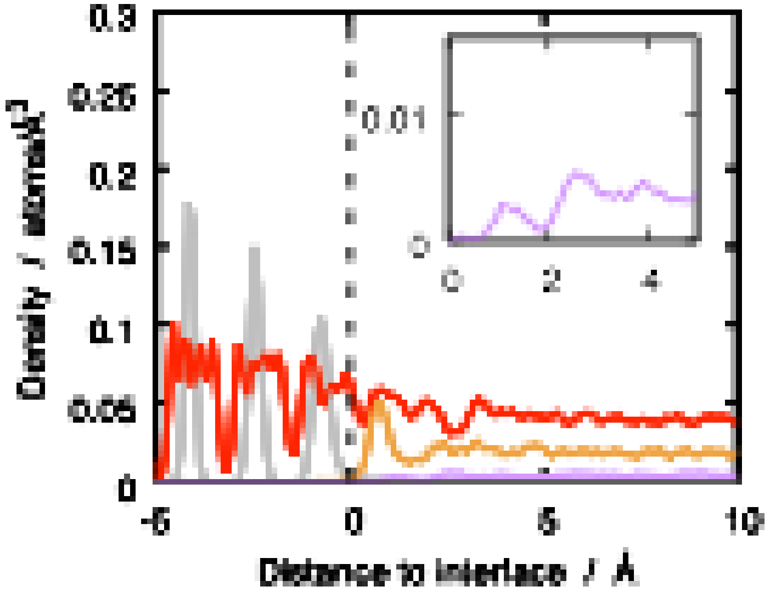

(121) interface; 10% Na_2O

Colour code:

Ti

O

Si

Na

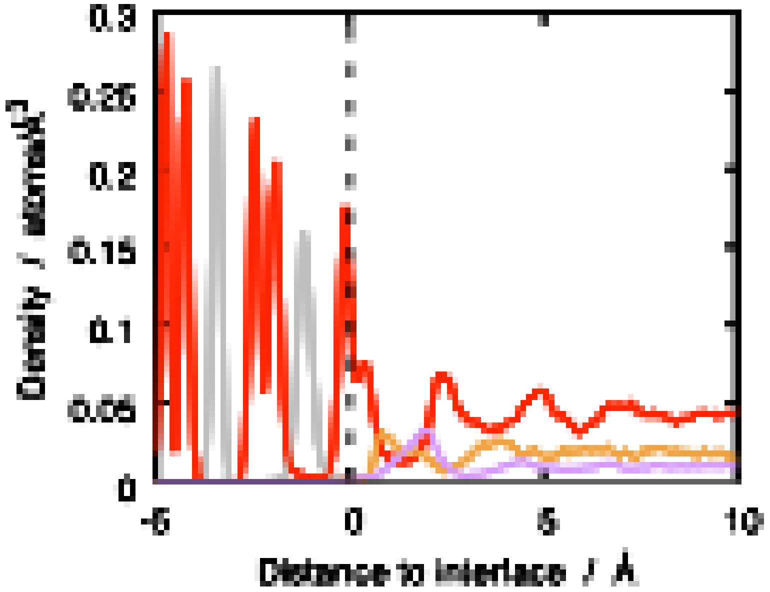

(100) interface; 20% Na_2O

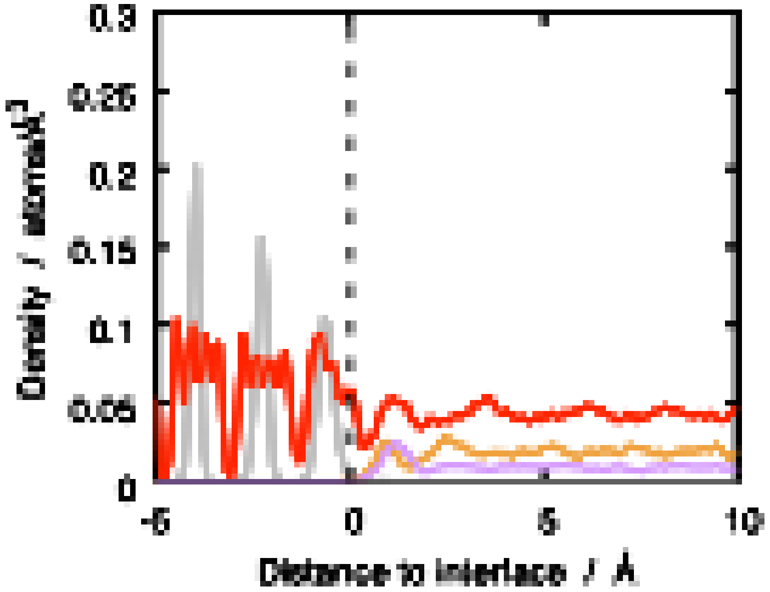

(121) interface; 20% Na_2O

z-density plots

- show concentration of each species as a function to distance from interface
- on the crystal side: clear, well-defined peaks for most interfaces
- on the glass side: 1 Si-rich layer, sometimes several successive layers

Ordering of the first glass layer: (100) interface

Representation of the first silicate layer

Colour code:

SiO_4 tetrahedra

Na ions

TiO_6 octahedra not shown

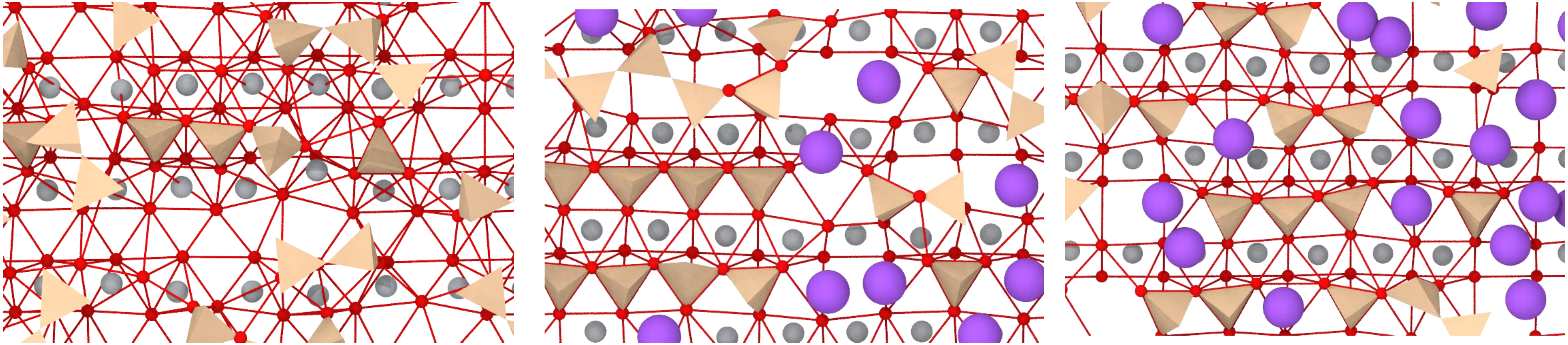

0% Na_2O

10% Na_2O: most tetrahedra are aligned

20% Na_2O: Na compete with tetrahedra

Sodium effect

- Na promotes ordering initially
- But then limits population of aligned SiO_4
- Higher Na concentration: Na lines
- With Na: most tetrahedra connected to the crystal by 3 O (face-connected)

Ordering of the first glass layer: (121) interface

Representation of the first silicate layer

Colour code:

SiO_4 tetrahedra

Na ions

TiO_6 octahedra not shown

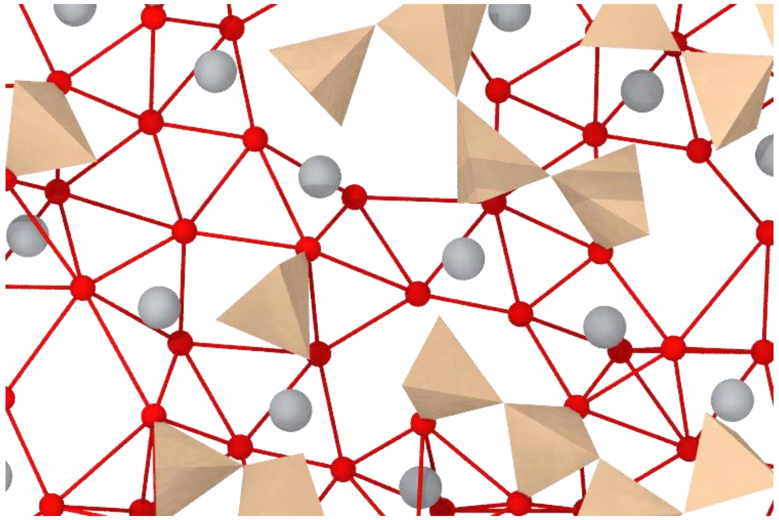

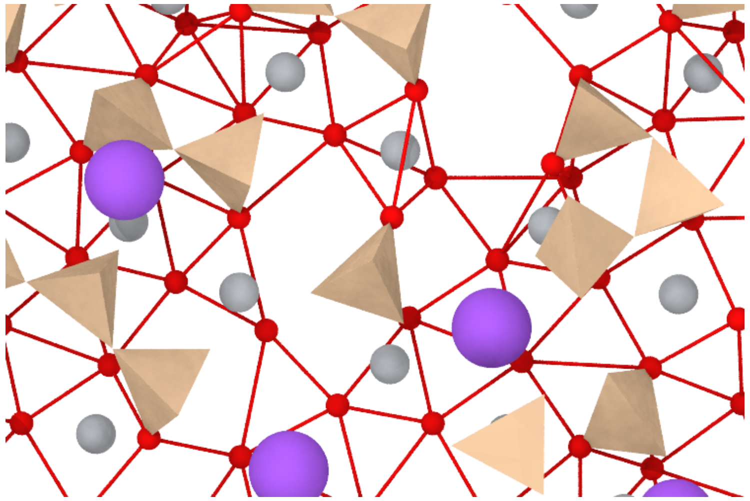

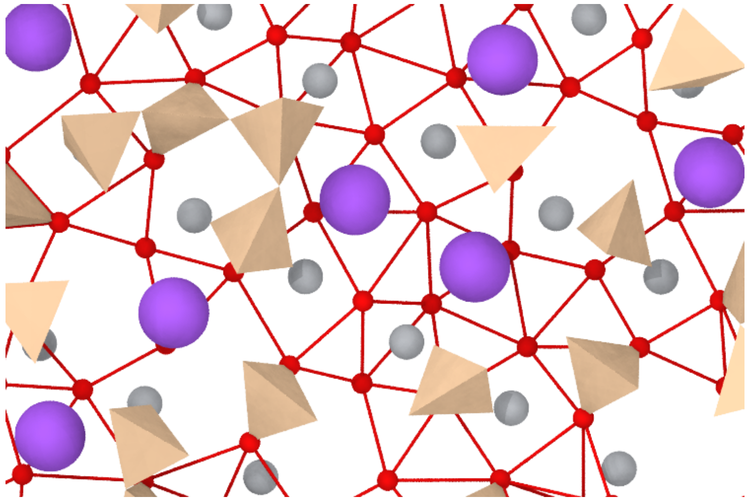

0% Na_2O

10% Na_2O

20% Na_2O: aligned Na

Sodium effect

- Na-rich channels
- Na concentration does not seem to change SiO_4 ordering
- Face-connected tetrahedra not dominant

Ordering beyond the first glass layer: (100) interface

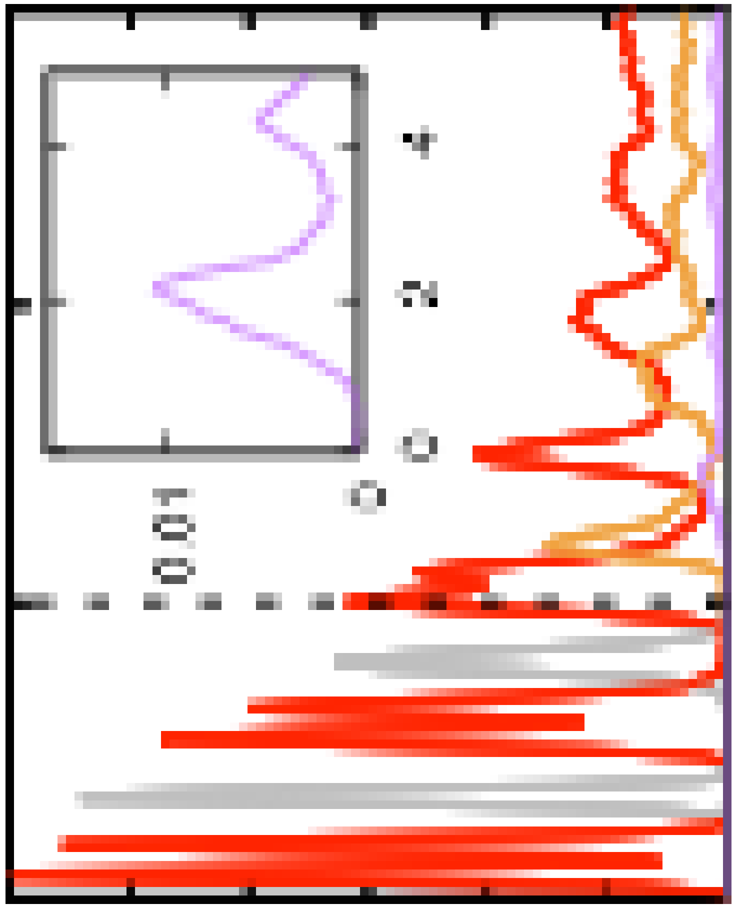

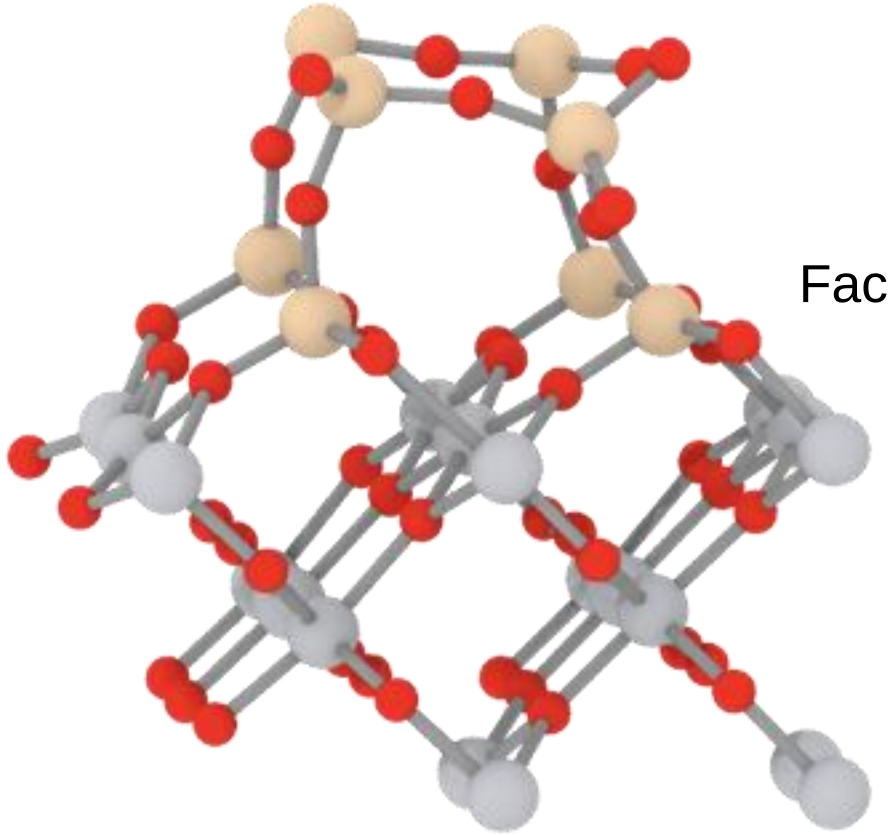

Arches: successive
rings with 4 Si and 1 Ti

Face-connected SiO_4

TiO_2 crystal

Face-connected tetrahedra

- Constrain the glass network
- Cause layering in the glass phase
- Open possible diffusion channels

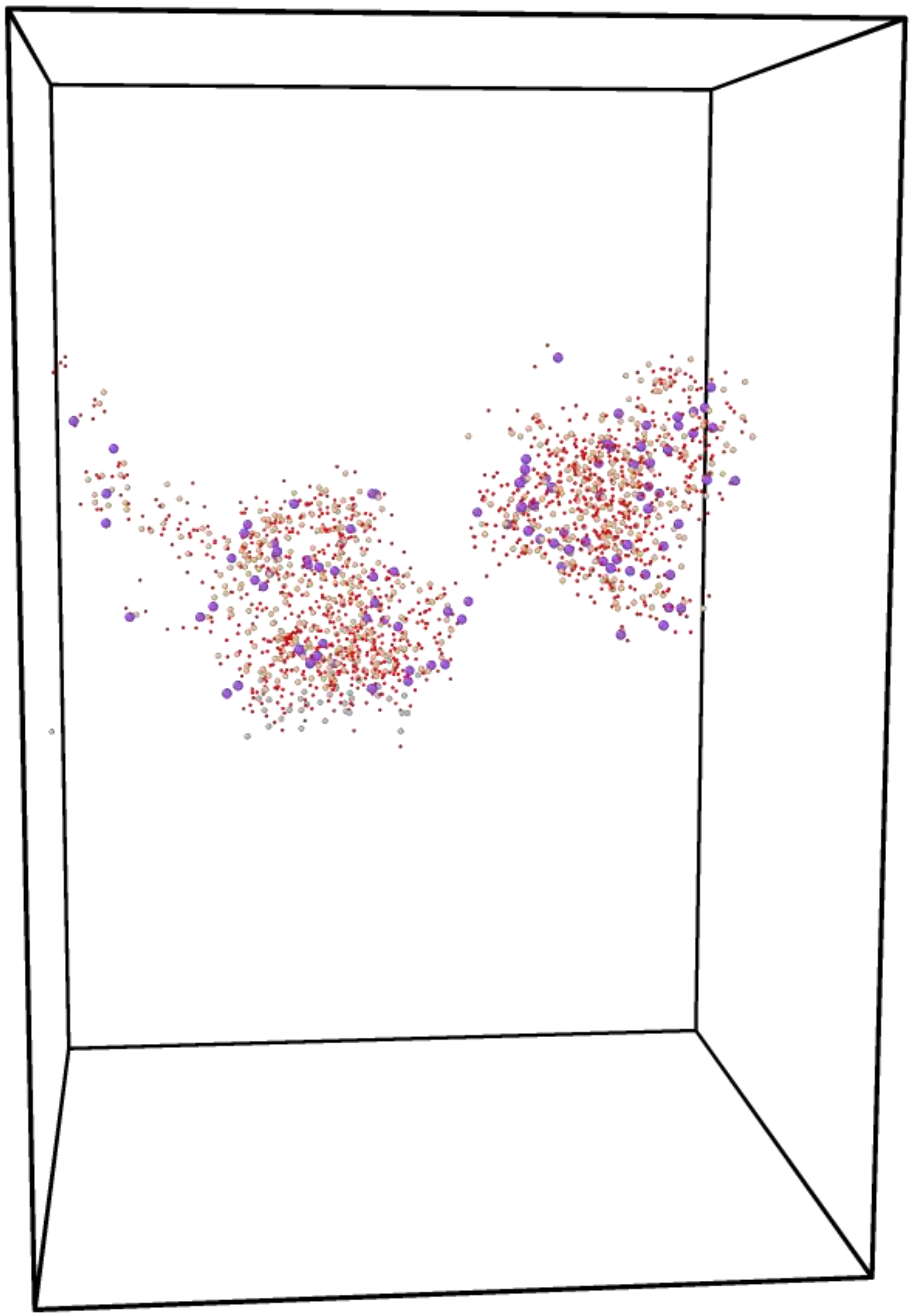

Radiation damage

Modelling approach

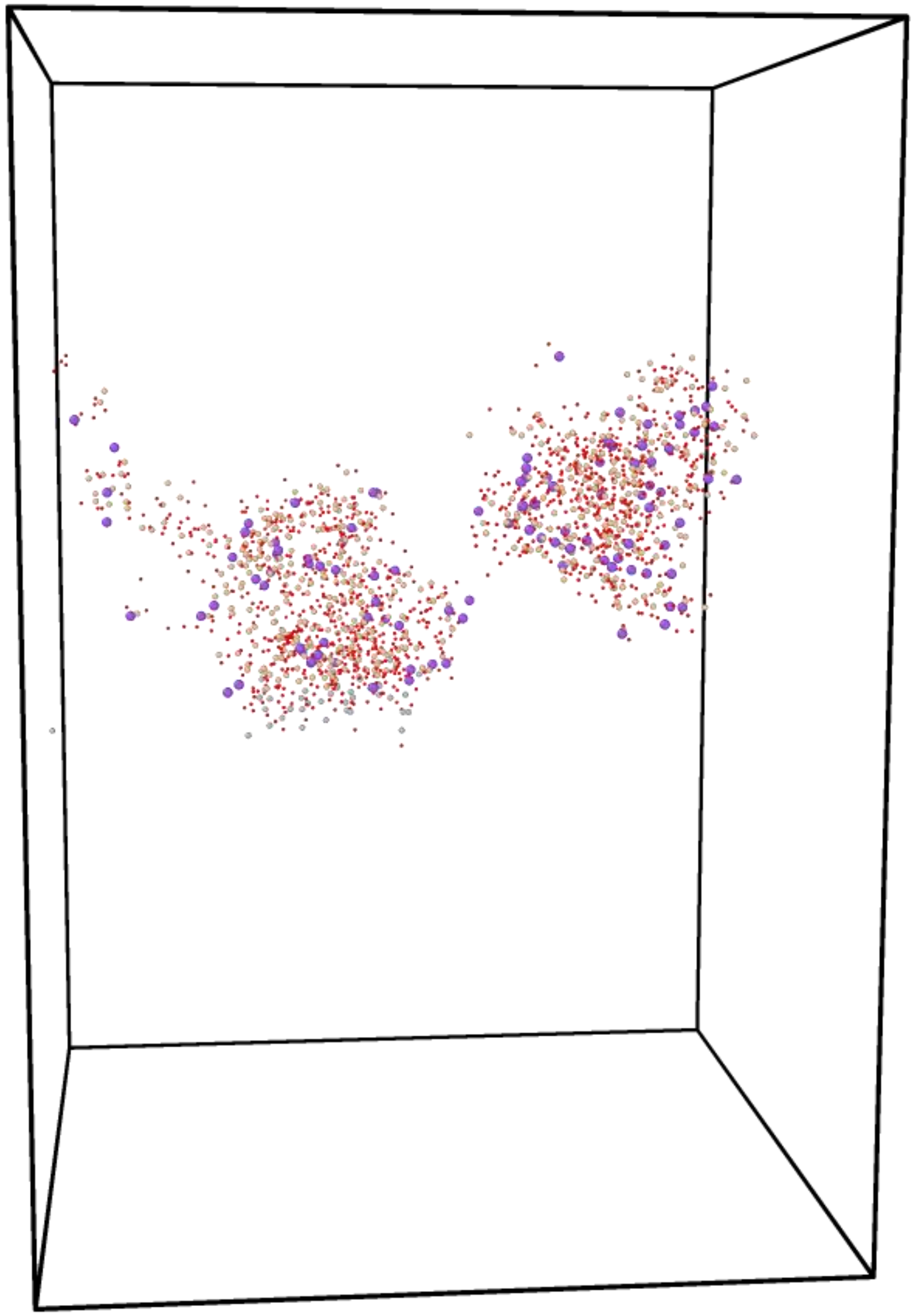

Displaced atoms during a 10 KeV cascade in glass with 10 wt% Na_2O

Cascades

- One initial high-energy atom (PKA)
- Energy spread along high-energy particles trajectories
- Branches
- ~ 10 keV range

Cascades: channeling

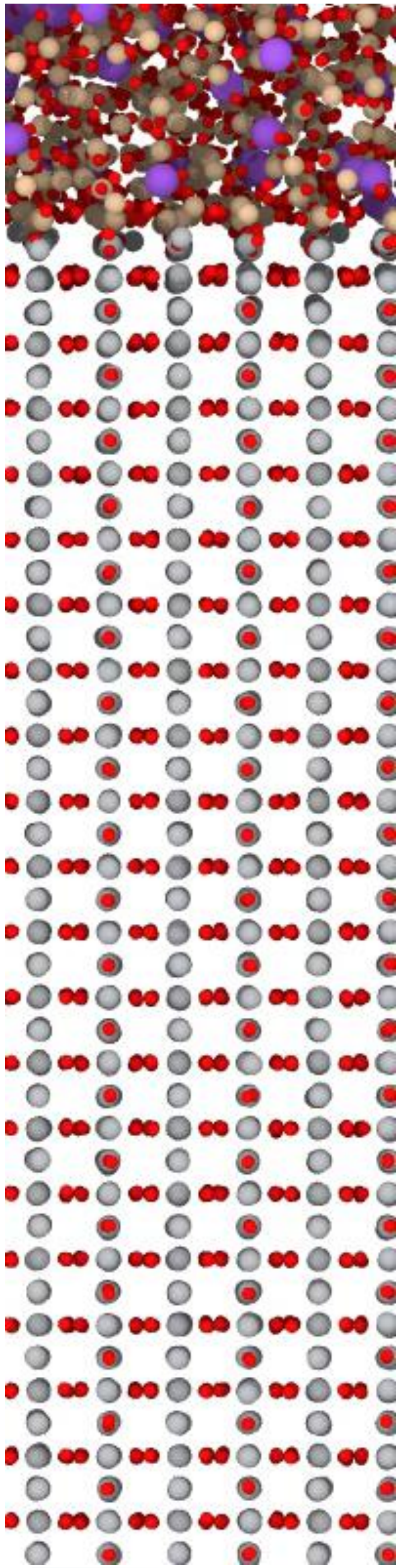

- Observed for both Na and Si
- Main direction: [001]

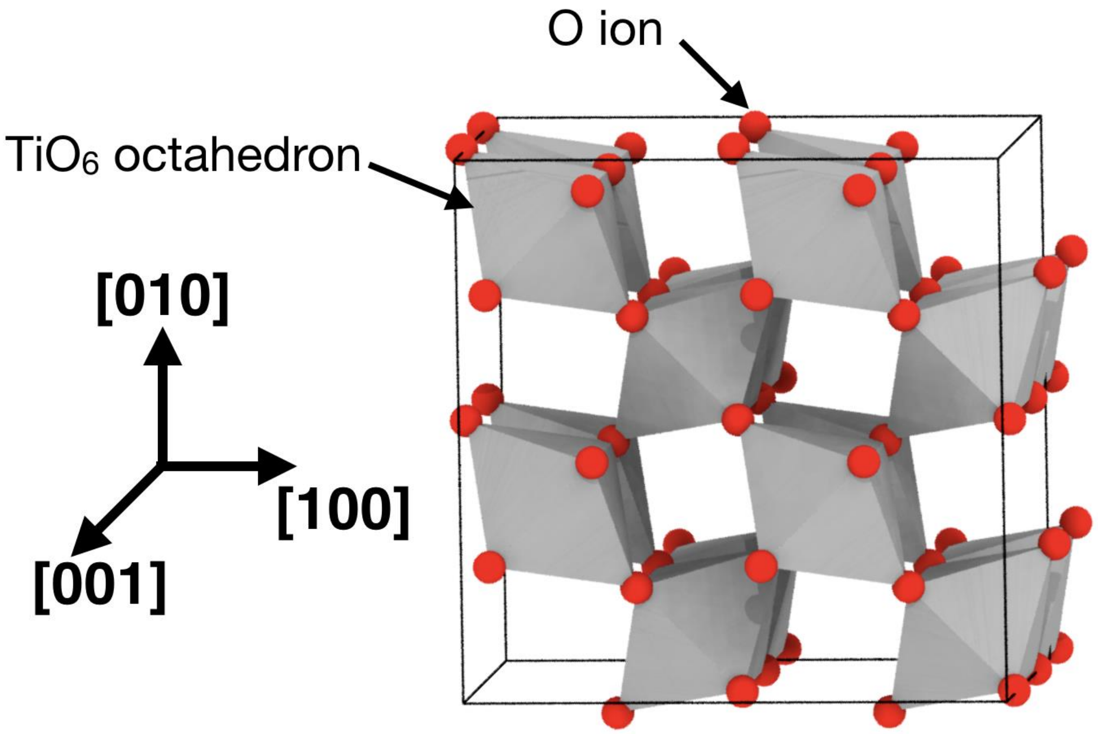

Channeled cations

- Tend to travel along channels far from interface
- Results in subcascades in the bulk crystal
- Not much energy is deposited close to the interface

10 keV cascade on (001) interface

Cascades: extrinsic defects

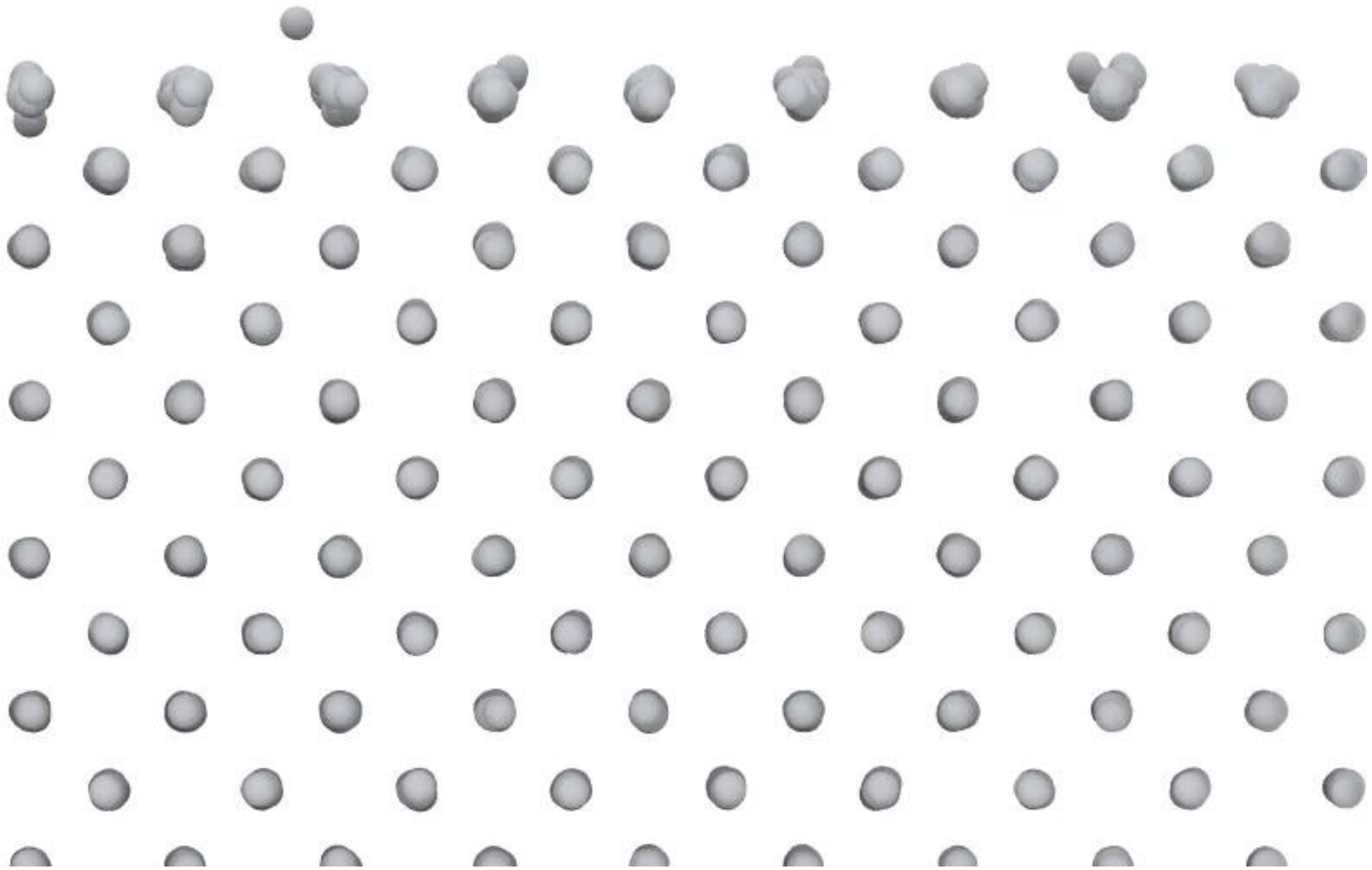

10 keV cascade on (100) interface;
only Ti ions and the PKA are shown

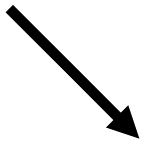

[110]

Some ion exchange

- Mostly Ti ➔ glass (rarely beyond the first layer)
- Some Na and Si ➔ crystal (channeled)

Cascades: defect energies

Defect	ΔE
$\mathrm{Ti}_{\mathrm{glass}}$	0.5 eV
Ti_{i}	3.5 eV
Na_{i}	0.7 eV
$\mathrm{Si}_{\mathrm{Ti}}$	1 eV

Estimates from simulations with x=0.1

- Driving force for Ti_{i} to move to the glass once they have formed
- Si tends to be substitutional
- Na tends to be interstitial

Cascades: interface ordering

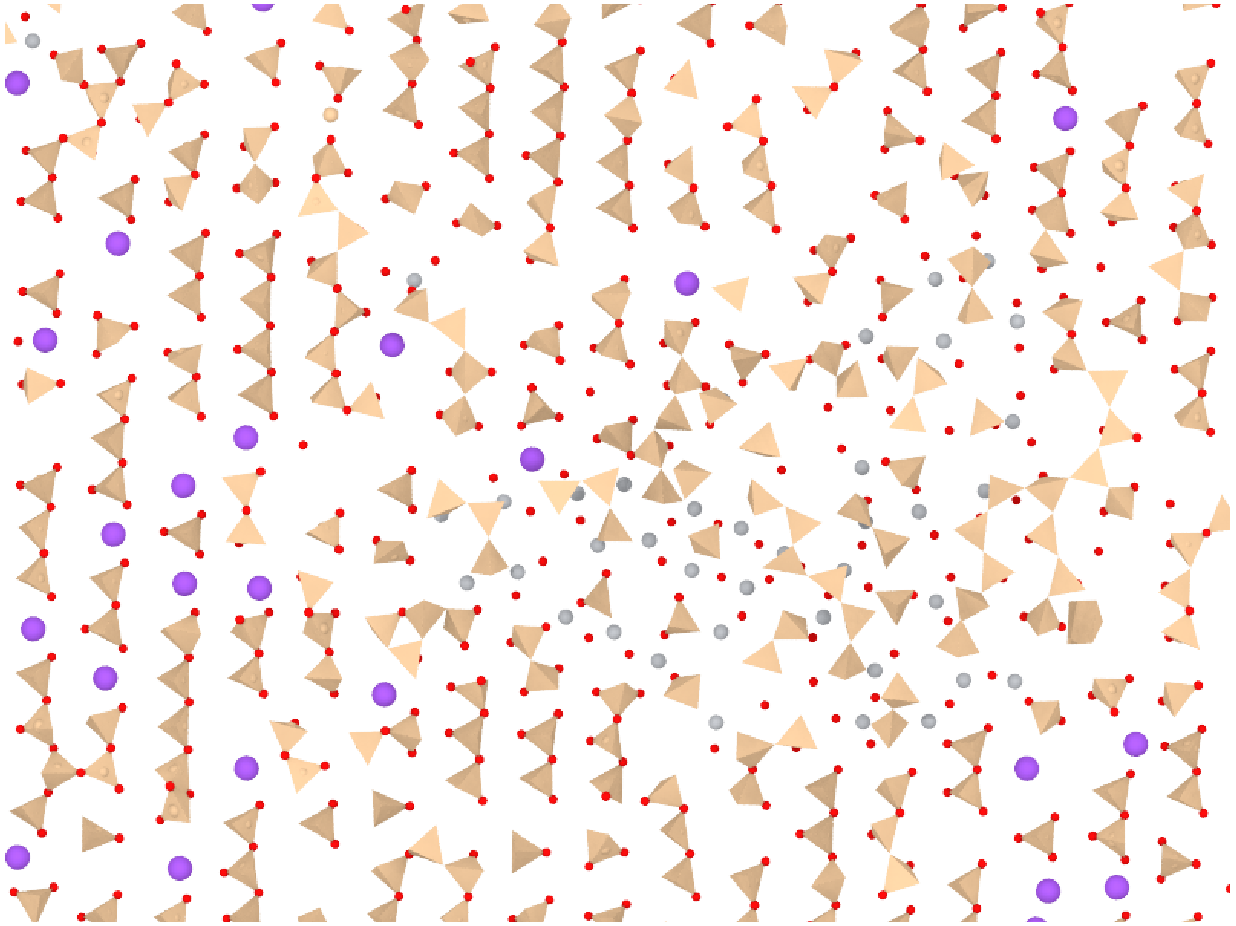

10 keV cascade on (100) interface (x=0.1)

Ordering perturbations

- Ti-rich regions in the silicate layer
- Ti coordination environments
    - 4 (tetrahedra)
    - 5 (truncated octahedra)
    - 6 (octahedra)
- Tend also to be poor in Na

Plan: Next steps

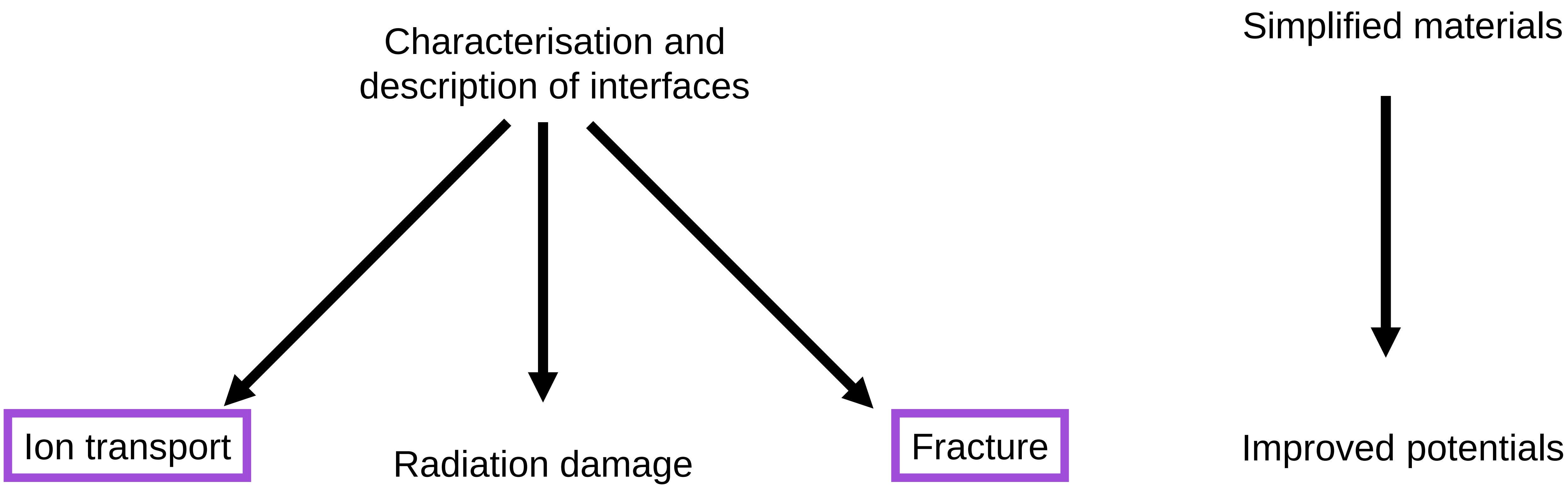

Characterisation and description of interfaces

Ion transport

Radiation damage

Fracture

Simplified materials

Improved potentials

Other crystal structures

- Spinel
- Zeolites

Acknowledgments

Erik Hansen
Robin Grimes

Computing facilities

- Imperial College HPC facilities
- Thomas (Tier-2 hub in Materials and Molecular Modelling)

Imperial College London

Centre for Nuclear Engineering

DISTINCTIVE

EPSRC
Engineering and Physical Sciences Research Council

Imperial College
London

Centre for Nuclear
Engineering

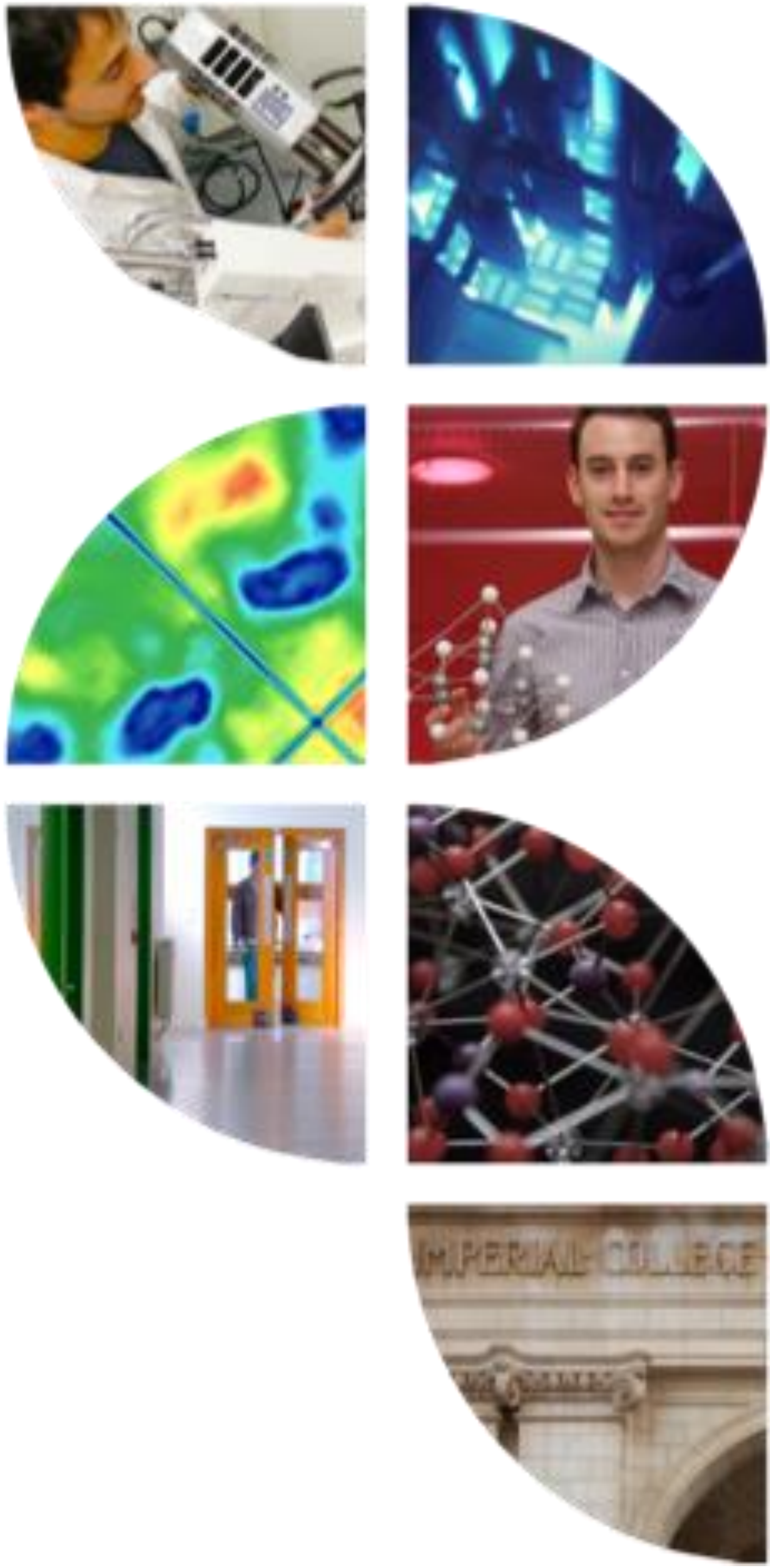

Durability of heterogeneous ILW glass/ceramic wasteforms

for complex waste streams

Paul C. M. Fossati, Michael J. D. Rushton & William E. Lee

p.fossati@imperial.ac.uk

DISTINCTIVE

16 October 2017

Switching on Ion Exchange in Metal Germanates

Ryan George

Research Councils UK Energy For a Low Carbon Future

DISTINCTIVE

Clinoptilolite (Clino)

- Natural zeolite used for Cs and Sr removal In SIXEP.
- Found worldwide – mined commercially in 16 countries.
- SIXEP clino shows high Cs and Sr selectivity.
- Composition varies, so does level of impurities.

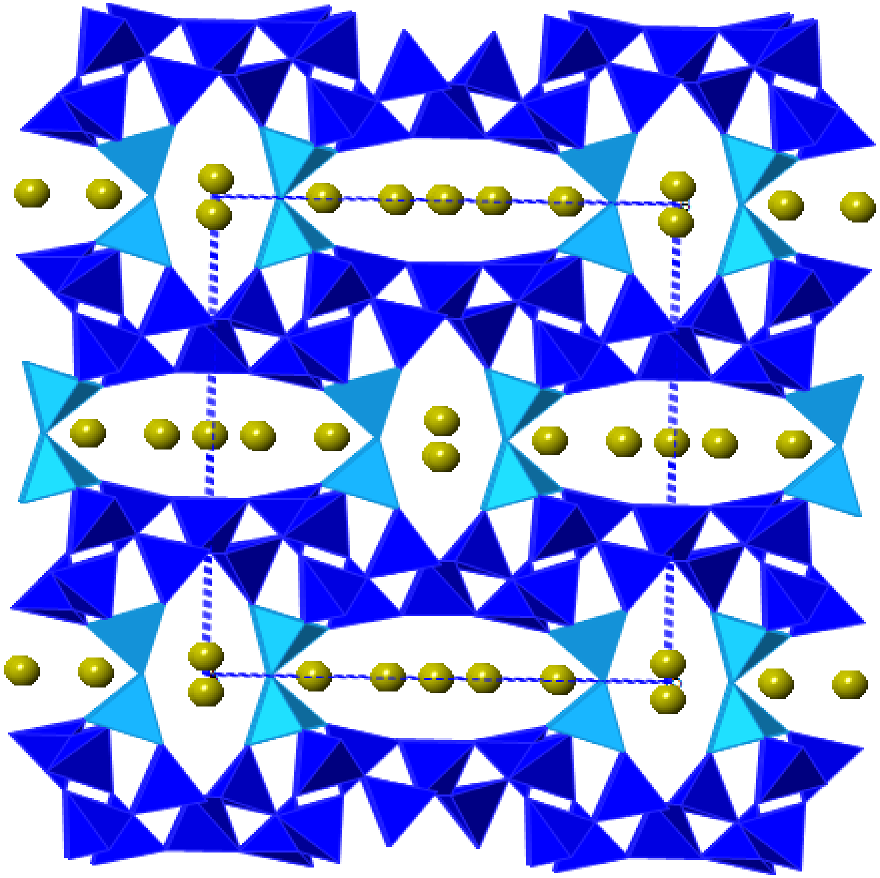

Design Principles

- Target ^{137}Cs and ^{90}Sr
- Design Principles
  - High thermal and chemical stability.
  - Potential direct thermal conversion to wasteform.
  - Medium sized pores (6-8 ring pore openings).
  - Hydrated cations located in channels, exchange K^+ for Na^+/H^+.

Octahedral-tetrahedral frameworks

- Some of these materials are naturally occurring.
- A wide range of materials have been synthesised with various different metal octahedra and Si tetrahedra.
- These materials are microporous and have hydrated cations in the channels, commonly sodium and potassium. Hence the interest as potential ion exchange materials.

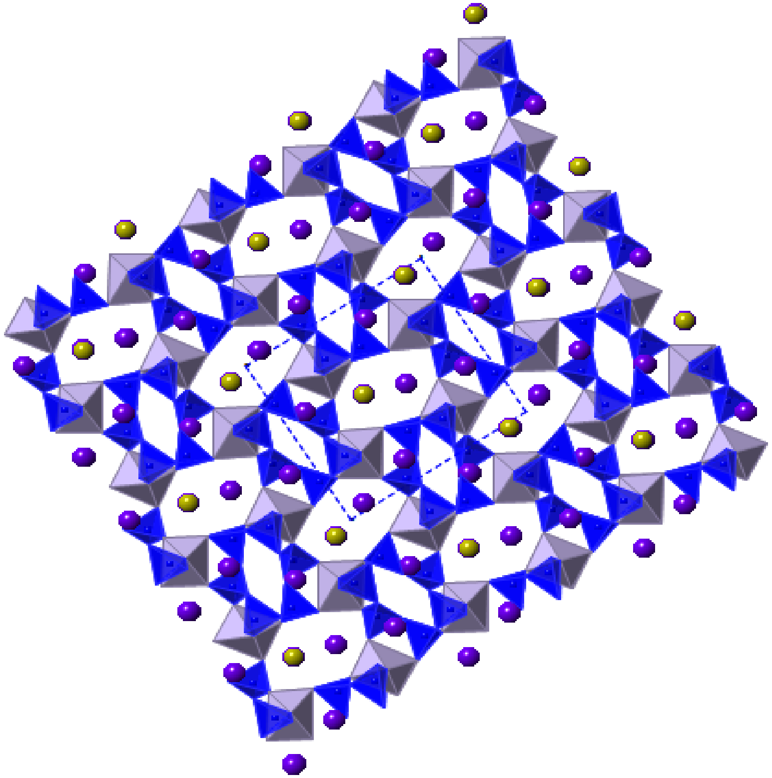

Octahedral-Tetrahedral frameworks

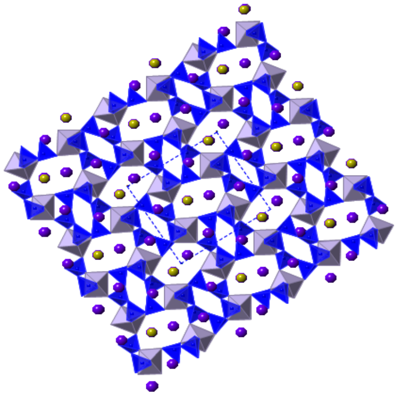

AV-7: $Na_{0.5}K_{1.5}SnSi_3O_9.H_2O$

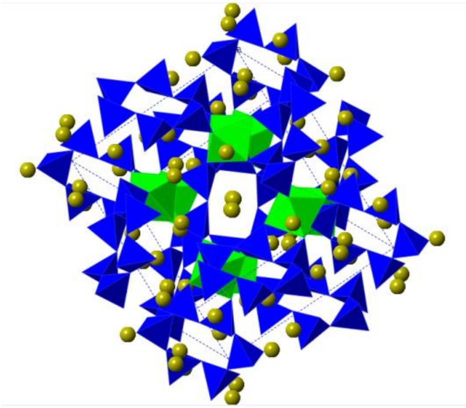

AV-13: $Na_{2.26}(Sn/Zr/Hf)Si_3O_9Cl_{0.26}.xH_2O$

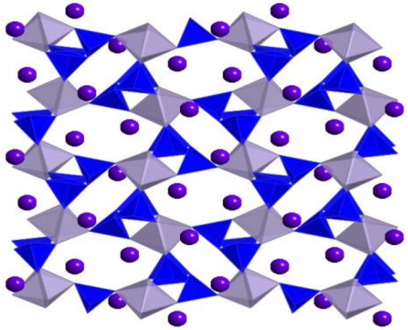

AV-6: $K_2(Sn/Zr/Ti)Si_3O_9\cdot H_2O$

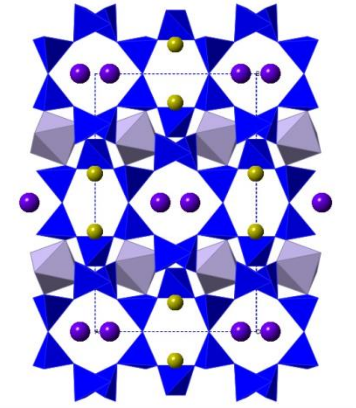

EMS-2: $Na_4K_4Sn_4Si_{20}O_{52}.12H_2O$

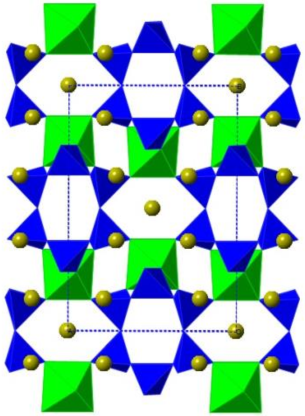

AV-3: $Na_5Zr_2Si_6O_{18}(Cl,OH)\cdot 2H_2O$

Ge vs Si

- Most of the published work covered focuses on changing the octahedral metal ion.
- Variation of the tetrahedral component may allow for further tunability.

Element	CN	Ionic radius
Si^{4+}	4	0.26 Å
Ge^{4+}	4	0.39 Å

OT Germanate phases

- Small number of microporous germanates are known.
- First phase of interest is $K_2ZrGe_3O_9.H_2O$, originally reported by Plevert *et al*., *Inorg. Chem*, 2003, **42**, 5954-5959.
- This is a germanate derivative of the natural zirconosilicate mineral Umbite.
- Ion exchange properties not explored in the literature.

Umbite type materials

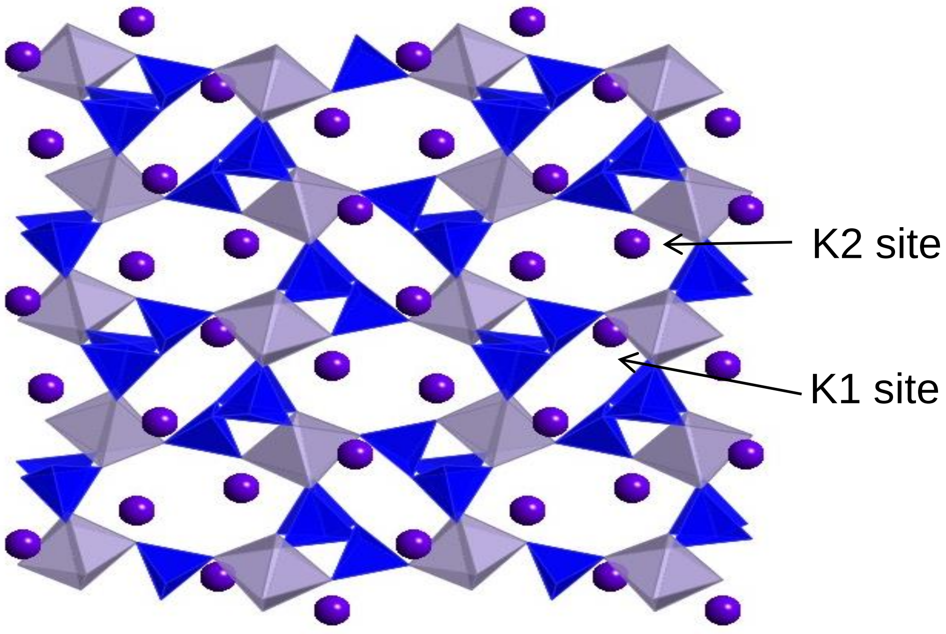

- $K_2MSi_3O_9.H_2O$ where M = Ti, Sn and Zr are all known with ion exchange properties explored.
- VT XRD shows conversion to Wadeite ($K_2MGe_3O_9$) at ~750°C

$K_2ZrGe_3O_9.H_2O$

- Hydrothermal synthesis optimised to produce multigram quantities (ca. 80% isolated yield) from GeO_2, $ZrOCl_2.8H_20$ and KOH at 200°C for 24 hours.
- Plevert *et al* recipe would yield around 0.3g per batch with a longer synthesis time.
- Next step was ion exchange

Ion exchange method

- 0.1M Cs/Sr nitrate solutions
- 1:100 w/v ratio of sample to solution
- 24 hour exchange at room temperature
- Sample shaken at 140 rpm
- Exchange analysed by XRF

Element	Uptake
Na	No
Mg	No
Ca	Very Low
Sr	Very Low
Cs	Very Low
Cs + K	Further reduces Cs uptake

Fused Beads

- Sample pre-treated at 800°C.
- Sample mixed with Li borate glass flux in a 1:10 ratio.
- Mixture heated in a platinum crucible at 1050°C with a 7:7:2 heating regime.
- Better data quality than loose powder and pressed pellet.

$K_2ZrGe_3O_9.H_2O$ Ion exchange

Element	Molar ratio	Expected ratio
Ge	1	1
Cs	0.02	-
Zr	0.41	0.33
K	0.68	0.66

- XRF analysis on fused beads

Nb substitution

Element	CN	Ionic radius
Zr^{4+}	6	0.72 Å
Ti^{4+}	6	0.605 Å
Sn^{4+}	6	0.69 Å
Nb^{5+}	6	0.64 Å

- $Nb^{5+} \longrightarrow Zr^{4+} + K^{+}$
- Single phase up to 30% Nb^{5+} for Zr^{4+}

Nb substitution

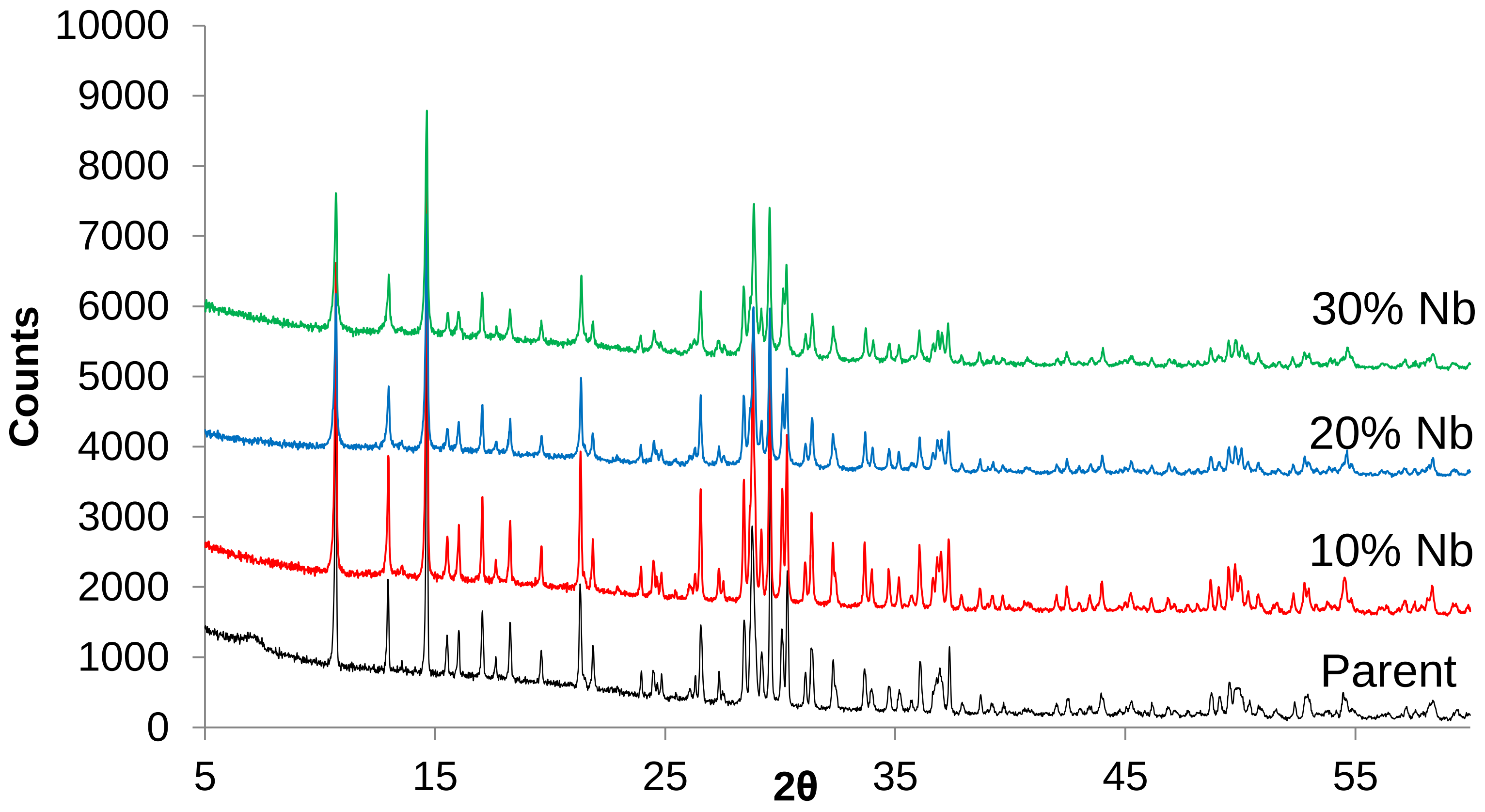

$K_{2-x}Zr_{1-x}Nb_xGe_3O_9.H_2O$ Ion exchange

	10% Nb	**20% Nb**	**25% Nb**
Element	**Molar ratio**	**Molar ratio**	**Molar ratio**
Ge	1	1	1
Cs	0.16	0.17	0.39
Zr	0.36	0.33	0.32
K	0.54	0.56	0.28
Nb	0.04	0.08	0.1

- XRF analysis on fused beads

Pharmacosiderites

- Sn, Ti substitutions and Nb 40% doping result in the formation of pharmacosiderite phases.

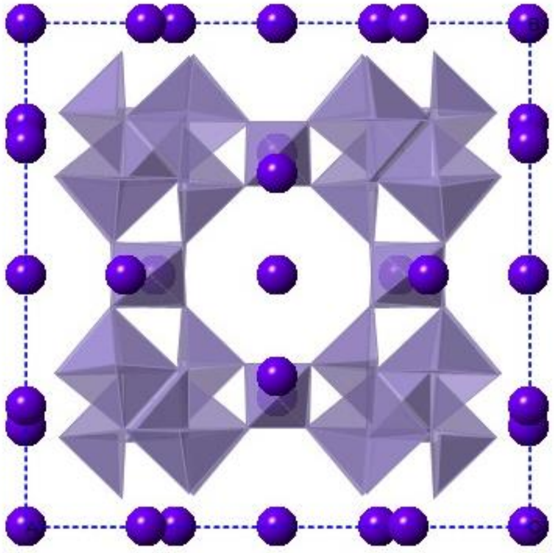

$HK_3Ge_7O_{16}.4H_2O$

Sn and 40% Nb as impurity

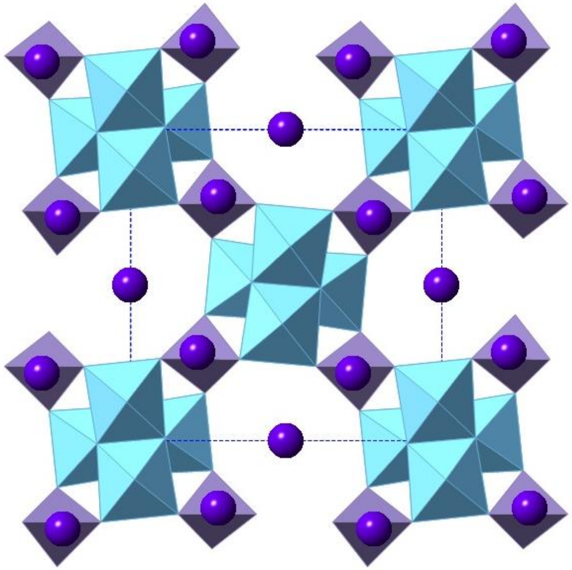

$HK_3Ti_4Ge_3O_{16}.4H_2O$

Ti source

Pharmacosiderites

$HK_3Ge_7O_{16}.4H_2O$

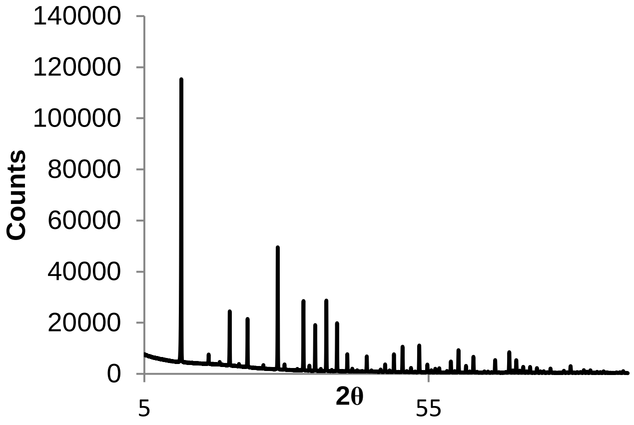

	Parent	Cs	Sr
Element	**Molar ratio**	**Molar ratio**	**Molar ratio**
Ge	1	1	1
K	0.47	0.18	0.44
Sr	-	-	0.03
Cs	-	0.38	-

$HK_3Ti_4Ge_3O_{16}.4H_2O$

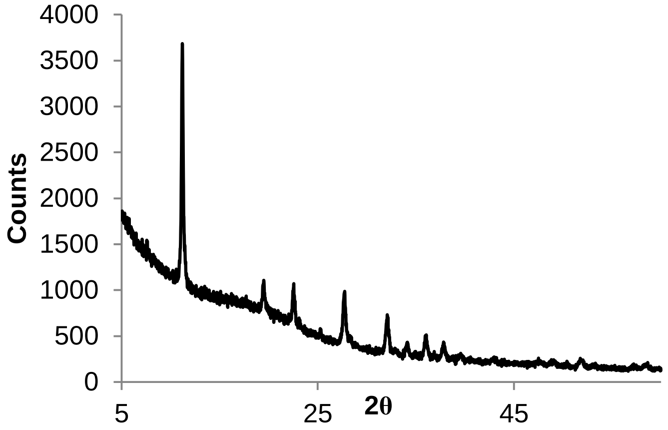

	Parent	Cs	Sr
Element	**Molar ratio**	**Molar ratio**	**Molar ratio**
Ge	1	1	1
Ti	1.12	1.08	1.13
K	0.86	0.21	0.29
Sr	-	-	0.28
Cs	-	1.05	-

Research Councils UK Energy For a Low Carbon Future

DISTINCTIVE

Summary

- Substitution of Ge for Si in the umbite structure does not improve ion exchange properties.
- Ion exchange can be switched on by doping Nb^{5+} for Zr^{4+}, with facile Cs^+ uptake in $K_{2-x}Zr_{1-x}Nb_xGe_3O_9.H_2O$.
- Other framework substitutions result in the formation of pharmacosiderite phases, which have also been shown to be good exchangers.

Further work

- Measuring K mobility.
- Studying thermal decomposition products of doped umbites and exchanged materials.
- Thermal decomposition of Pharmacosiderites and exchanged materials.
- Studying sodium exchange in ZrGeUmbite.

Acknowledgements

- Dr Joe Hriljac
- Dr Tzu-Yu Chen

EPSRC
Engineering and Physical Sciences
Research Council

PER AD
ARDUA ALTA
UNIVERSITY OF
BIRMINGHAM

investing
in **your** future
European Regional Development Fund
European Union

Advantage
West Midlands
www.advantagewm.co.uk

Research Councils UK
Energy
For a Low Carbon Future

DISTINCTIVE

Investigations into dynamic shear based filtration of ferric floc

Keith Schou

Supervised by R.Holdich and M.Dragosavac

Background

During micro and ultrafiltration, filter blocking rapidly reduces the flux.

Shear enhanced (or Dynamic) filtration has been shown to have very large increases in flux up to 17x(1)

Typical increases in pseudo steady state flux is in the region of 2-4x.
(flux is the flow rate of liquid across the filter)

[1] M.Y. Jaffrin, L-H Ding, O. Akoum, A. Brou, A hydrodynamic comparison between rotating disk and vibratory dynamic filtration systems. *J Memb Sci*. 2004; 242: 155-167.

Dynamic Shear

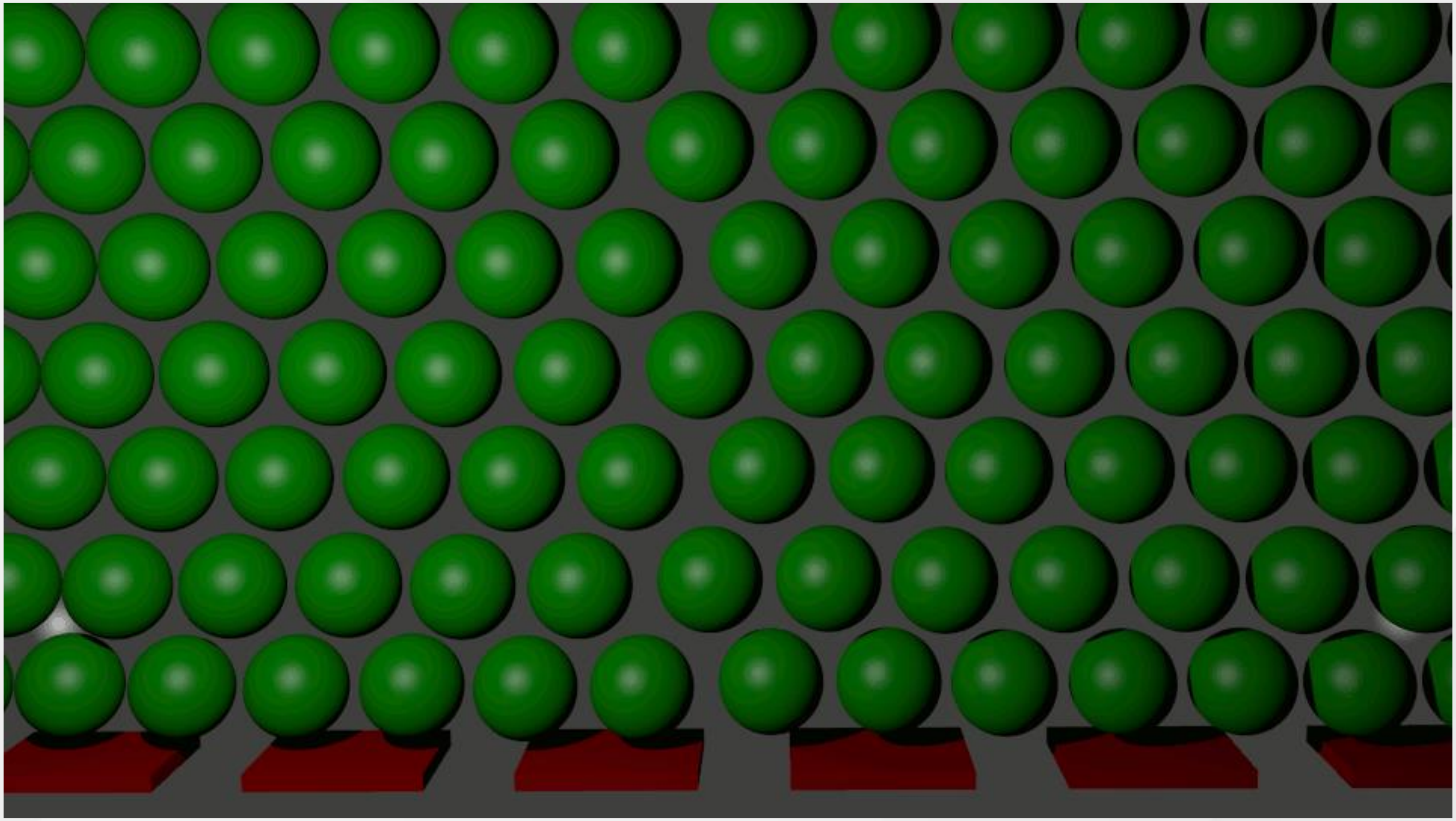

Oscillating membrane wall

Axial and Azimuthal

Azimuthal

Oscillating up to 100Hz

Axial

Calcite – what is it?

Calcium carbonate in cubic crystals.

Aka chalk

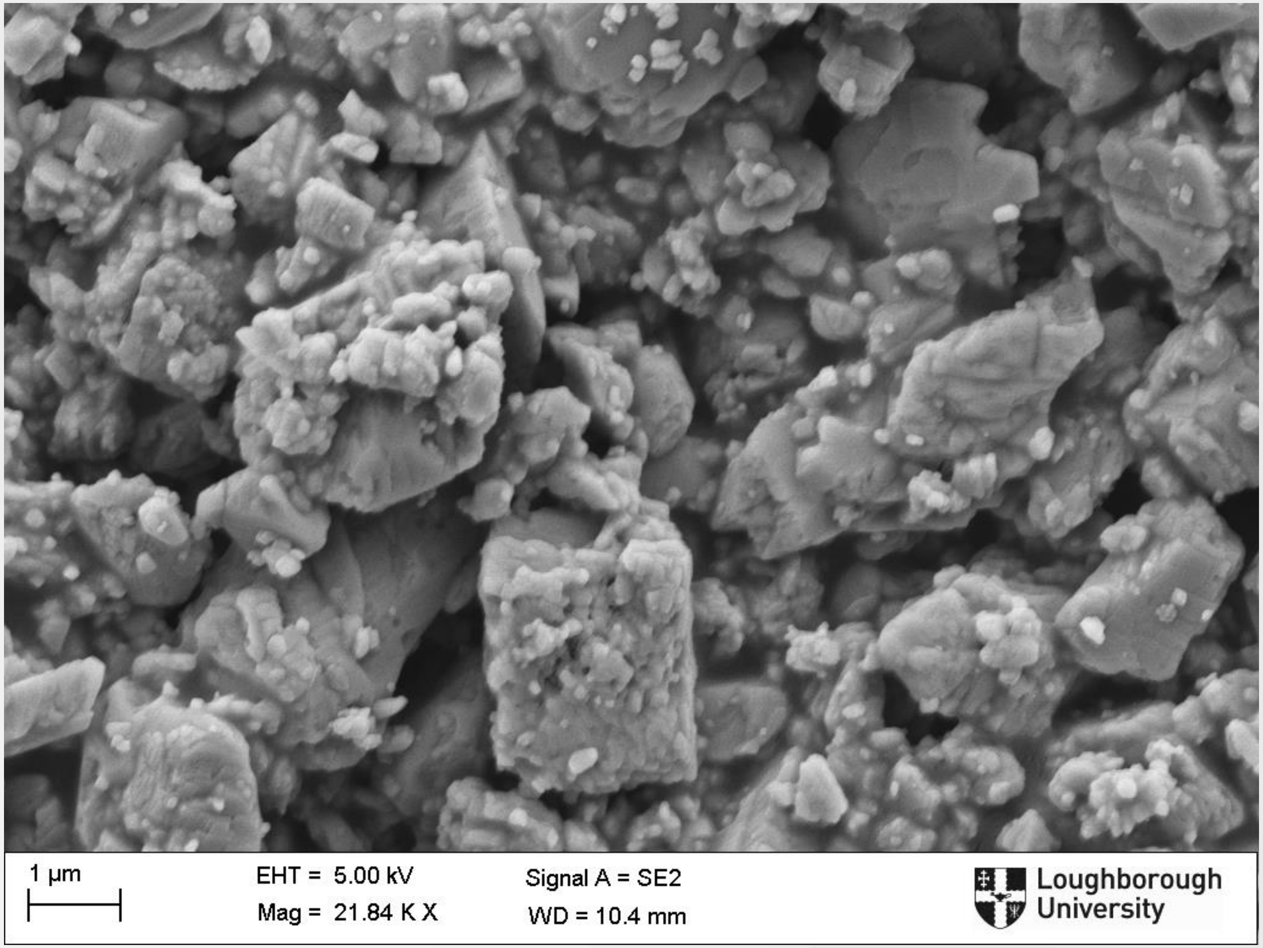

Calcite – PSD

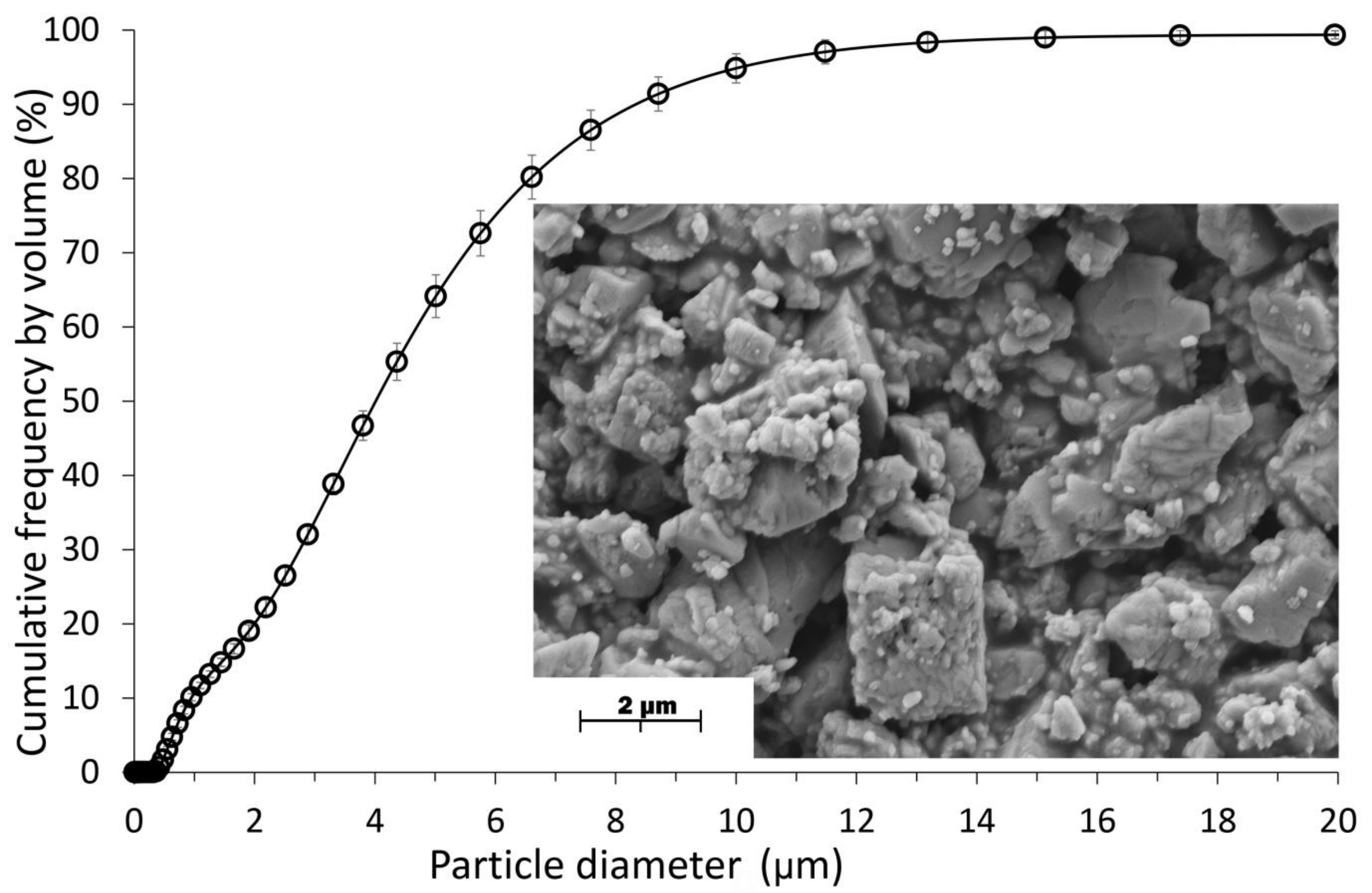

Cumulative frequency by volume (%)
100
90
80
70
60
50
40
30
20
10
0
0
2
4
6
8
10
12
14
16
18
20
Particle diameter (μm)
2 μm

Calcite - Cake

The cake is an average of 37% by volume, found from 27 gravimetric tests.

Rheogram of ~37% Calcite

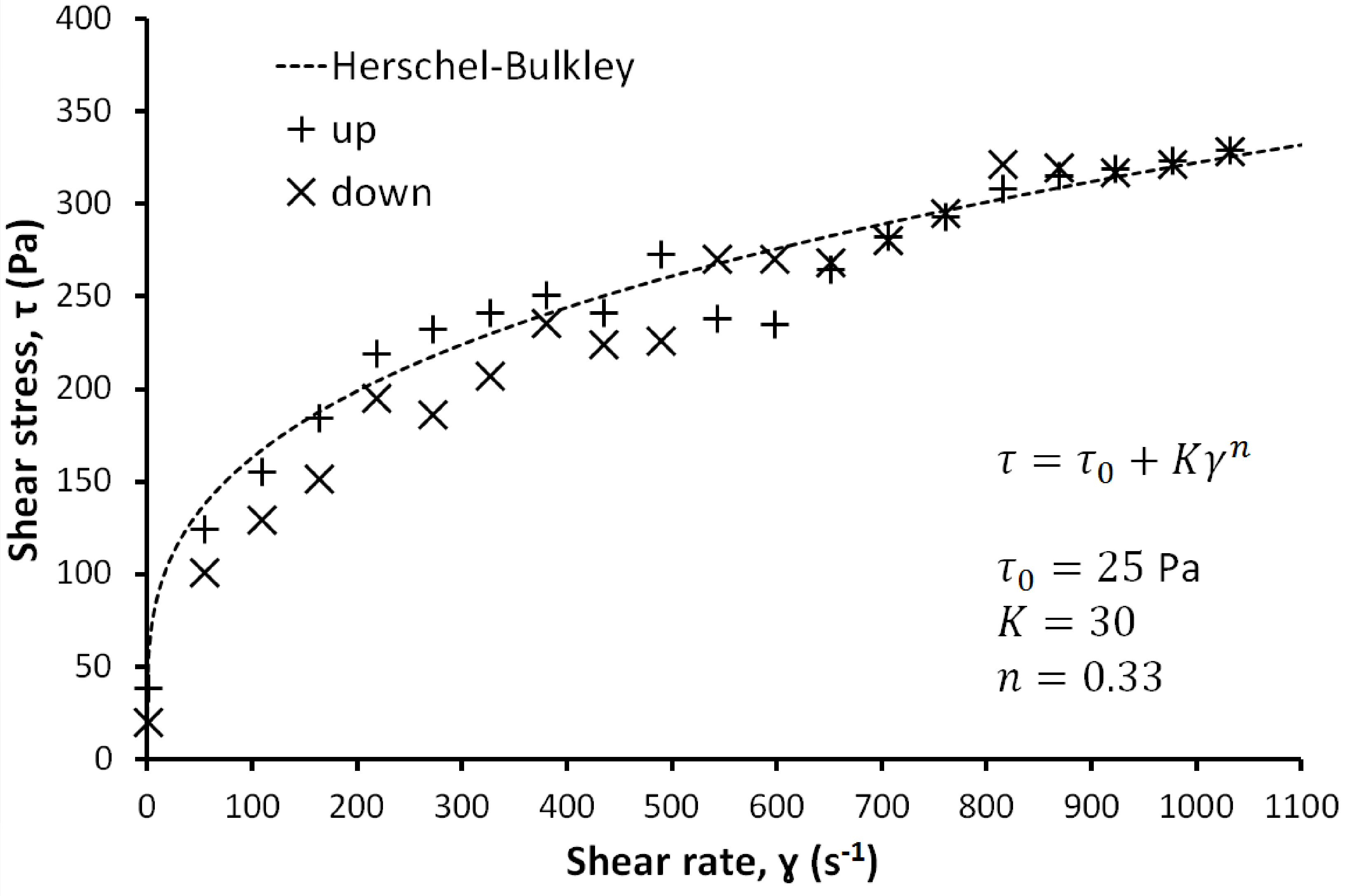

$$\tau = \tau_0 + K\gamma^n$$

$\tau_0 = 25$ Pa
$K = 30$
$n = 0.33$

Experimental Setup - Diagram

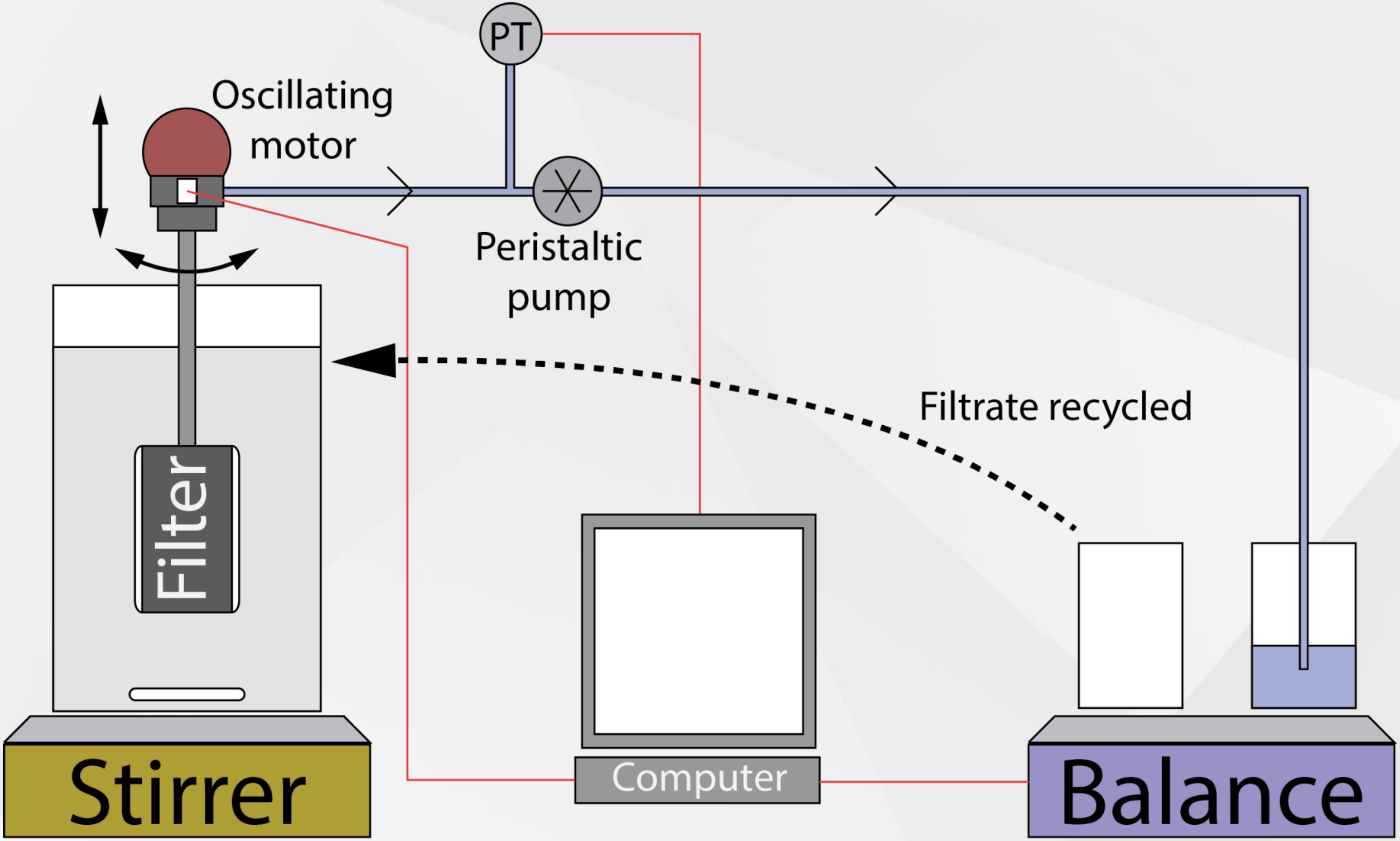

Experimental Setup - Filters

Nominal pore size 1µm

Ceramic Filter

Nickel

Slots 400µm x 7µm

The Filters

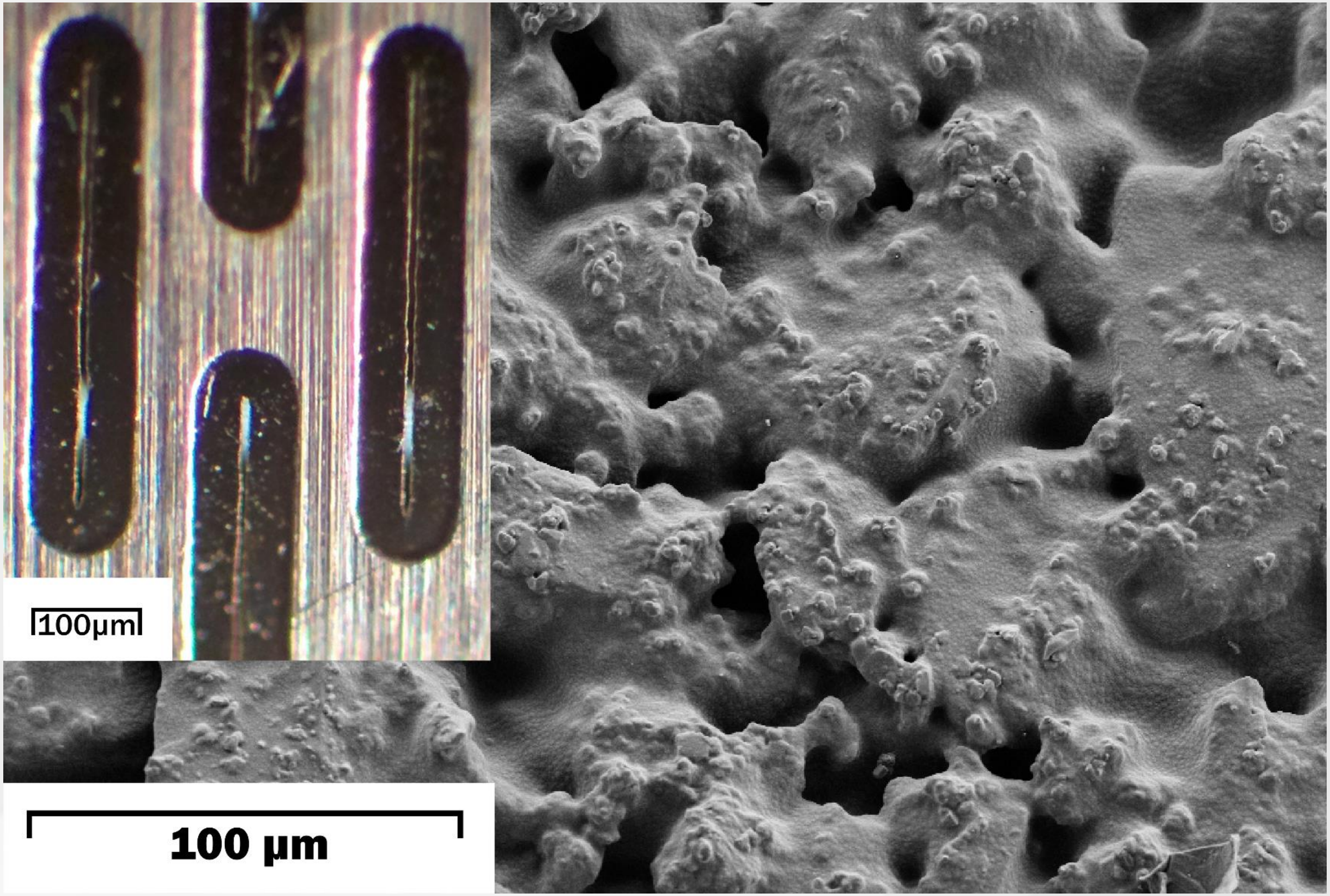

Flux vs time

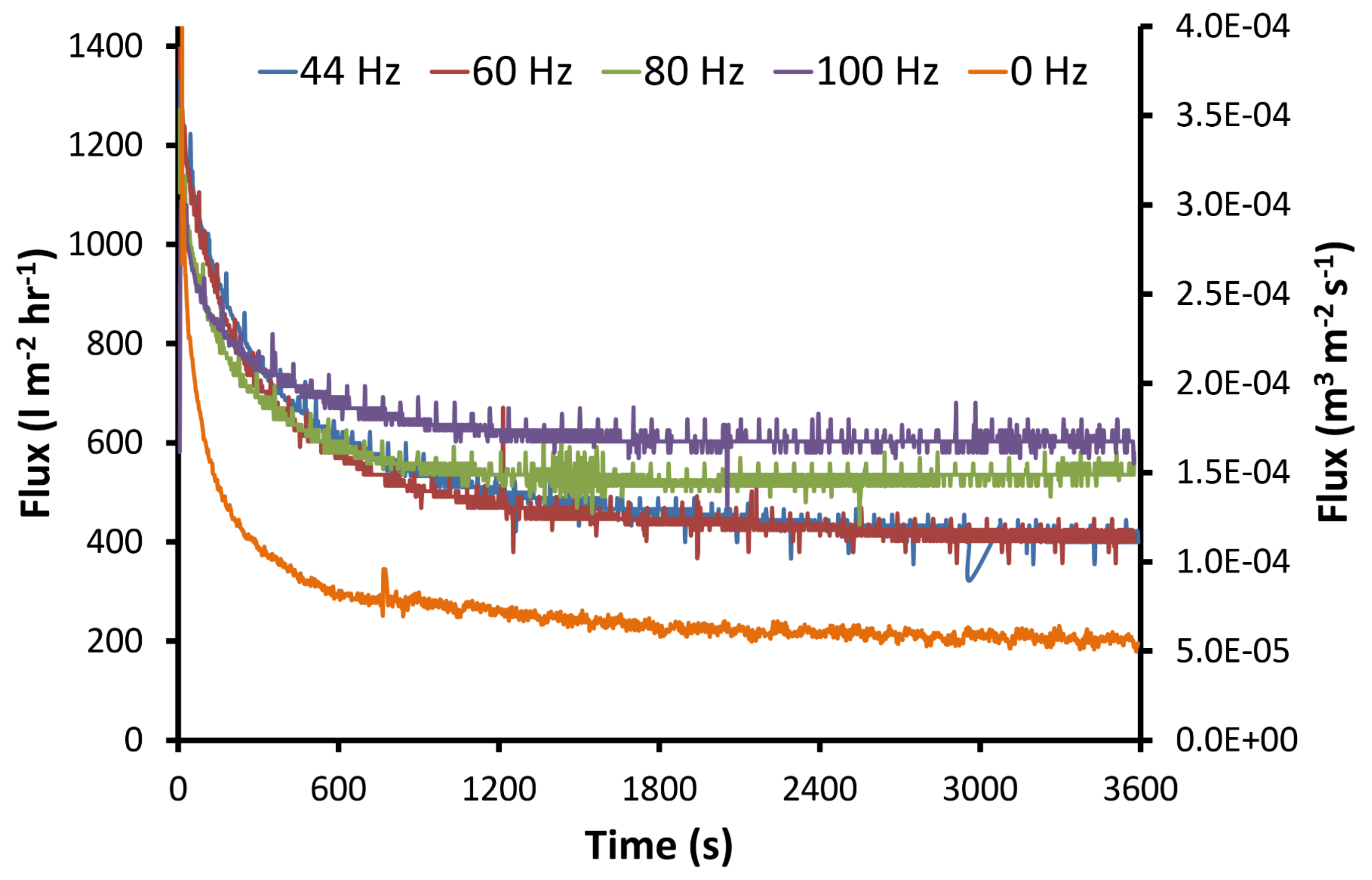

44 Hz
60 Hz
80 Hz
100 Hz
0 Hz
Flux (l m^{-2} hr^{-1})
0
200
400
600
800
1000
1200
1400
Flux (m^3 m^{-2} s^{-1})
0.0E+00
5.0E-05
1.0E-04
1.5E-04
2.0E-04
2.5E-04
3.0E-04
3.5E-04
4.0E-04
Time (s)
0
600
1200
1800
2400
3000
3600

Resistance vs shear

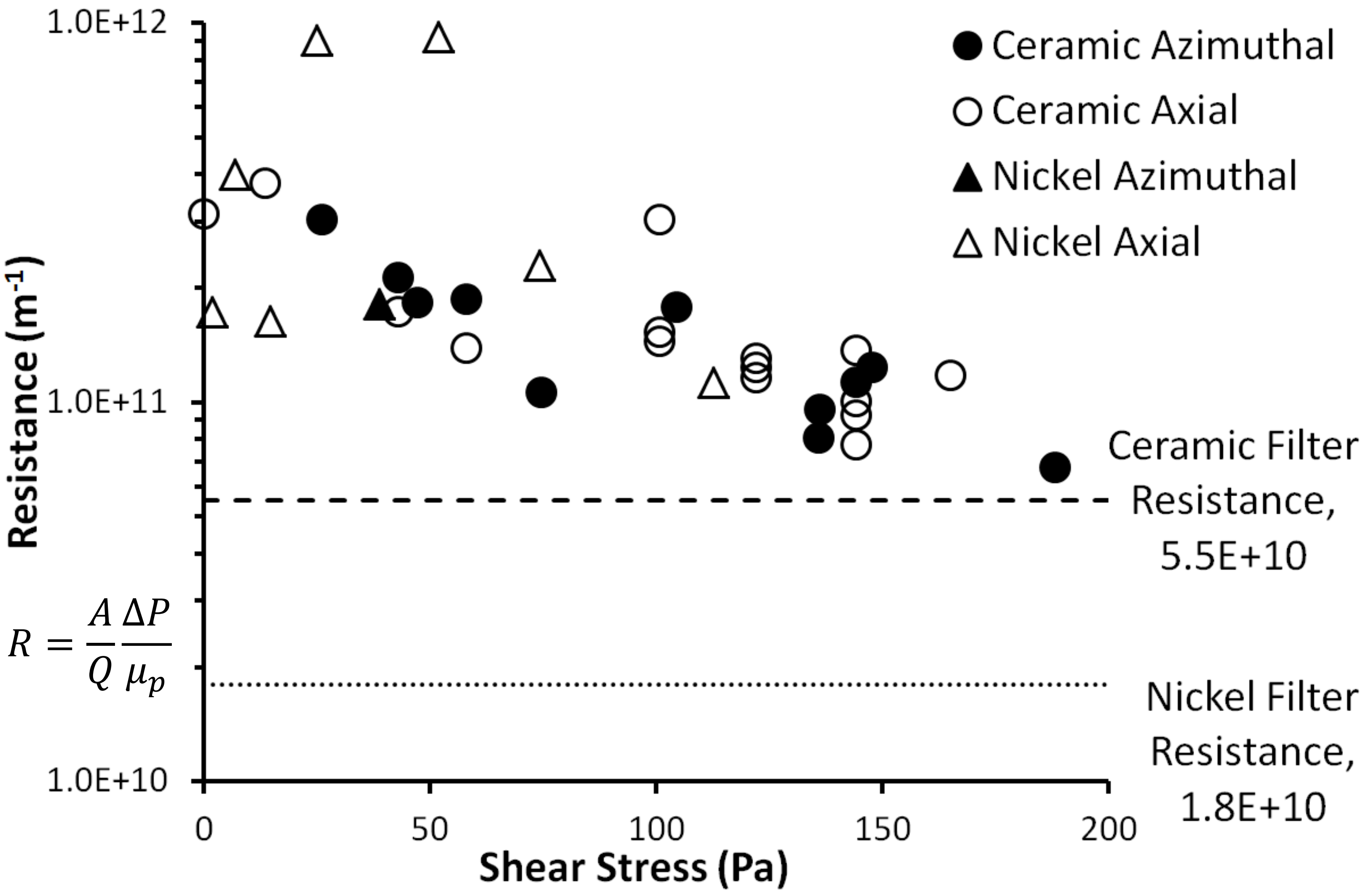

$$R = \frac{A}{Q}\frac{\Delta P}{\mu_p}$$

Cake thickness vs shear

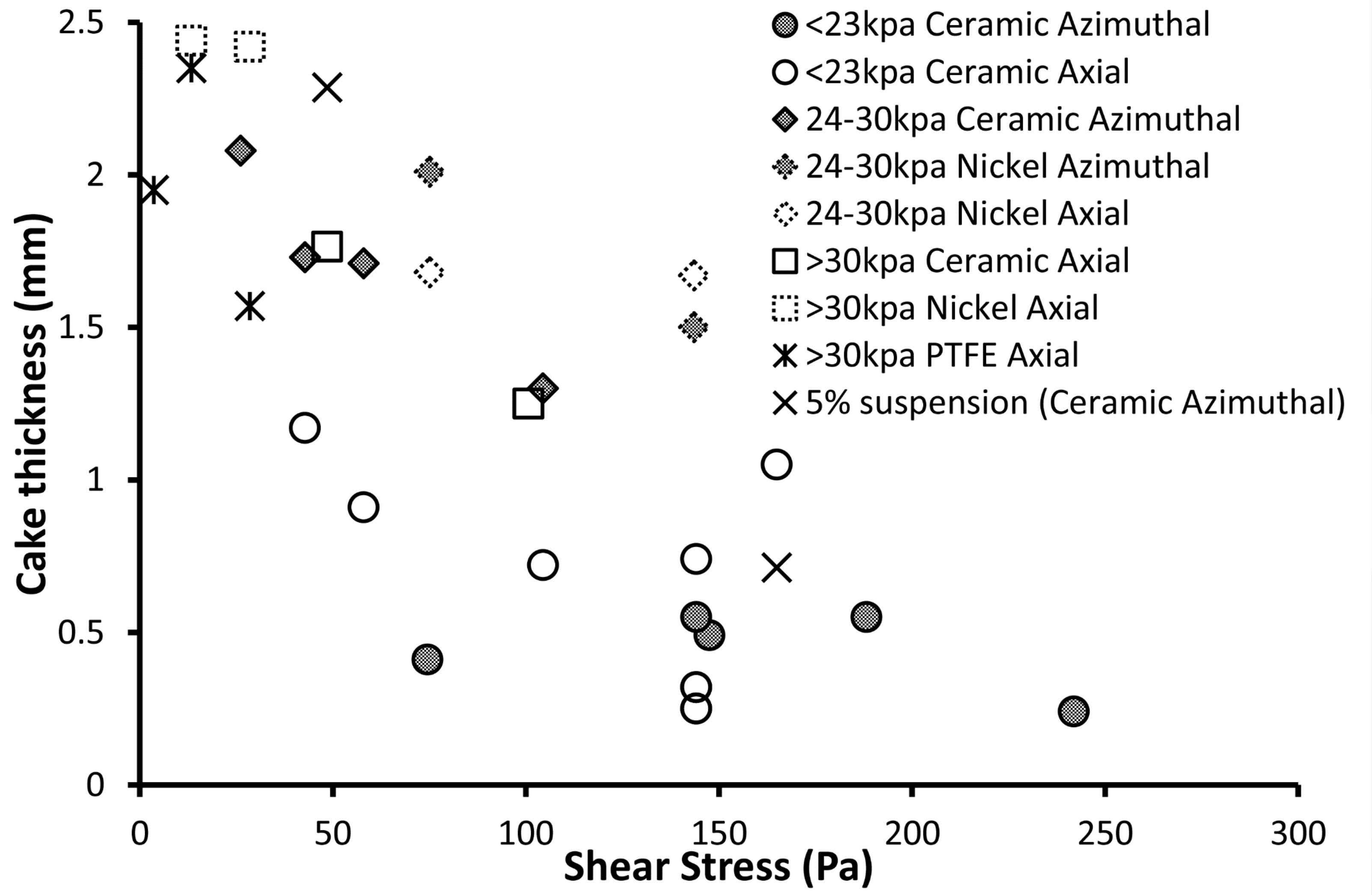

J vs tau

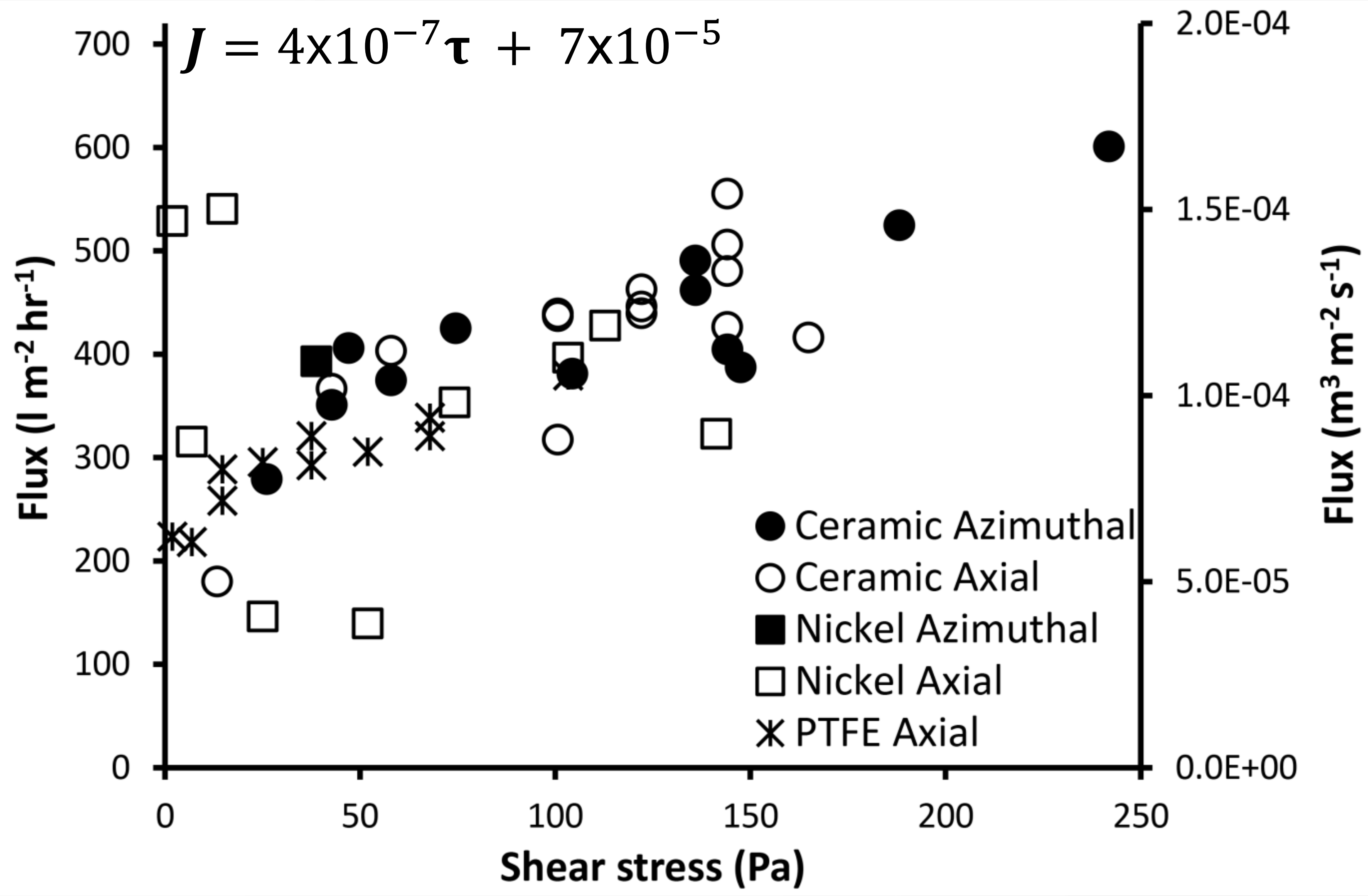

$J = 4\text{x}10^{-7}\boldsymbol{\tau} + 7\text{x}10^{-5}$
700
600
500
400
300
200
100
0
Flux (l m^{-2} hr^{-1})
2.0E-04
1.5E-04
1.0E-04
5.0E-05
0.0E+00
Flux (m^3 m^{-2} s^{-1})
0
50
100
150
200
250
Shear stress (Pa)
● Ceramic Azimuthal
○ Ceramic Axial
■ Nickel Azimuthal
□ Nickel Axial
✳ PTFE Axial

High Speed Photography

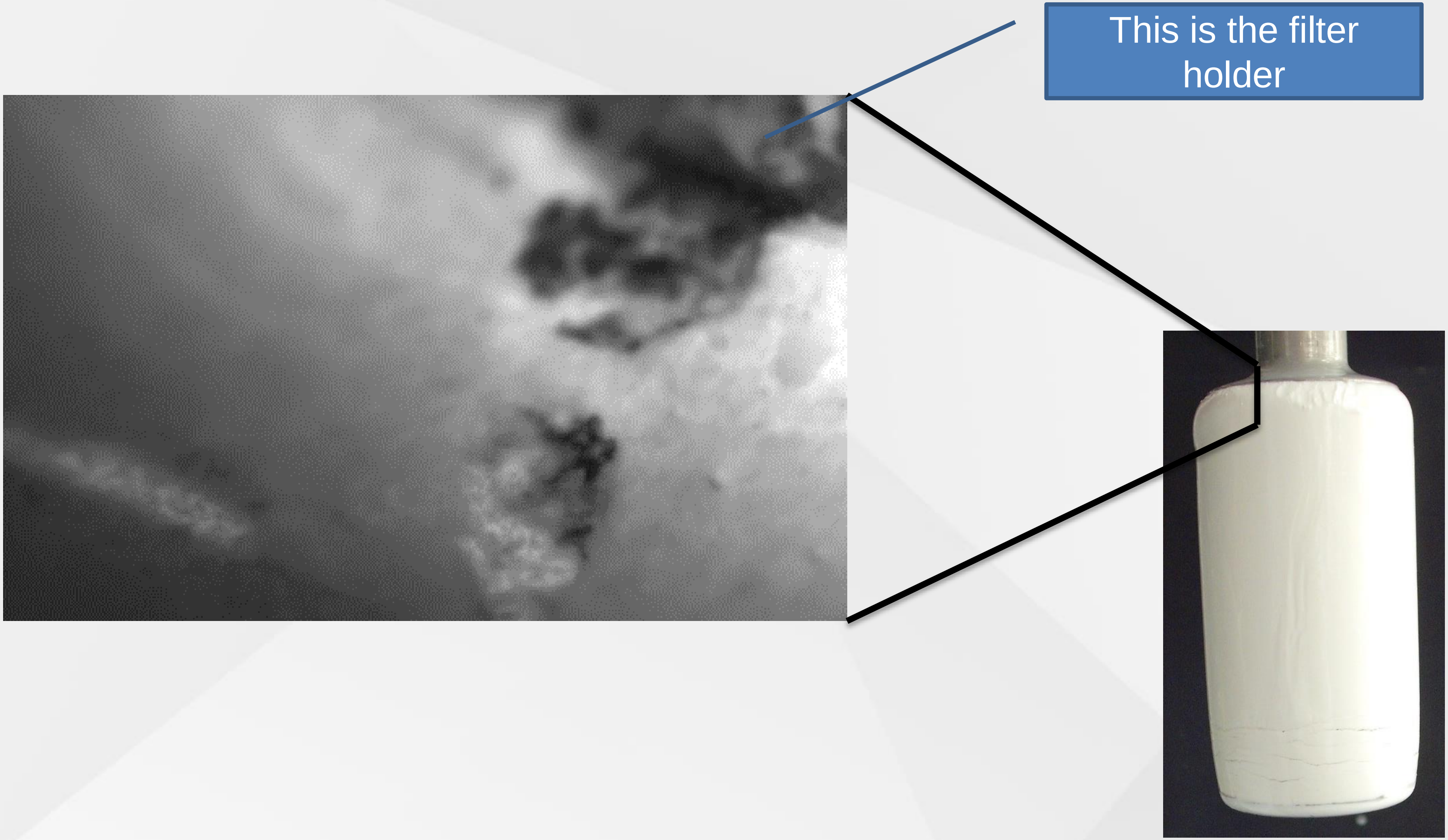

This is the filter holder

Comsol - Simulation

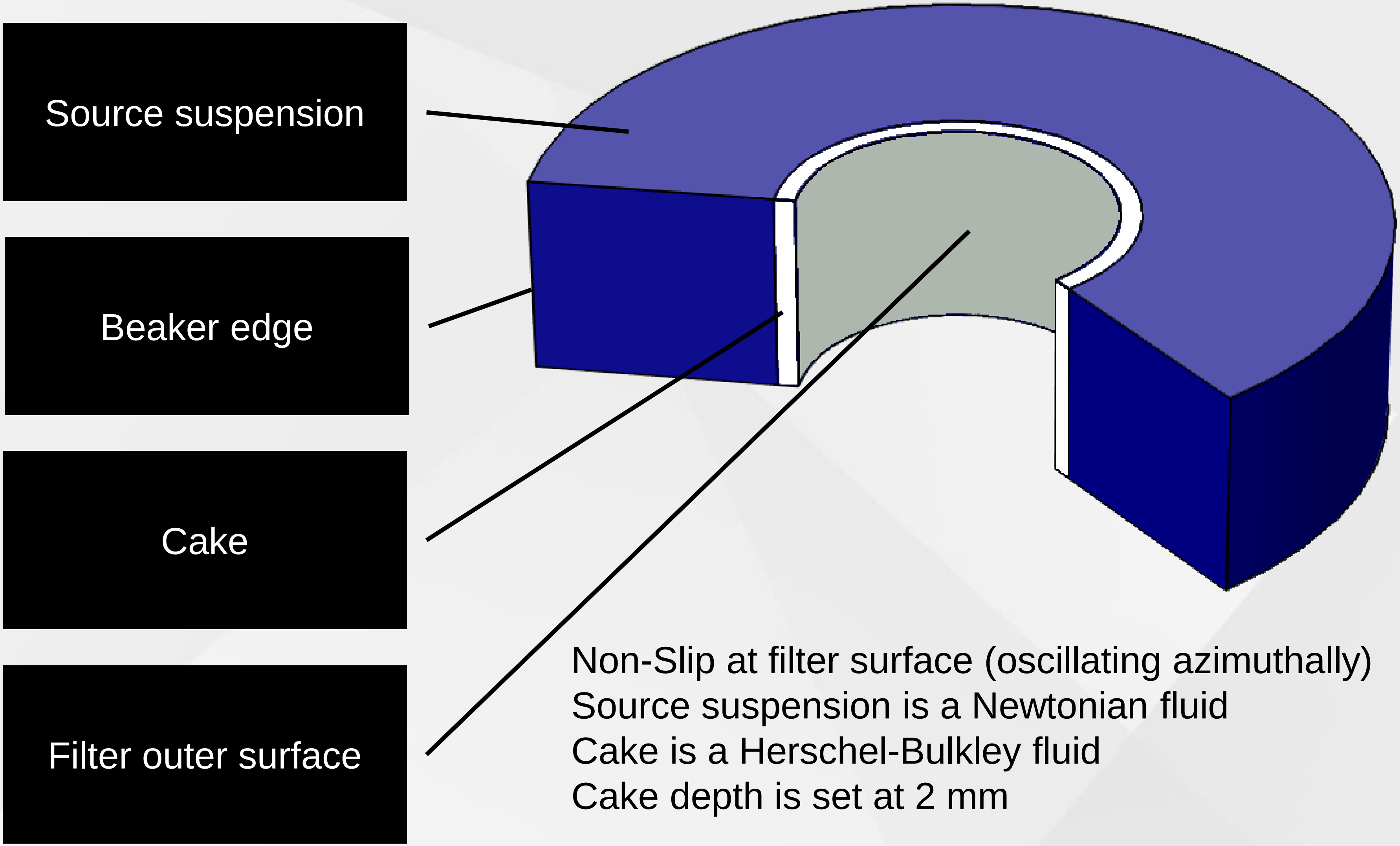

Source suspension

Beaker edge

Cake

Filter outer surface

Non-Slip at filter surface (oscillating azimuthally)
Source suspension is a Newtonian fluid
Cake is a Herschel-Bulkley fluid
Cake depth is set at 2 mm

Comsol - Results

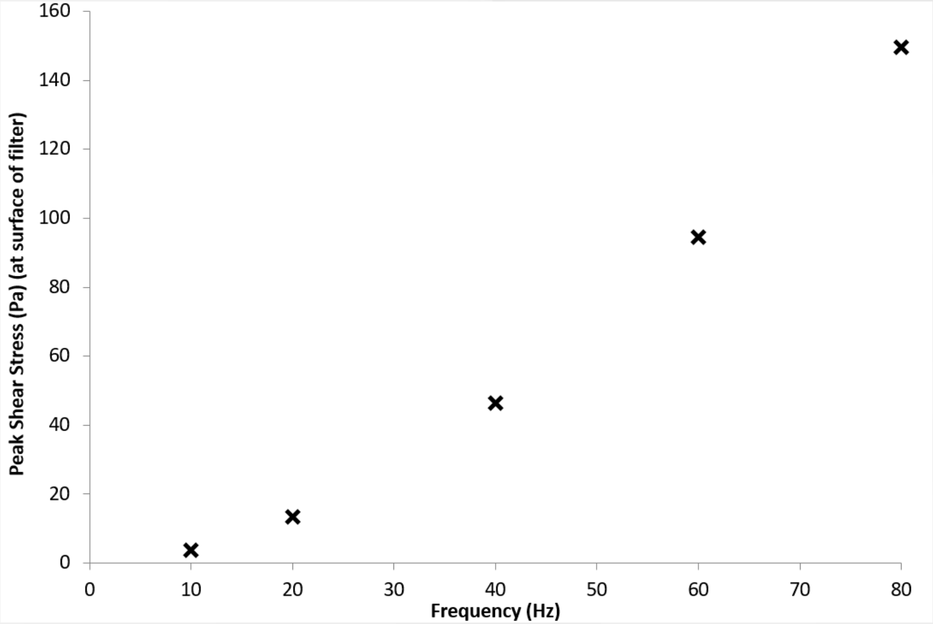

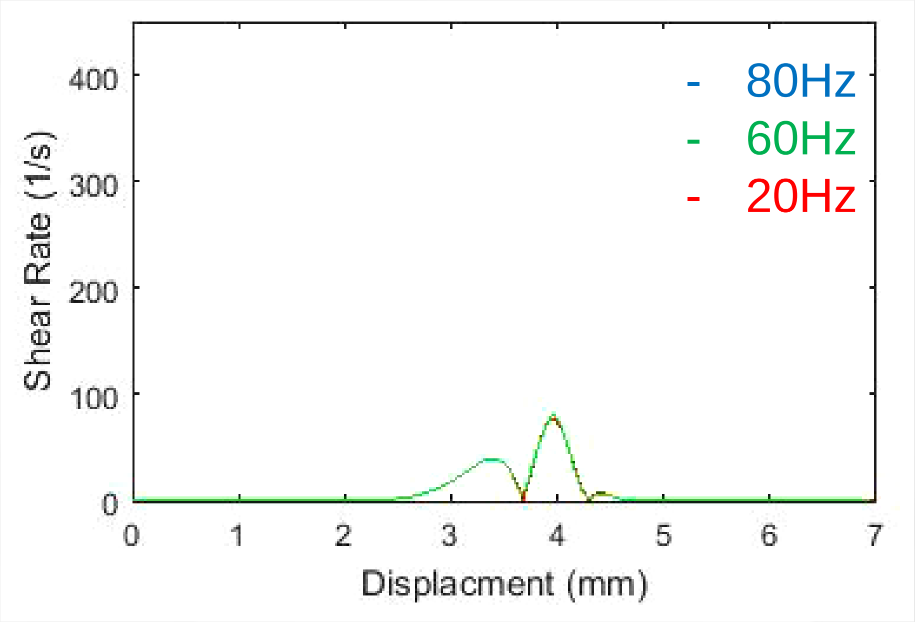

The purpose of this is to give an accurate shear stress (τ) value.

Loughborough University

#InspiringWinners since 1909

Modelling

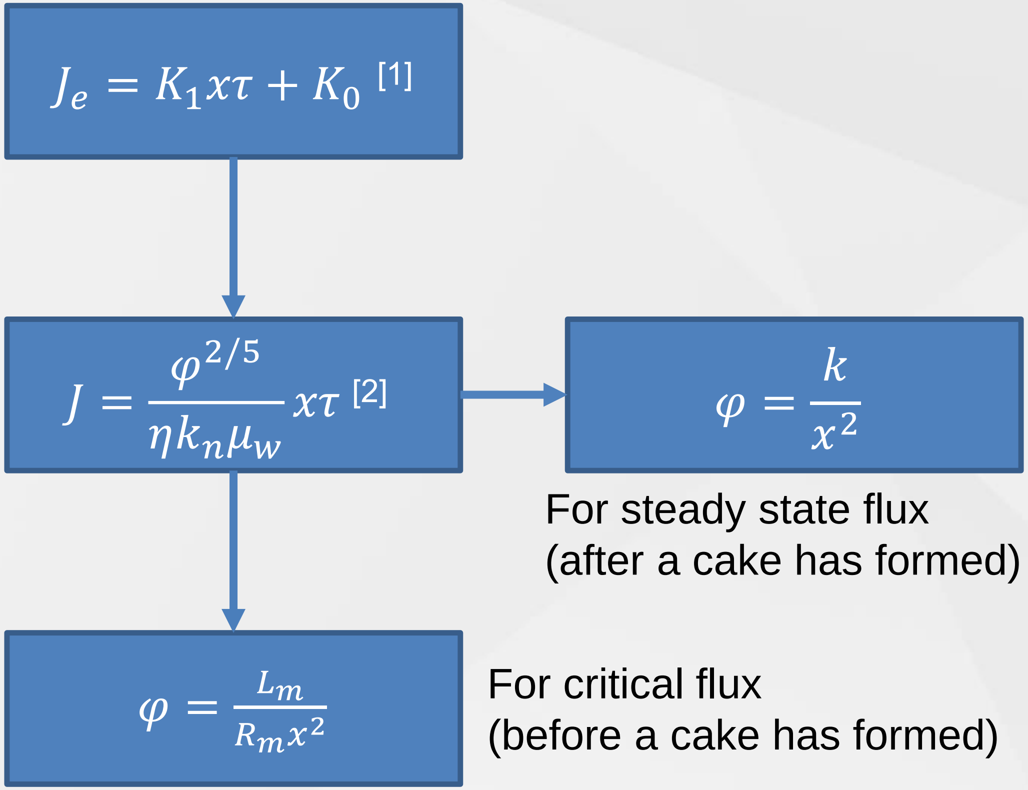

$$J_e = K_1 x\tau + K_0$$ [1]

$$J = \frac{\varphi^{2/5}}{\eta k_n \mu_w} x\tau$$ [2]

$$\varphi = \frac{k}{x^2}$$

For steady state flux
(after a cake has formed)

$$\varphi = \frac{L_m}{R_m x^2}$$

For critical flux
(before a cake has formed)

$$k = \frac{\left(2-3C^{\frac{1}{3}}+3C^{\frac{5}{3}}-2C^2\right)}{\left(3+2C^{\frac{5}{3}}\right)} \frac{x^2}{12C}$$ [3] (other permeability models exist)

C	cake concentration (vol)
J	flux
J_e	equilibrium flux
k	permeability
k_n	constant in the Stokes drag equation
K_0	constant from interparticle forces
K_1	constant from frictional forces
L_m	membrane thickness
η	frictional coefficient
R_m	membrane resistance
τ	Shear Stress
μ_w	Viscosity of permeate (water)
x	Particle diameter
φ	Dimensionless number

[1] N.J. Blake, I.W. Cumming, M. Streat, Prediction of steady state crossflow filtration using a force balance model. *J Memb Sci*. 1992; 68: 205-215.
[2] G. Foley, Membrane Filtration a problem solving approach with MATLAB, Cambridge University Press, Cambridge, UK, 2013.
[3] Happel and Brenner, Low Reynolds number hydrodynamics, Kluwer Boston, Inc., Hingham, USA, 1983.

Magnesium Hydroxide – PSD

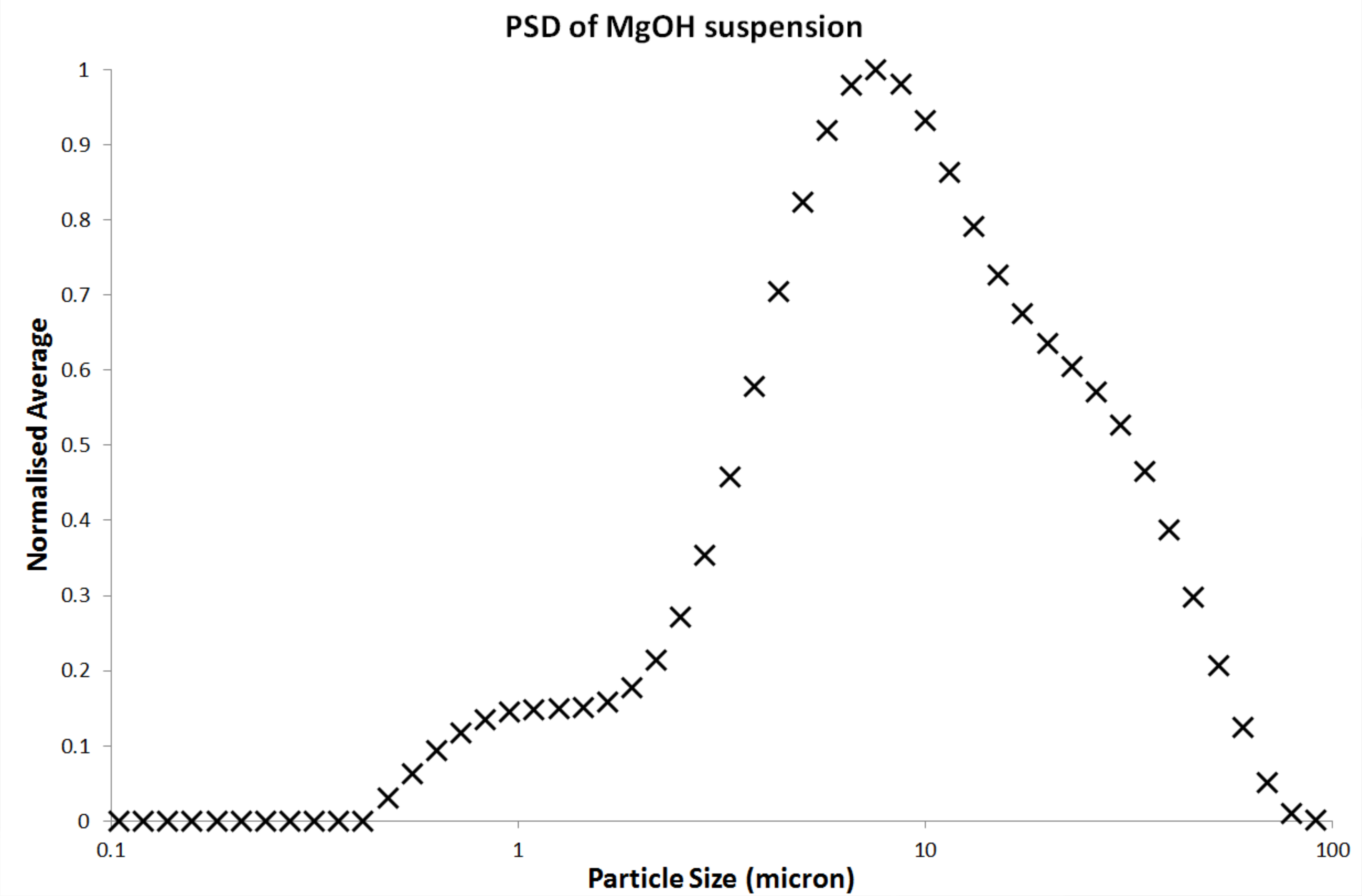

MgOH - Cake

Similar to calcite

Magnesium Hydroxide – SEM

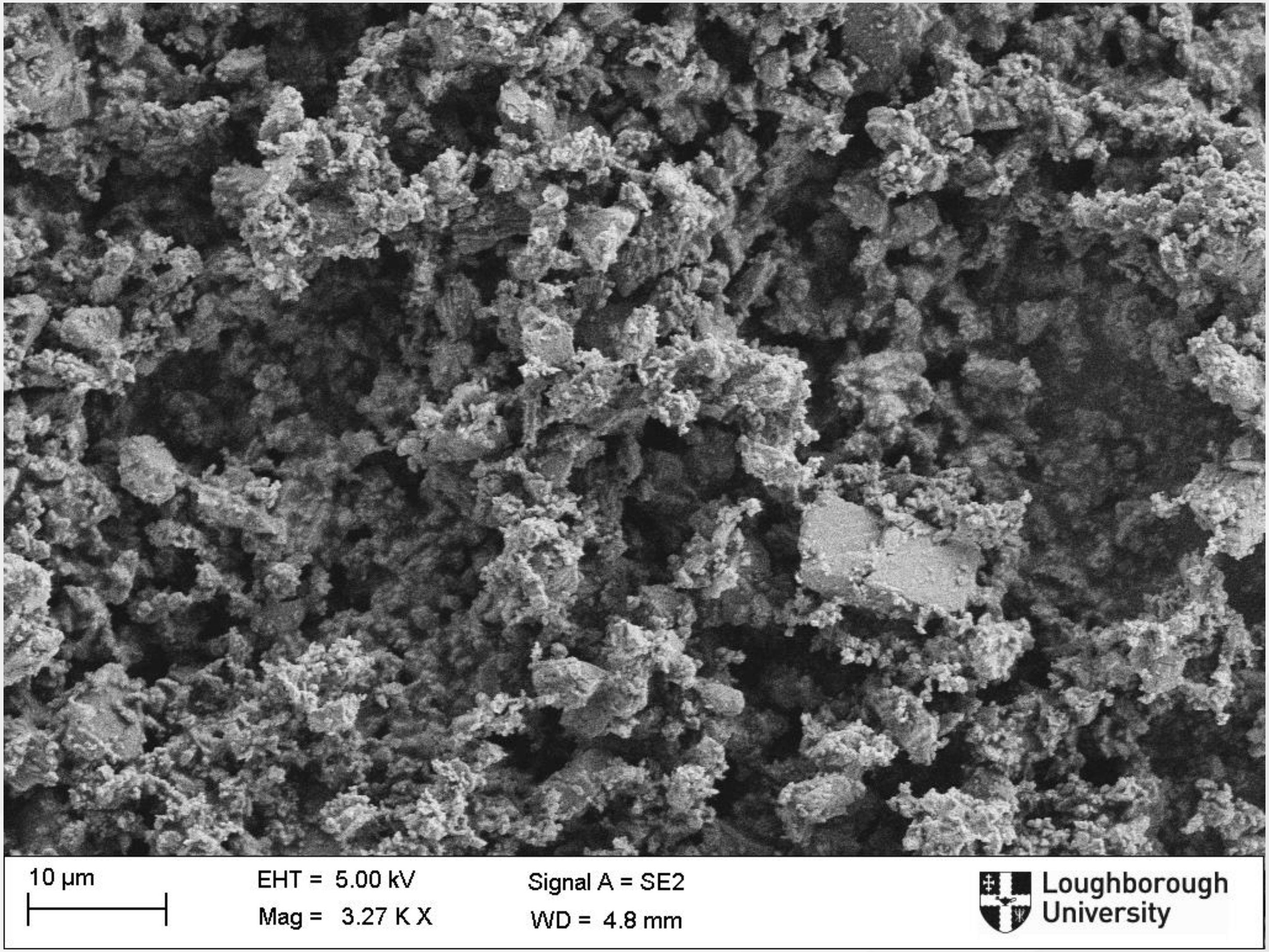

Ferric floc – what is it?

A ferric floc is a substance which sticks to colloids, precipitates, then clump together to produce a large structure which settles.

In situ TEM images show a common 'clump' of ~1μm

Reaction structures

Nano-particulates ~ 2– 4 nm in diameter.

Sometimes reported as:
$Fe(III)(OH)_3$

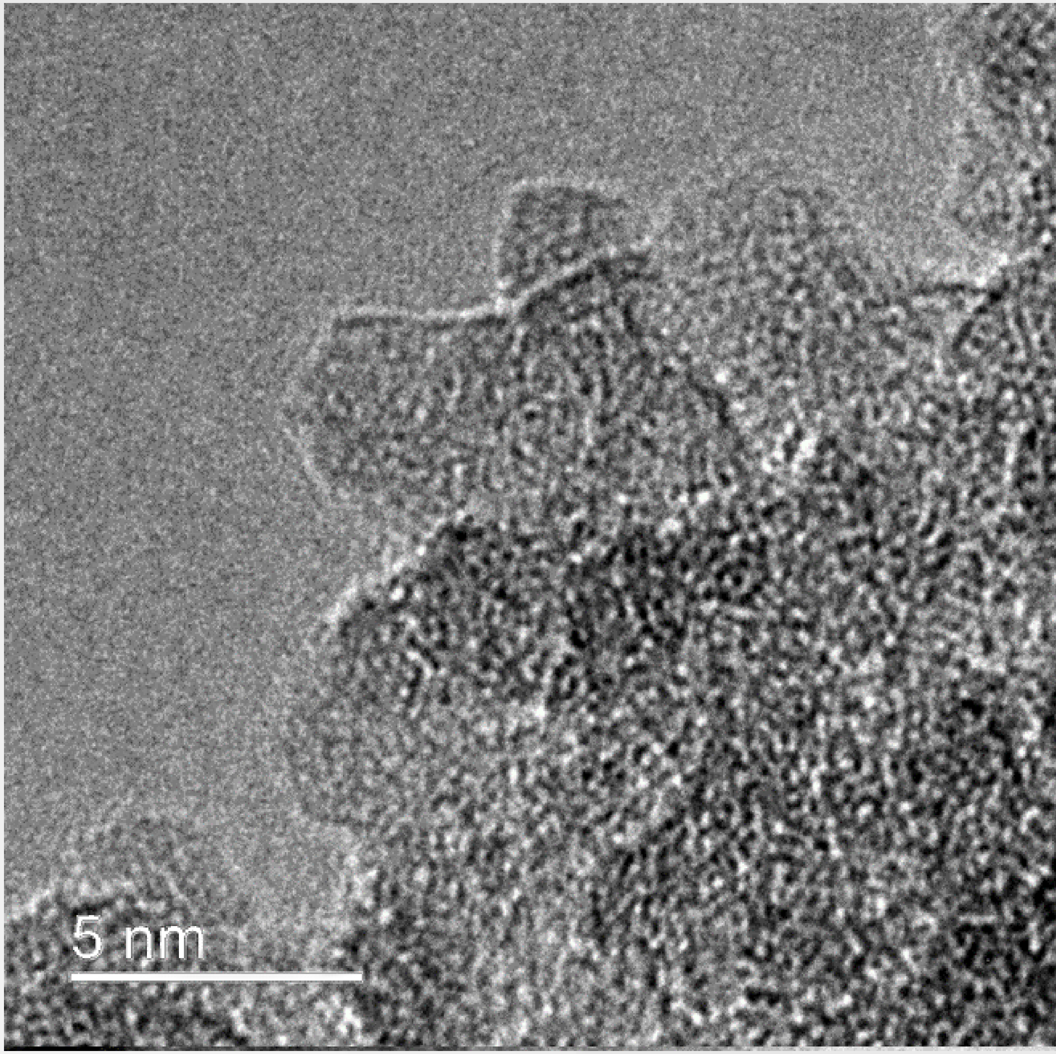

Images taken from work by Josh Weatherill with permission

Ferric floc – how is it made

$Fe(III)(NO_3)_3$ + 3NaOH -> FeO(OH) + $3NaNO_3$+$3H_2O$

NaOH +HNO_3 -> $NaNO_3$ + H_2O

$2OH^-$ -> H_2O + O^{2-}

Fe^{3+} + O^{2-} -> FeO^+

FeO^+ +OH^- -> FeO(OH)

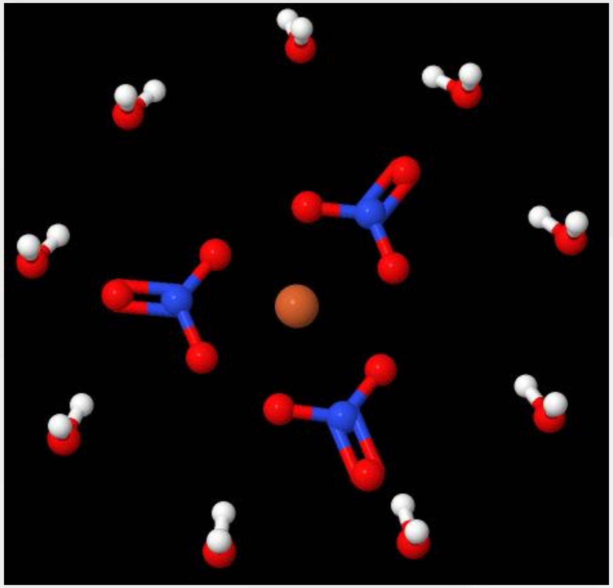

pH	H^+ ions
3	$1.0x10^{-3}$
4	$1.0x10^{-4}$
5	$1.0x10^{-5}$
6	$1.0x10^{-6}$
7	$1.0x10^{-7}$
8	$1.0x10^{-8}$
9	$1.0x10^{-9}$

Iron nitrate Nonahydrate is dissolved in 1M HNO_3, and then brought to pH 3 with a 7M NaOH solution. This is then brought up to pH 9 with a 0.2 M NaOH solution.

Ferric OxyHydroxide precipitates between pH2.8 and 9.

Floc Cake

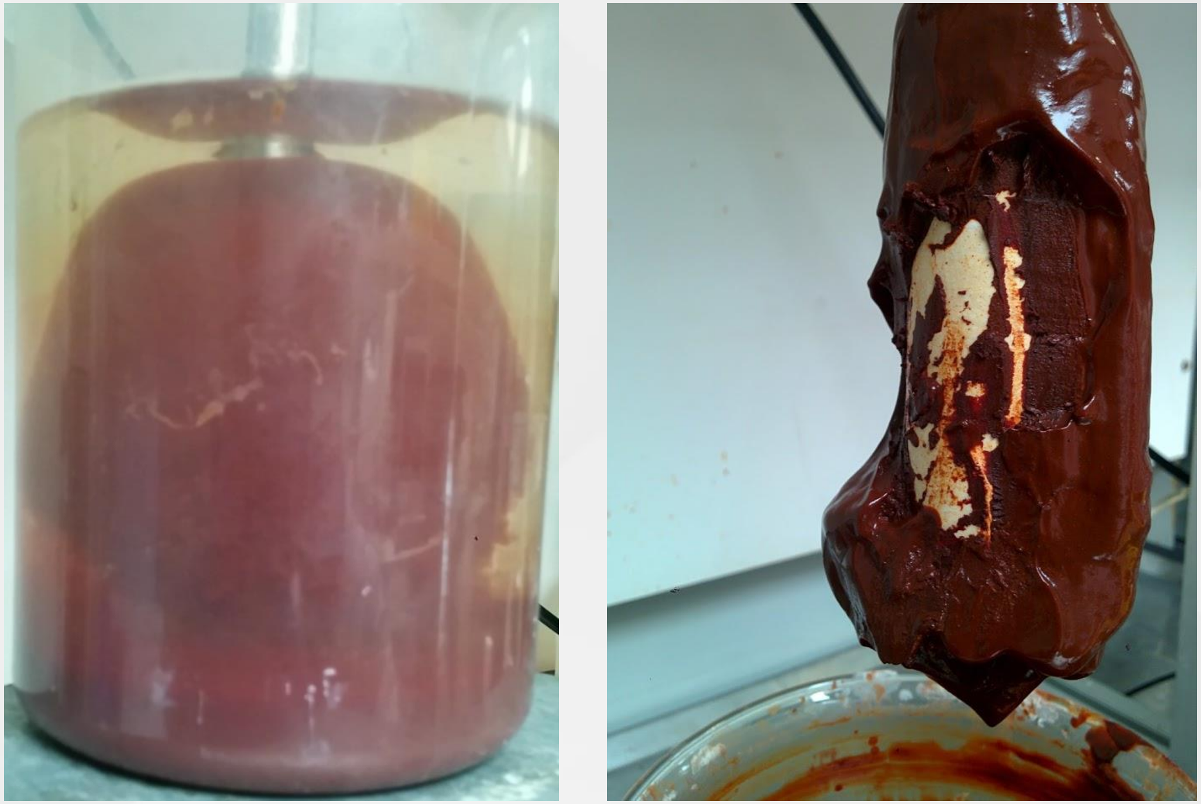

Cake formed on ceramic filer without shear before (left) and cutaway after being removed from water (middle)*

Versapor clad filter under shear

*this is not actually true, but demonstrates the point well

Floc filtration

- With an inappropriate filter, a large fluffy cake forms
- This fluffy cake inhibits filtration.
- This fluffy cake has a dense centre, and much fluffier outside.
- By applying a 0.45 µm nominal pore size polycarbonate filter (Versapor) to the outside of the filter, the fluffy cake does not form.
- This leads to much more efficient filtration
- Cake depths after cladding with Versapor to the surface are too small to measure accurately.
- Similar results were gained by pre-coating with Dematiaceous earth

*this is not actually true, but demonstrates the point well

Versapor

- 0.45 µm nominal pore size polycarbonate filter (Versapor) was wrapped around filter and sealed with silicone sealant.

- EDS sampling indicates complete iron retention

EDS Sampling	Fe (%)
Used filtering surface	4.95
Used non-filtering surface	0

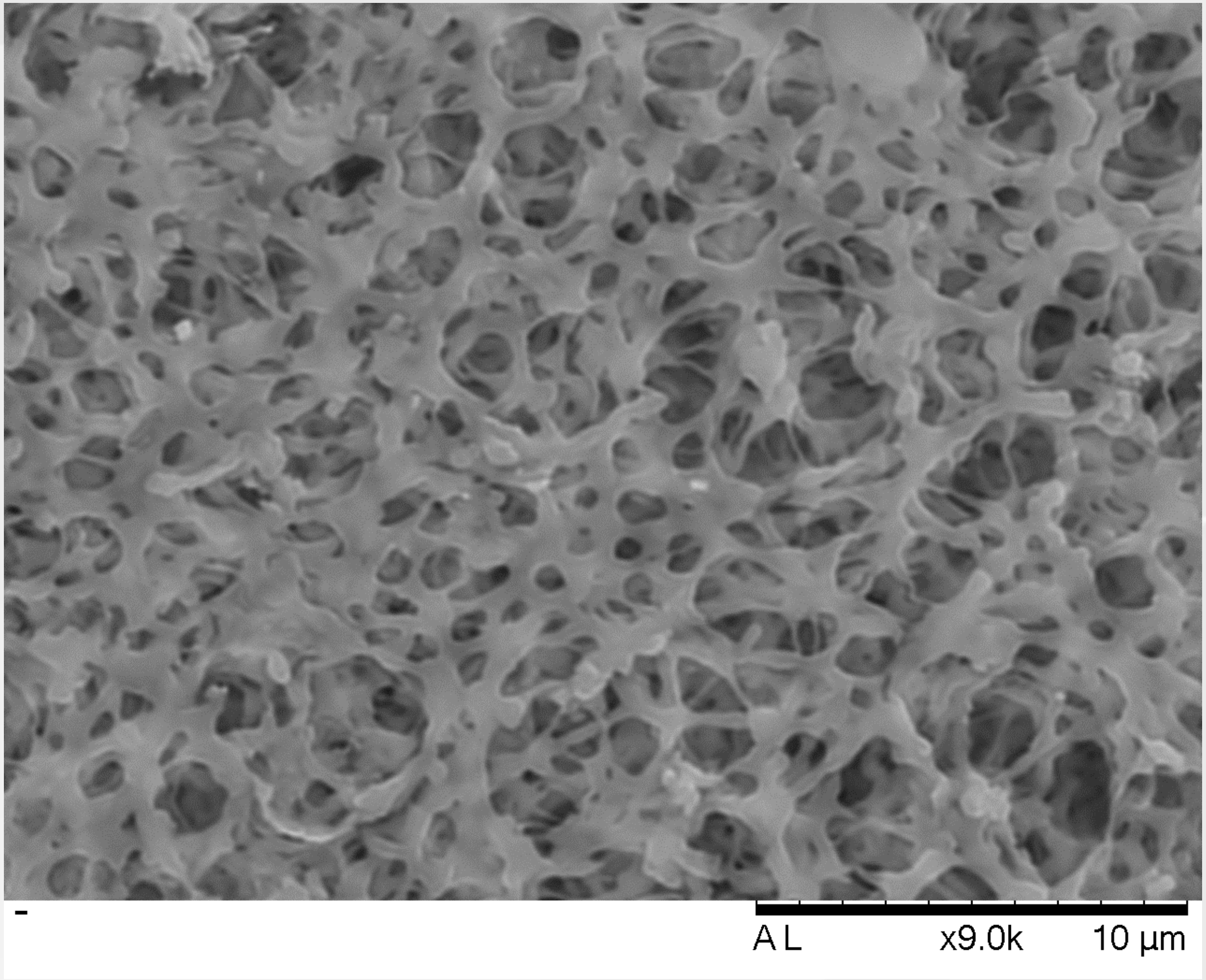

0.45 µm nominal pore size Versapor

*this is not actually true, but demonstrates the point well

Floc aging

Ferric floc converts to haematite (~200 micron crystals) and goethite over time.[2]

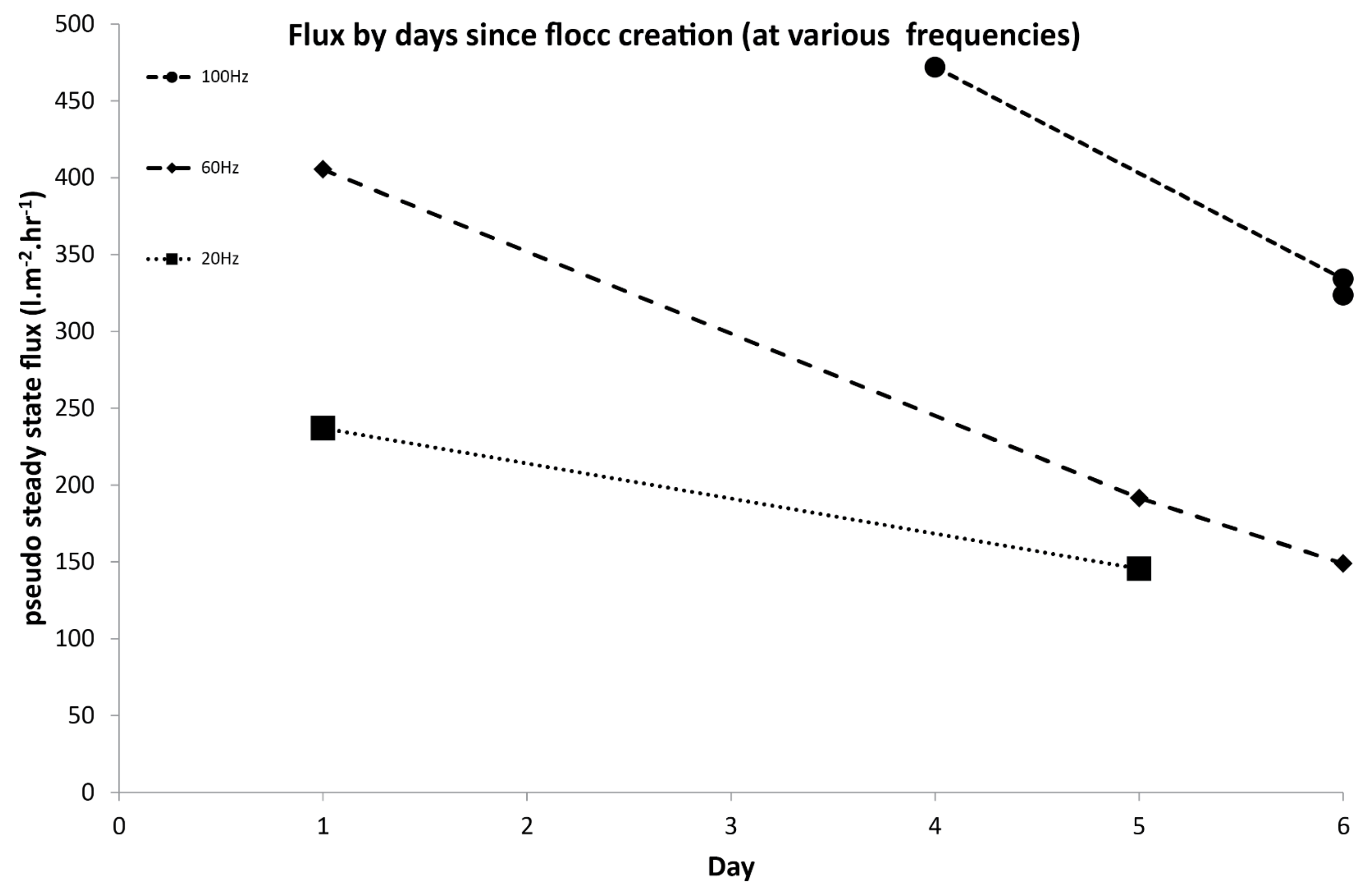

Comparison of shear based filtration on days after the floc was generated

[2] "Ferrihydrite Formation: The Role of Fe13 Keggin Clusters" Joshua S. Weatherill, Katherine Morris, Pieter Bots†, Tomasz M. Stawski, Arne Janssen, Liam Abrahamsen, Richard Blackham, and Samuel Shaw, Environ. Sci. Technol., 2016, 50 (17), pp 9333–9342 DOI: 10.1021/acs.est.6b02481

Floc aging

- Ferric floc converts to haematite (bright red) (~200 micron crystals) and goethite (yellow) over time.[2]
- This aging can be observed by slight colour changes*
- A reduction in settled volume of 5-10% per day is also observable*
- Aged floc does not dissolve in acids as easily as fresh floc*

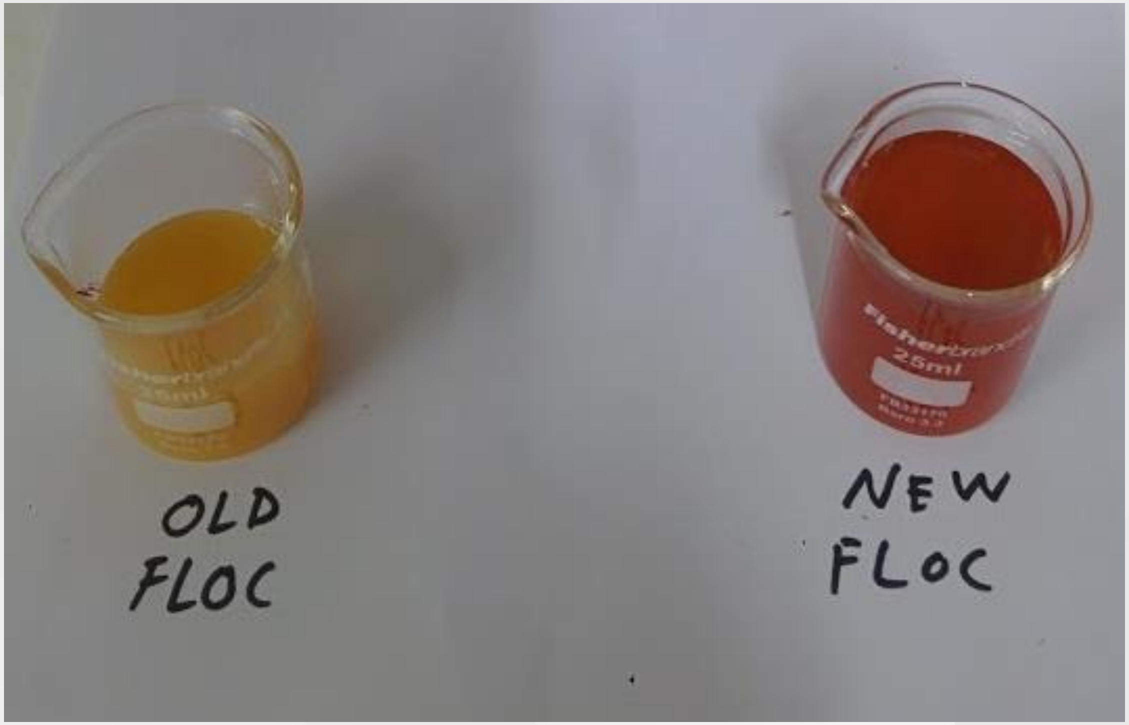

Colour comparison of aged and non-aged floc. The sample on the left is a couple of months old, the sample on the right is freshly made

[2] "Ferrihydrite Formation: The Role of Fe13 Keggin Clusters" Joshua S. Weatherill, Katherine Morris, Pieter Bots†, Tomasz M. Stawski, Arne Janssen, Liam Abrahamsen, Richard Blackham, and Samuel Shaw, Environ. Sci. Technol., 2016, 50 (17), pp 9333–9342 DOI: 10.1021/acs.est.6b02481

*(not yet quantified)

Ferric floc – Settling and Aging

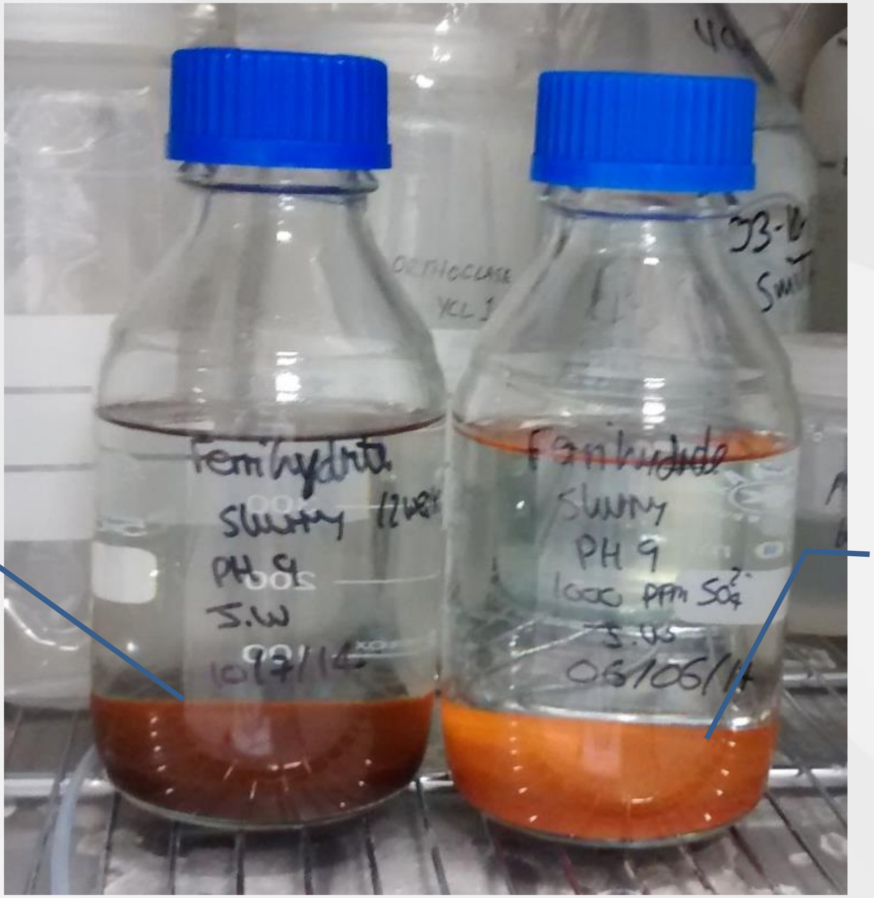

New Floc

Old Floc

Images taken from work by Josh Weatherill with permission

Floc filtration with shear

Flux is increased as a function of shear, this effect appears to only hold up to 100 Hz

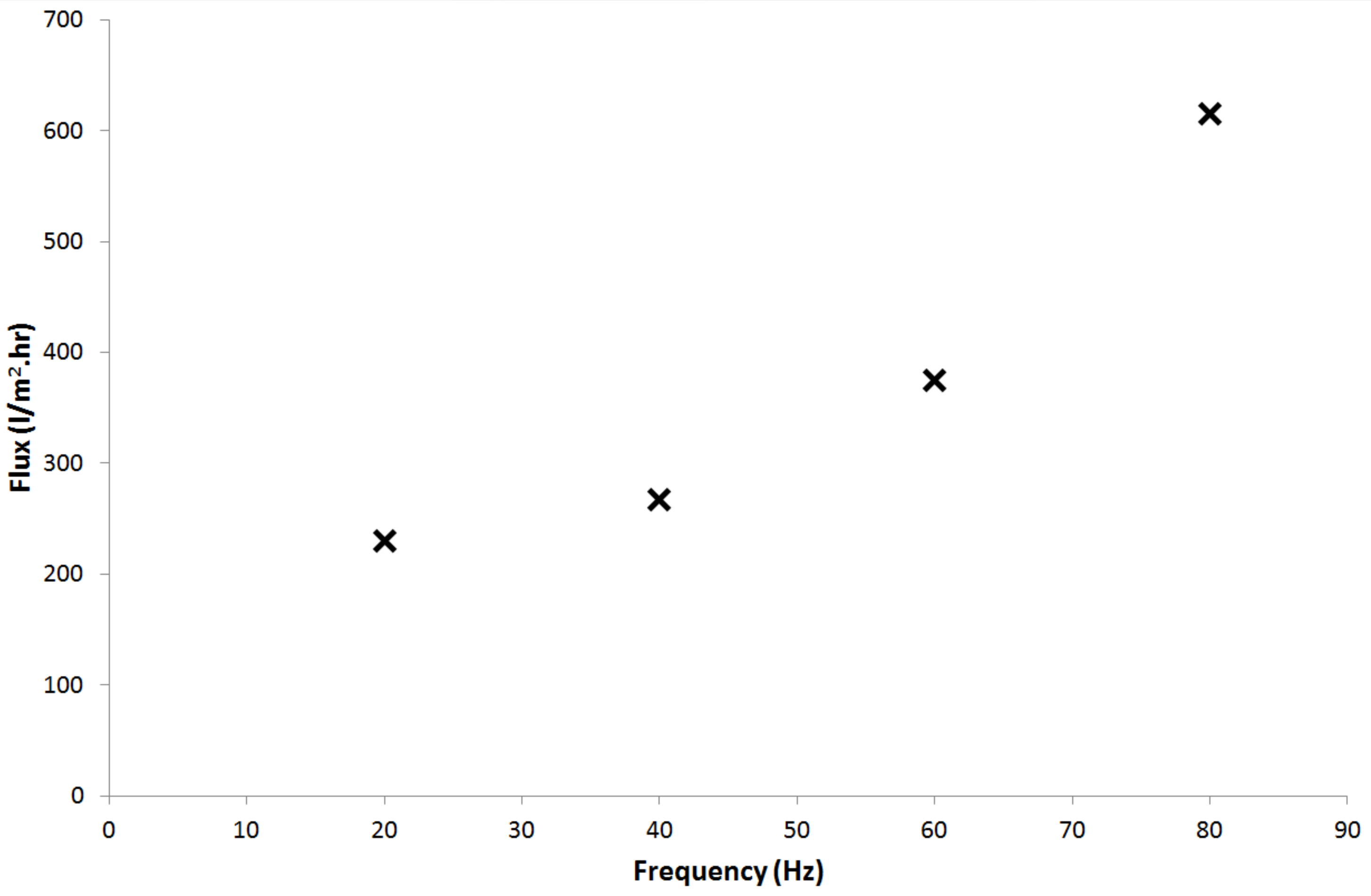

Pseudo steady state flux as a function of frequency (8 g Fe /l, floc made same day)

Floc filtration with shear

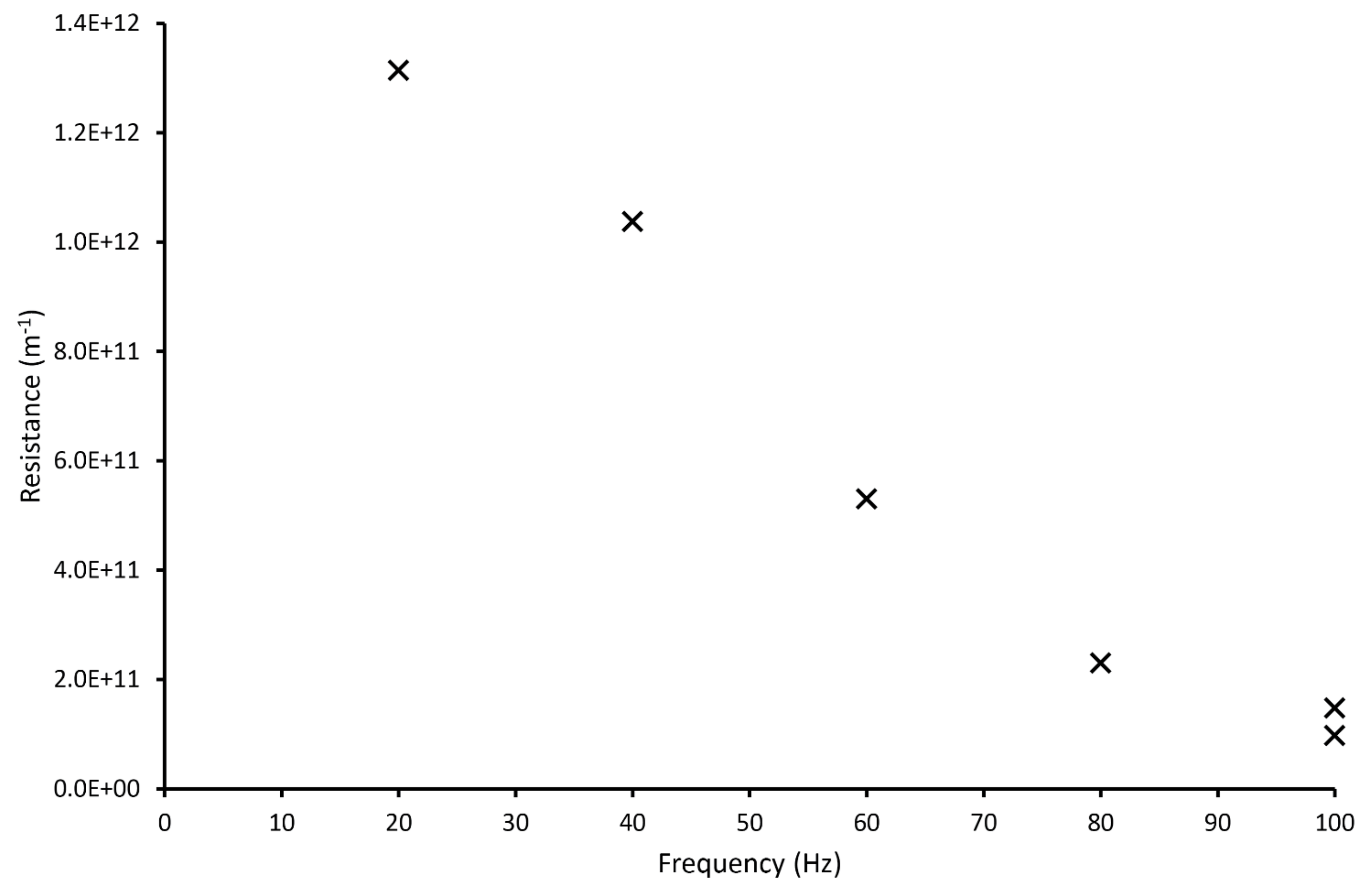

Pseudo steady state resistance as a function of frequency (8 g Fe /l, floc made same day)

Floc filtration, trans-membrane pressure

- Increasing trans membrane pressure (TMP) when filtering ferric floc under shear does **not** increase (or decrease) flux.

- TMP’s of just 0.1 bar can effectively filter with flux’s of ~500 $l.m^{-2}/hr^{-1}$

- This has not yet been quantified (or repeated enough to provide a reliable graph), however has been observed to be a consistent effect.

- This is consistent with shear enhanced diffusion theory.

Conclusions

Calcite

- There is no difference in azimuthal and axial oscillation improving filtration of calcite.
- There is no difference in to the type of filter used and the flux obtained.
- There is a strong correlation between cake thickness and shear applied.
- It is possible to model this effect.

Ferric floc

- Ferric floc is a challenging material to filter.
- Ferric floc does not filter well on itself, and must have a more appropriate filter.
- Ferric floc ages in just a couple of days, and a significant drop off in flux is observed.
- Ferric floc does not benefit from having large trans membrane pressures
- Ferric floc benefits from shear likely due to shear enhanced diffusion.
- Cake build-ups with appropriate filters and shear rates are almost negligible
- There is a maximum improvement with shear. (at about 100Hz with 0.7mm amplitude)

Further Work

- Investigate the shear based filtration of ferric floc:
    - Quantify the independence of TMP to flux during shear enhanced filtration
    - Concentration testing – how shear effects the concentration process, rather then filtering a constant concentration. (Dewatering of floc from 0.03 g/l Fe to 160 g/l Fe)
    - Kinetic filtration model for mineral suspensions– what happens during shear enhanced filtration as a function of time.
    - Filtering ferric floc with non-polymer filters.
    - Quantifying the shear enhanced filtration of ferric floc (in a similar way to with calcite)

Acknowledgments

I would like to thank my sponsor Sellafield Ltd. and my supervisors Richard Holdich and Marijana Dragosavac for allowing me the opportunity to study this.
I would also like to thank Hemaka Bandulasena for his help with the Comsol® work.

Questions

* Also happy Americans fireworks day

?

Background

During micro and ultrafiltration, filter blocking rapidly reduces the flux.

Shear enhanced (or Dynamic) filtration has been shown to have very large increases in flux up to 17x(1)

Typical increases in pseudo steady state flux is in the region of 2-4x.
(flux is the flow rate of liquid across the filter)

[1] M.Y. Jaffrin, L-H Ding, O. Akoum, A. Brou, A hydrodynamic comparison between rotating disk and vibratory dynamic filtration systems. *J Memb Sci*. 2004; 242: 155-167.

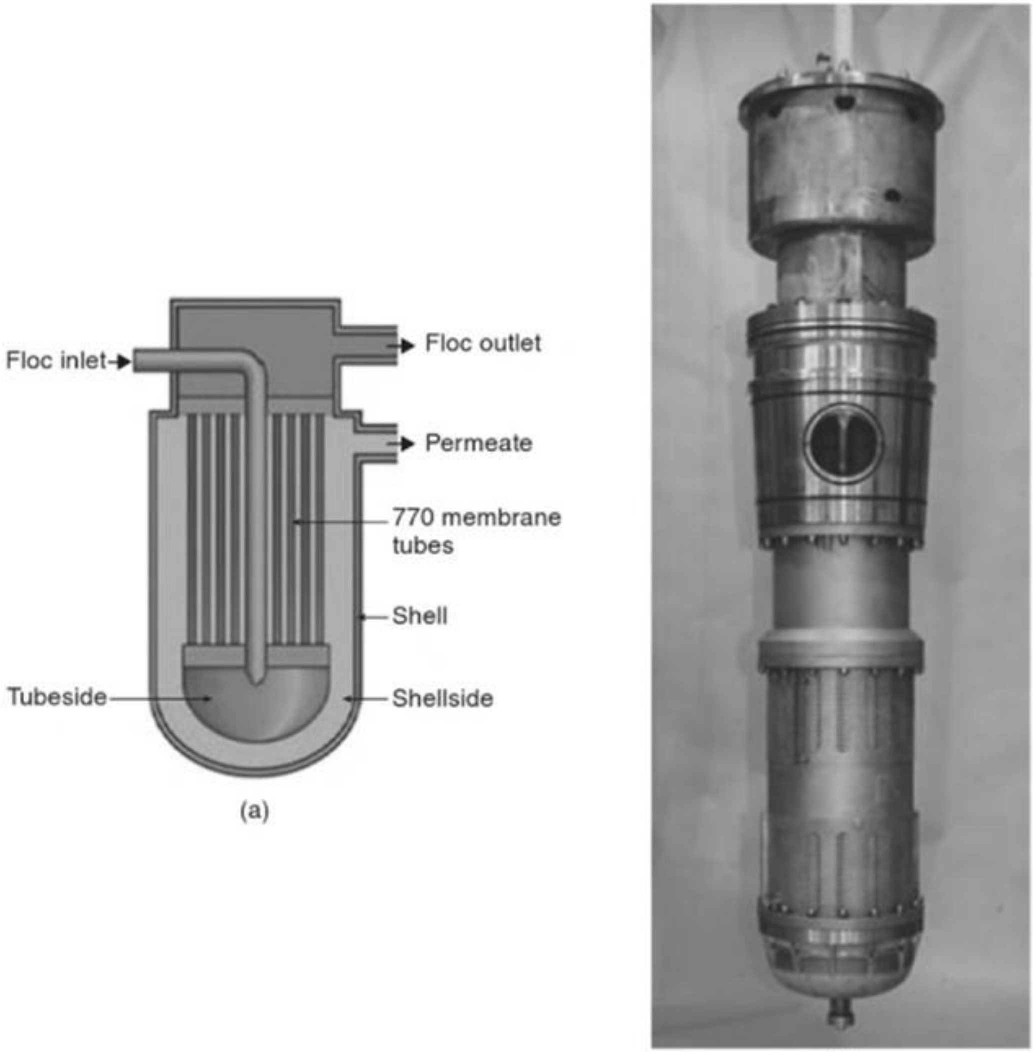

(a)

(b)

3.6 a and b Schematic representation and photograph of an EARP ultrafilter module. b Source: Nuclear Decommissioning Authority ("NDA"), copyright: Nuclear Decommissioning Authority ("NDA").

Floc Results

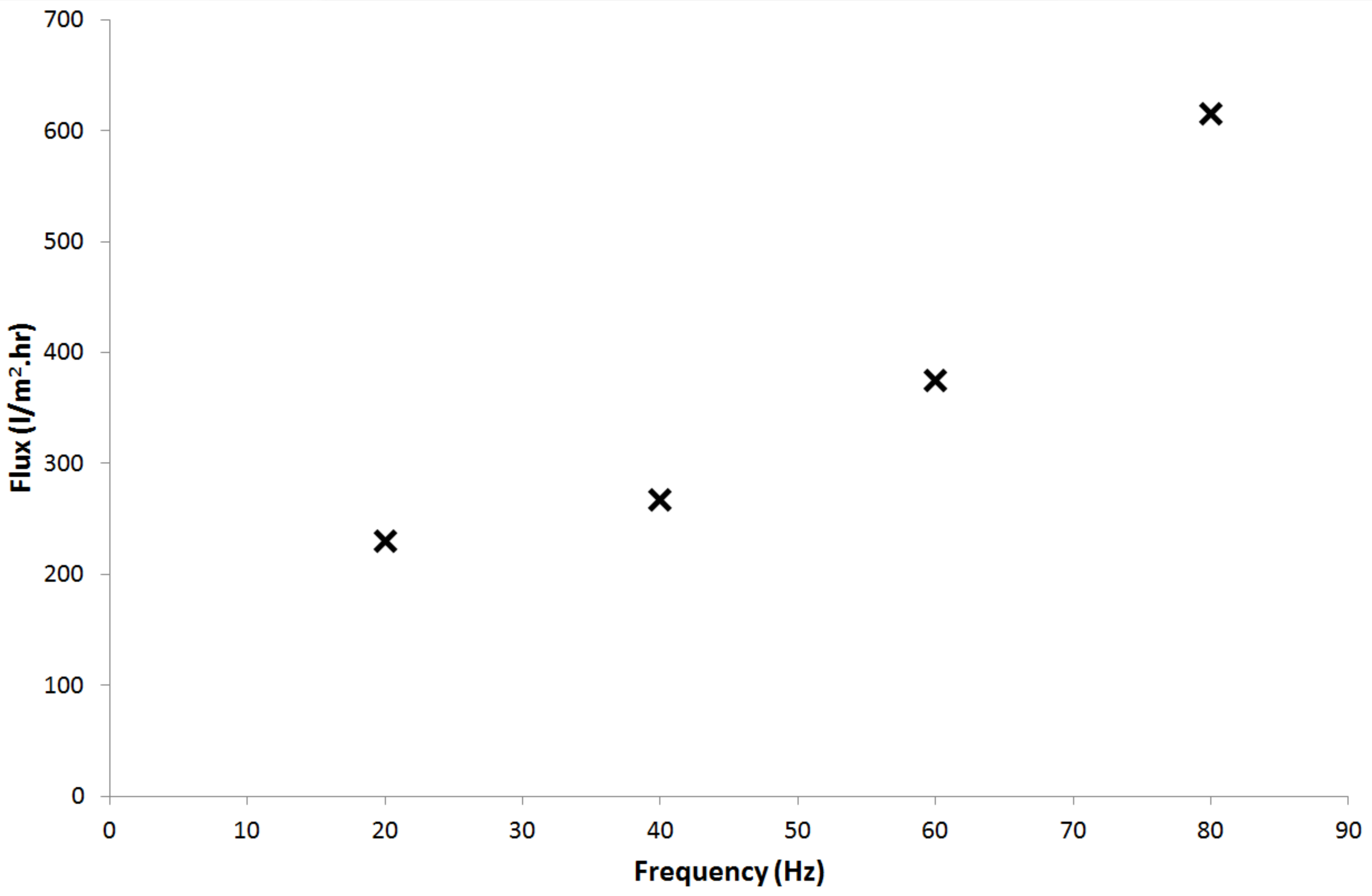

Floc Results

School of Chemical and Process Engineering
Faculty of Engineering

UNIVERSITY OF LEEDS

Characterisation of Flocculated Dispersions using Acoustic Backscatter Systems

Alastair Tonge

Supervisors: Dr Tim Hunter, Prof. Steven Freear & Prof. Jeff Peakall

Experimental Setup

UNIVERSITY OF LEEDS

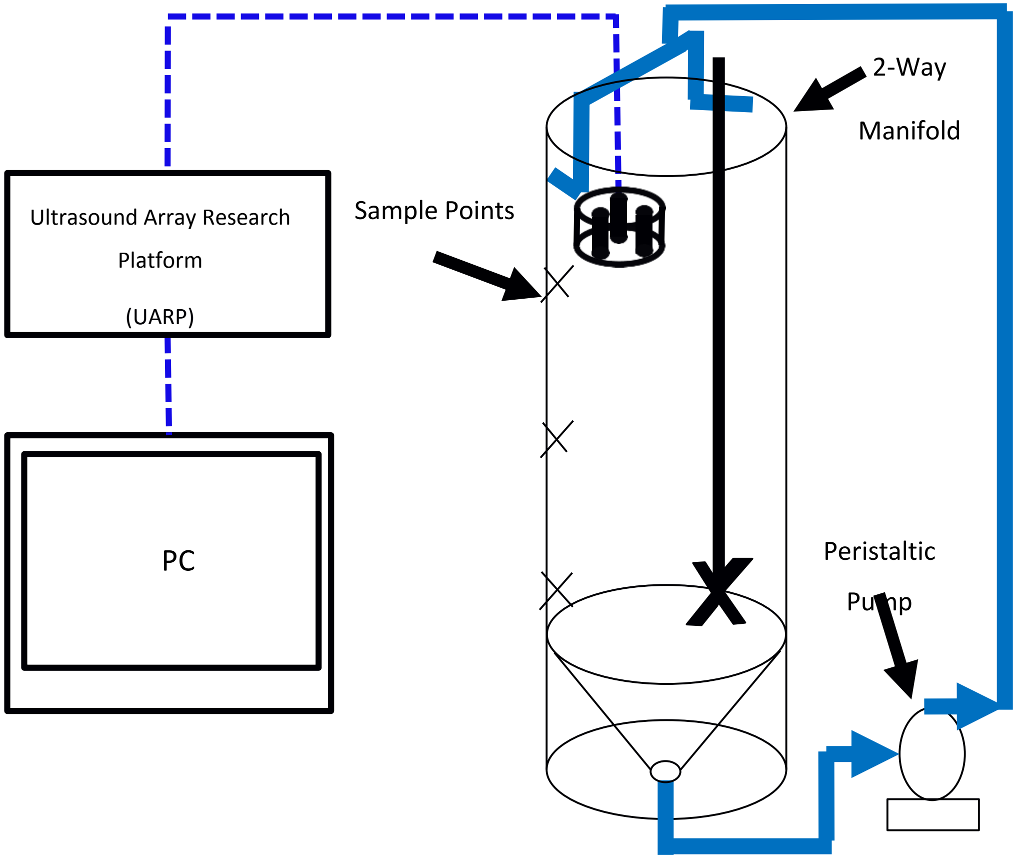

Ultrasound Array Research Platform

(UARP)

PC

Sample Points

2-Way

Manifold

Peristaltic

Pump

Experimental Setup

Ultrasound Array Research Platform (UARP)

- High resolution concentration & interfaces from backscatter echo strength.
- Up to **sixteen** individually adjustable, multi-frequency channels.

Specification	UARP
Maximum Output Voltage	5 Level ± 100V, ± 50V, GNS
Transmit Frequency	0.5 MHz to 15 MHz
Number of channels	16 per module (Max: 256)
Raw data transfer to computer	PCI Express Gen 3 (Max : 64Gbps)
Analog Digital Converter	AFE5807 (Max 80MSPS)
Mechanical aspects	Communications via PCIe Dedicated Clock and Synchronisation signals.

a

b

D.M.J. Cowell et. Al. 10.1109/ULTSYM.2015.0165

Measurement principle

$$V_{\mathrm{rms}} = \frac{k_s k_t}{r} M_W^{\frac{1}{2}} e^{-2r(\alpha_w + \alpha_s)}$$

k_s	particle species backscatter co-efficient
k_t	transducer constant
r	distance from transducer face
M_W	mass concentration
α_w	attenuation of water
α_s	attenuation of suspended particles

P. D. Thorne and D. M. Hanes, “A review of acoustic measurement of small-scale sediment processes,” *Continental Shelf Research,* vol. 22, pp. 603-632, 2002.

Measurement principle

$$G = \ln(\psi r V_{\mathrm{rms}}) = \ln(k_{sh} k_t) + \frac{1}{2}\ln M_W - 2r(\alpha_w + \alpha_{sh})$$

k_{sh}	particle species backscatter co-efficient (under homogeneous conditions)
k_t	transducer constant
ψ	near field correction factor
r	distance from transducer face
M_W	mass concentration
α_w	attenuation of water
α_{sh}	attenuation of suspended particles (under homogeneous conditions)

P. D. Thorne and D. M. Hanes, "A review of acoustic measurement of small-scale sediment processes," *Continental Shelf Research,* vol. 22, pp. 603-632, 2002.

Measurement principle

$$\frac{\partial G}{\partial r} = -2(\alpha_w + \alpha_s)$$

$$\alpha_w = 0.05641 f^2 \mathrm{e}^{\left(-\frac{T}{27}\right)} \qquad \alpha_s = \xi_h M_W \qquad \xi_h = -\frac{\frac{1}{2}\left(\frac{\partial G}{\partial r}\right)}{\partial M_W}$$

~~k_s~~	~~particle species backscatter co-efficient~~
~~k_t~~	~~transducer constant~~
ψ	near field correction factor
r	distance from transducer face
M_W	mass concentration
α_w	attenuation of water
α_s	attenuation of suspended particles

H. Rice *et al*, “Measuring particle concentration in multiphase pipe flow using acoustic backscatter: Generalization of the dual-frequency inversion method,” *J. Acoust. Soc. Am.*, vol. 136, no. 1, pp. 156-169, 2014.

Glass Particle Acoustic Calibration Procedure

UNIVERSITY OF LEEDS

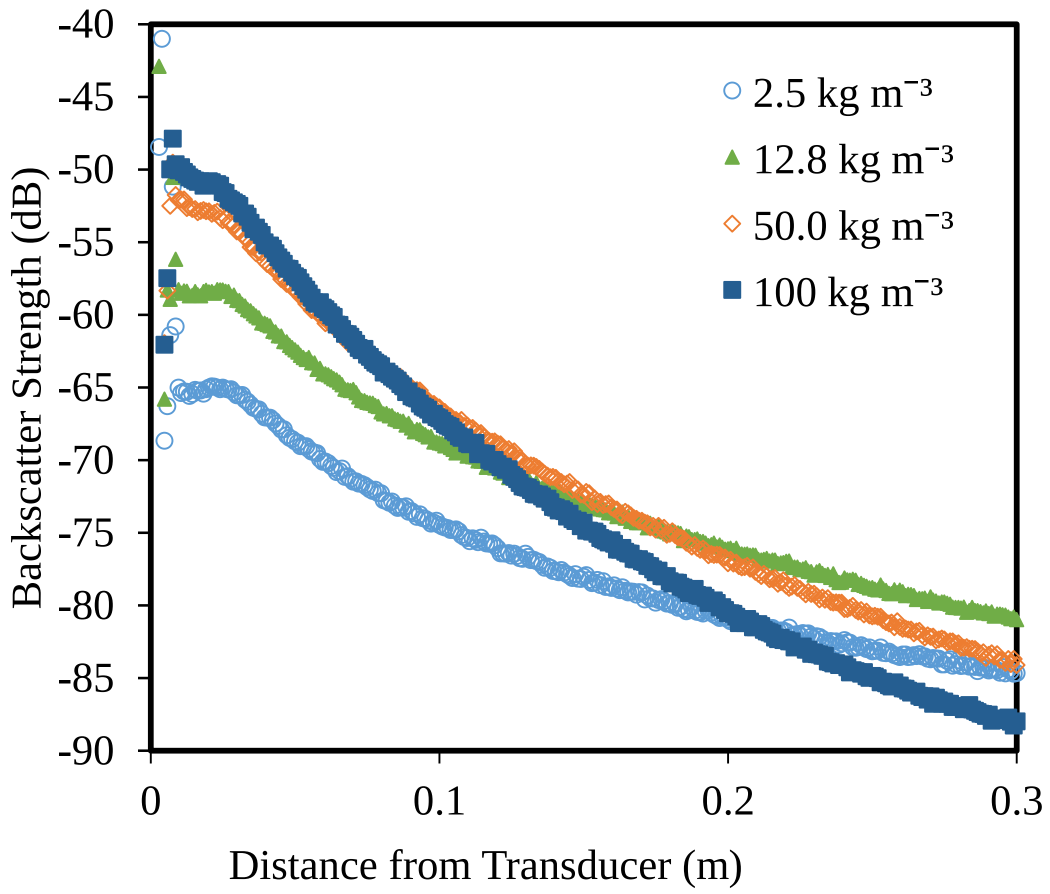

Glass Particle Acoustic Calibration Procedure

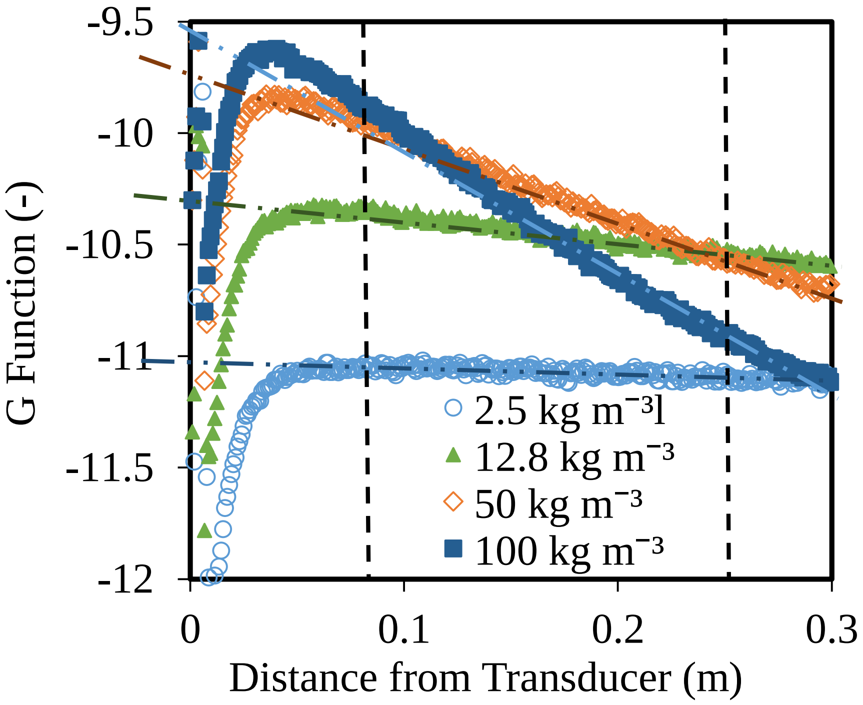

Glass Particle Calibration Data (Honite-16)

UNIVERSITY OF LEEDS

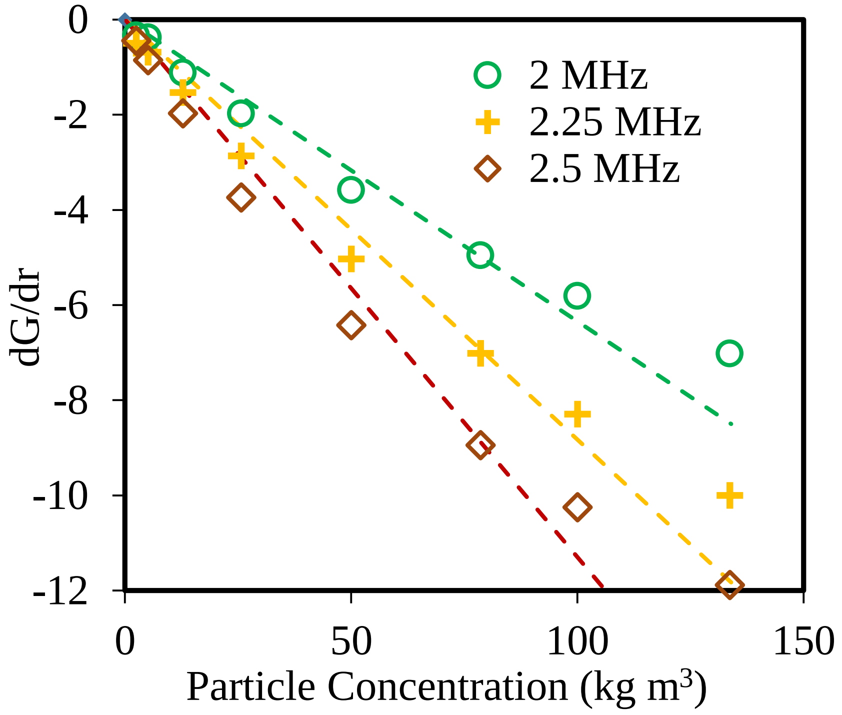

Concentration Profile Inversion

UNIVERSITY OF LEEDS

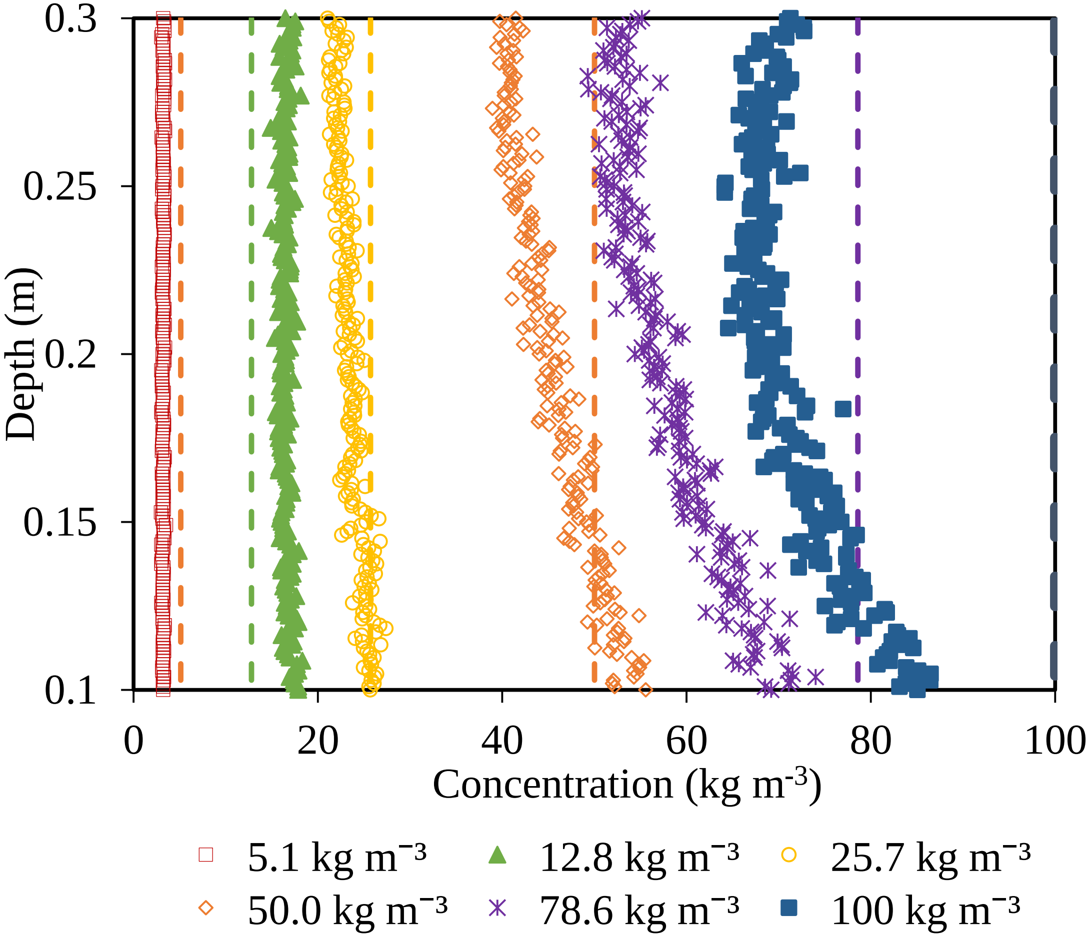

CALCITE FLOC STUDIES

Flocculation Study – Materials Used

UNIVERSITY OF LEEDS

- Calcite (Calcium Hydroxide) was chosen as our test sediment as it has been shown to be a good nuclear simulant for sediment transport processes at Sellafield and used in NSG trials previously.

- The flocculant used is FLOPAM - AN93SH a high molecular weight, negatively charged polymer produced by SNF Ltd.

- The medium charge density of the polymer allows it to neutralise the positive charge of the calcium while binding to the particles and forming bridges to others to induce flocculation.

Test Material Development

UNIVERSITY OF LEEDS

- Flocculate with anionic polyelectrolytes (heterogeneous, multi-component sludges).

SNF (UK) LIMITED

Name	Charge type	Charge density
AN 934SH	Anionic	Medium
AN 945SH	Anionic	High

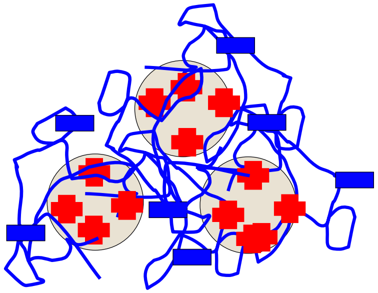

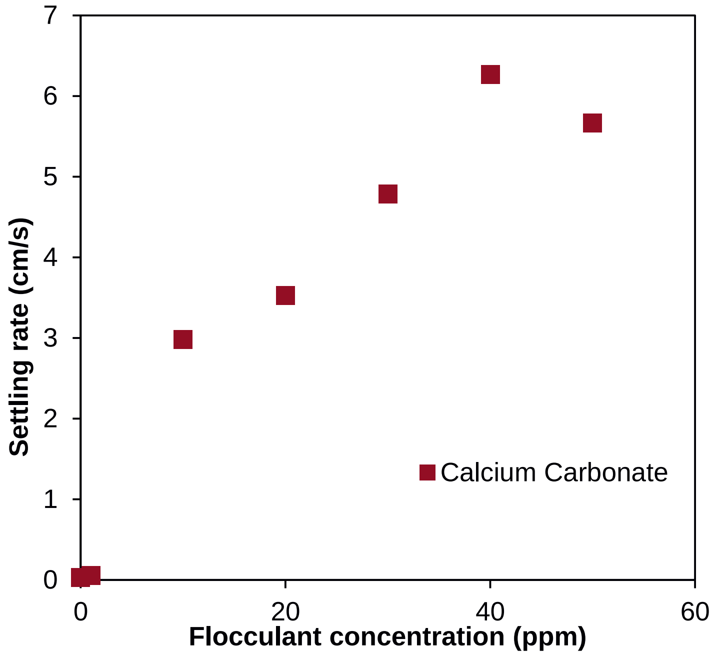

G-function profiles for Calcite Flocs

UNIVERSITY OF LEEDS

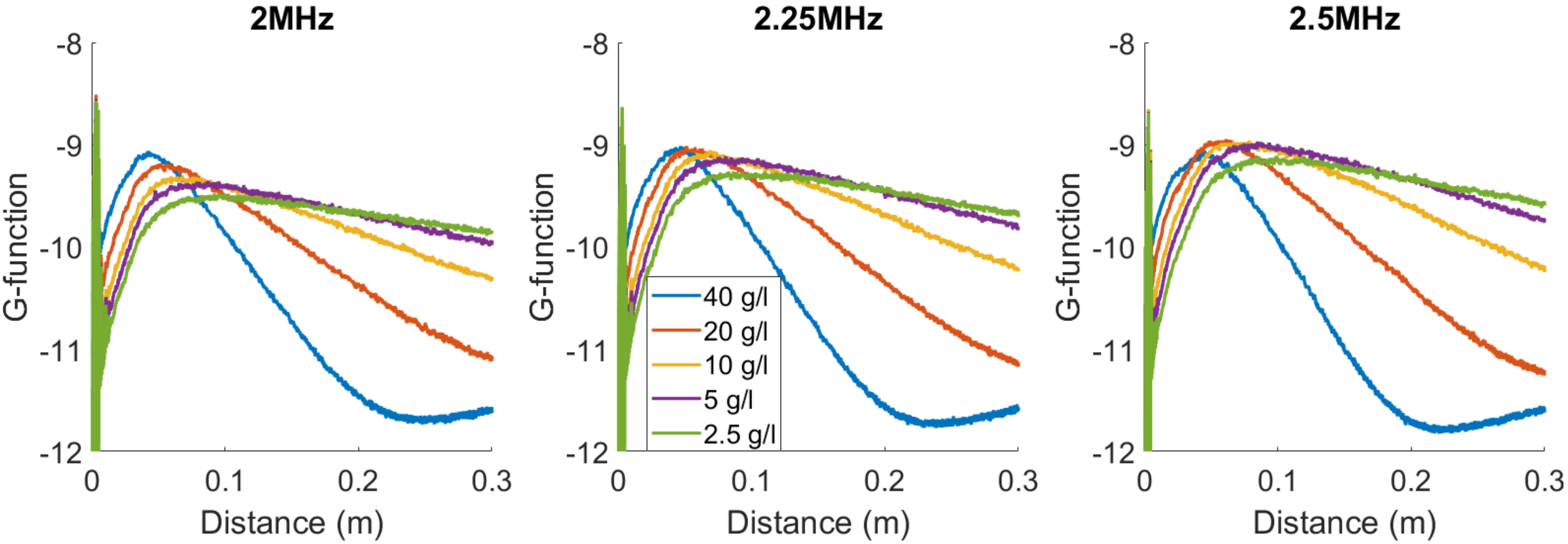

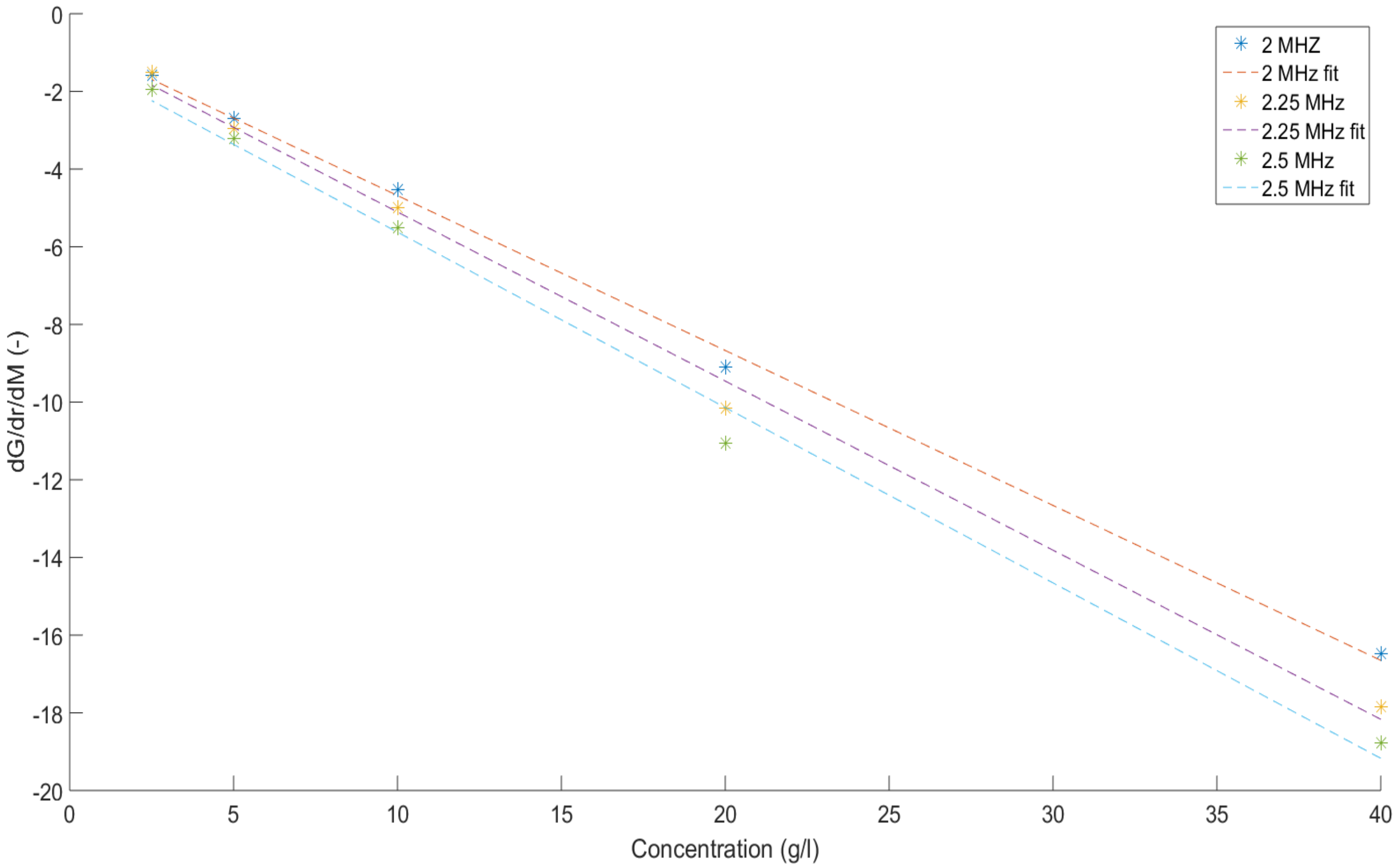
0
-2
-4
-6
-8
-10
-12
-14
-16
-18
-20
dG/dr/dM (-)
0
5
10
15
20
25
30
35
40
Concentration (g/l)
2 MHZ
2 MHz fit
2.25 MHz
2.25 MHz fit
2.5 MHz
2.5 MHz fit

Fractal Dimension Measurement Principle

$$N = k_0 \left(\frac{R_g}{a}\right)^{D_f}$$

N	Number of Primary particles
R_g	Radius of gyration of floc
a	Radius of monomer
D_f	Fractal Dimension
k_0	Constant of order unity

Sorensen, C.M., “Light Scattering by Fractal Aggregates: A Review” Aerosol Science and Technology. vol. 35, pp. 648–687, 2001

Fractal Dimension Measurement Principle

UNIVERSITY OF LEEDS

$$I(q) \propto n_q N_q^2$$

For $R_g^{-1} < q < a^{-1}$

$$I(q) \propto N^2 (q.R_g)^{-D_f}$$

N	Number of Primary particles/ scatterers
R_g	Radius of gyration of floc
a	Radius of monomer
D_f	Fractal Dimension
I	Scattered light intensity
q	Scattering wave vector

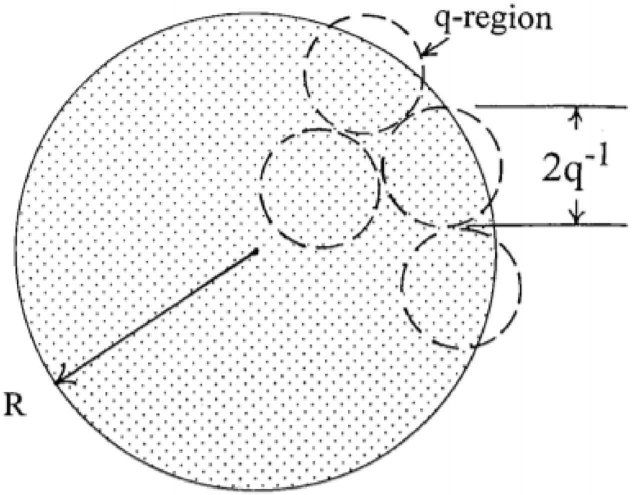

Sorensen, C.M., “Light Scattering by Fractal Aggregates: A Review” Aerosol Science and Technology. vol. 35, pp. 648–687, 2001

Calcite Floc Fractal Dimension Measurements

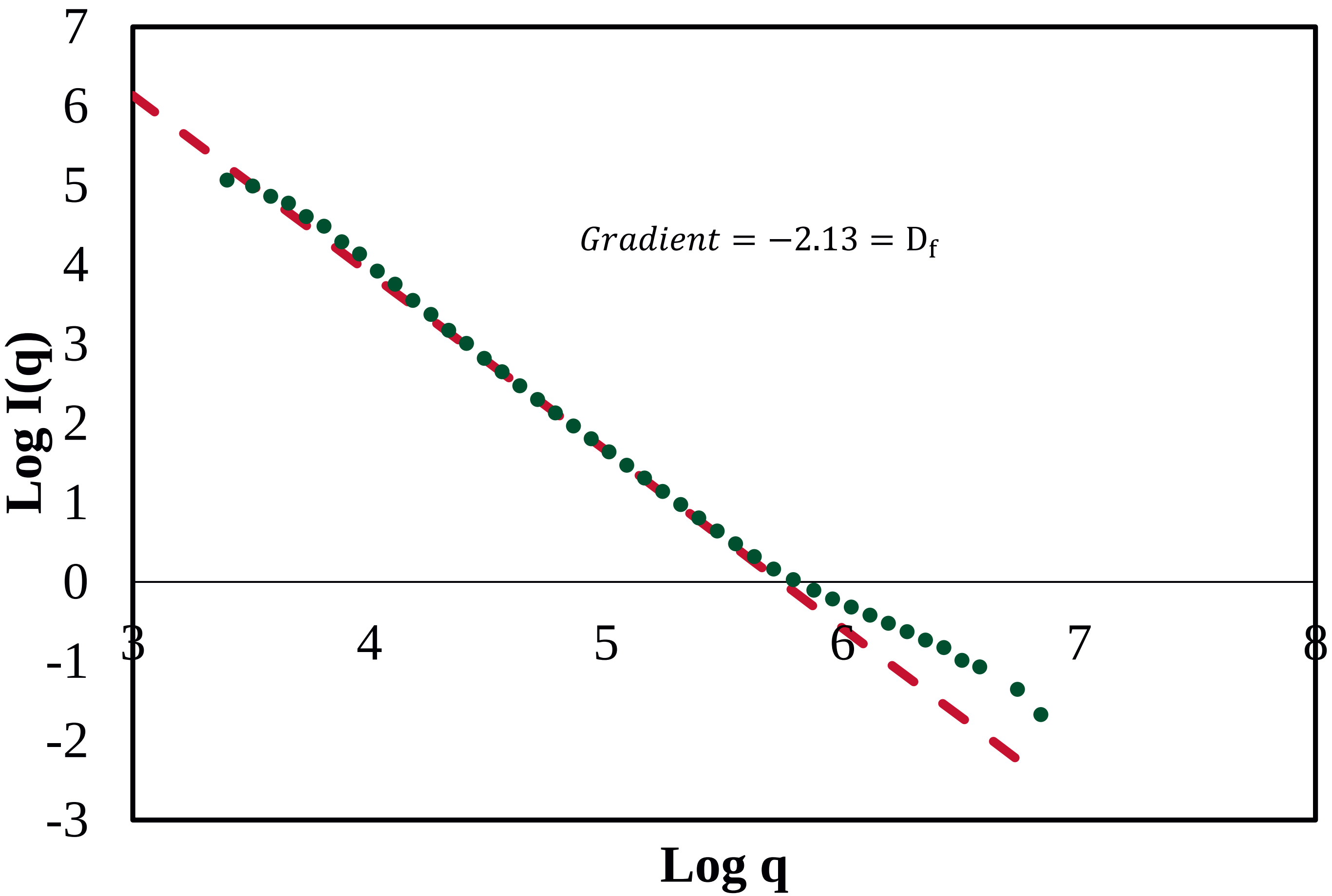

Comparison of Experimental Data to Betteridge et al. Model

UNIVERSITY OF LEEDS

$$k = \frac{2\pi}{\lambda}$$

$$\chi = \frac{4\,a\rho_s\,\xi}{3}$$

χ = Scattering Cross-section (-)
ξ_h = Sediment attenuation coefficient
a= Particle diameter (m)
ρ_s = Sediment particle density (kgm^{-3})

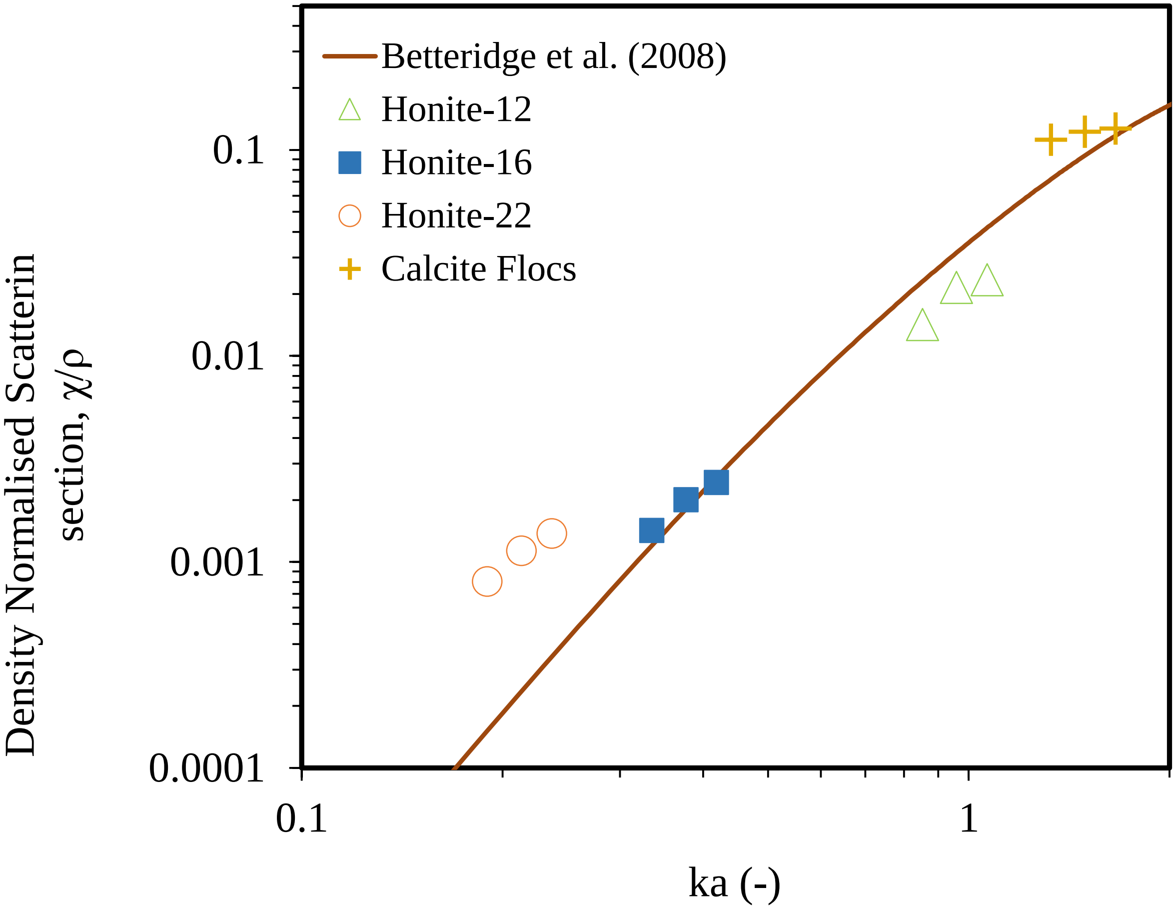

K. Betteridge, P. Thorne and R. Cooke, "Calibrating multi-frequency acoustic backscatter systems for studying near-bed suspended sediment transport processes," *Continental Shelf Research 28,* pp. 227-235, 2008.

ANY QUESTIONS?